UNIVERSITÀ DEGLI STUDI DI PADOVA

Dipartimento di Fisica e Astronomia "Galileo Galilei"

Master Degree in Astrophysics and Cosmology

Final Dissertation

Cosmic Microwave Background Spectral Distortions and Primordial Gravitational Waves

Thesis supervisor
Prof. Nicola Bartolo

Candidate
Marienza Caldarola

Thesis co-supervisors
Prof. Jens Chluba
Dr. Andrea Ravenni

Academic Year 2020/2021

"Viviamo in un mondo di ombre, Daniel, e la fantasia è un bene raro."

— C. R. Zafón

Abstract

Distortions of the Cosmic Microwave Background (CMB) spectrum in the frequency domain provides a new window onto a variety of cosmological phenomena, including the physics of the early Universe. These spectral distortions are tiny departures of the CMB frequency spectrum from a pure blackbody which are created whenever the energy or the number density of the CMB photons is changed and therefore encode information about the thermal history of the Universe. They can be produced by a number of processes occurring at the early stages of cosmic history and therefore allow us to probe the standard picture of cosmology. The energy spectrum of the CMB is extremely close to that of a perfect blackbody with a temperature of 2.725 K [1, 2]. However, at redshifts $z \lesssim 2 \times 10^6$, several mechanisms can modify the CMB spectrum and introduce departures from a blackbody spectrum. Spectral distortions are created by processes that drive matter and radiation out of equilibrium. This could be related to early energy injection, for instance, the dissipation of acoustic waves from inflation. In this process, the baryons heat up and transfer part of their excess energy to the surrounding CMB photon bath. Depending on the moment of injection, this causes a distortion which can be of two main types, namely the so-called μ-type and y-type distortions. The parameters associated with these distortions are a measure for the total amount of energy that was injected into the CMB and also provide estimates about the time when the injection occurred [3]. Therefore, CMB spectral distortions constitute a powerful probe of the physics of the early Universe. The current best observational limits are due to COBE/FIRAS, that are $|\mu| < 9 \times 10^{-5}$ and $|y| < 1.5 \times 10^{-5}$ (95% CL) [1, 2, 4]. With proposed experiments, it will be possible to detect these distortions and therefore probe inflation at small scales, which are not accessible by CMB temperature polarization and anisotropies [5–7].

As said, the standard cosmological model predicts the production of CMB spectral distortions, thanks to various effects, one of which is the dissipation of acoustic waves of the photon-baryon plasma through the Silk-damping effect. Such distortions can be used to constrain the power spectrum (i.e., the Fourier transform of the two-point correlation function) of the primordial density perturbations arising from inflation in the range $1\ \mathrm{Mpc}^{-1} \lesssim k \lesssim 10^4\ \mathrm{Mpc}^{-1}$. Moreover, a fundamental prediction of inflationary models is the production of primordial gravitational waves (GWs), i.e., a stochastic background of tensor perturbations of the metric. Interestingly, it has recently been shown how the effects of primordial GWs on CMB spectral distortions can indeed fill in a gap in a portion of GW frequency neither covered by CMB anisotropies nor by direct interferometric measurements [8].

The first main goal of this Thesis is to present a general overview of CMB spectral distortions. Moreover, this work will include an original part focused on the possibility

of generating statistically anisotropic features in the CMB spectral distortions and on sources of these anisotropic features. Within many candidates, there are the so-called *inflationary fossils*, models in which the scalar field that drives inflation couples to a new primordial degree of freedom, a fossil field, which could be a scalar, a vector or a tensor field. In particular, *tensor* fossils refer to long-wavelength relic GWs from inflation that produce a quadrupolar modulation of curvature perturbations. The tensor fossils no longer interact, or interact very weakly, during late-time cosmic evolution. Therefore, the unique observational effect due to the coupling with the inflaton field would be to give rise to local departures from statistical isotropy, or from Gaussianity, in the primordial curvature perturbation field [9–11].

In practice the original contribution of this Thesis will consist in the study of how this new tensor degree of freedom can distort the primordial scalar curvature two-point correlation function. In order to evaluate this, the mixed bispectrum (the Fourier transform of the three-point correlation function) involving tensor-scalar-scalar fluctuations will be computed in the so-called *squeezed limit configuration* (namely when the wavenumber of the tensor perturbations in Fourier space is much smaller than the other two associated with the scalar perturbations), which gives rise to an anisotropic power spectrum of curvature (density) perturbations, as it will be explained.

Hence, in this work, after an introduction about the standard cosmological model in general, we discuss more in details the CMB, focusing on temperature anisotropies and deriving some of the results which are generally useful. After that, we delve into CMB spectral distortions, pointing out the main features and their importance. Moreover, we derive the cross-correlation between CMB anisotropies and CMB spectral distortions, which is a useful observable to constrain primordial non-Gaussianity [12, 13]. We then focus on the study of the imprints of the tensor fossils on cosmic structures. Starting from these ingredients, we will see how tensor fossils can leave a signature in the CMB spectral distortions, by evaluating the ensemble average of the μ-distortion modulated by the long-wavelength tensor mode. Then, we will also compute the corresponding cross-correlation between CMB anisotropies and μ-distortions, computing the tensor-scalar-scalar and the scalar-tensor-tensor bispectra, both in the case of modulation.

As far as CMB spectral distortions are concerned, we expect that their expression will be modified as a consequence of such primordial correlation between scalar and tensor modes and the induced anisotropic power spectrum. Our goal is to make a detailed study of the theoretical predictions that such tensor fossils could imprint into CMB spectral distortions, focusing mainly on μ-distortions.

Contents

Chapter 1

The Standard Cosmology

Cosmology is a very wide research field continuously evolving, stimulated by increasingly precise experimental data and by the corresponding emergence of new ideas, new models, new scenarios for the early Universe, in close contact with the progress of theoretical high energy physics. At the beginning of the twentieth century people started elaborating a scientific theory to describe the Universe as a whole. In particular, the astronomer and astrophysics E. Hubble discovered the expansion of the Universe we live in. The idea was that if the Universe is expanding, then galaxies should be moving away from each other and we should consequently see galaxies receding from us, actually confirmed by his studies [14]. From that moment on, cosmology has increasingly grown. In particular, the turning point was the discovery of the Cosmic Microwave Background (CMB) by Penzias and Wilson (1965) [15]: this marked the very birth of modern cosmology. Then, first models were proposed, essentially based on nearly scale invariant and adiabatic initial conditions and on an almost homogeneous and isotropic Universe, whose evolution is described by the Einstein's Field Equations. This is the second pillar upon which the Big Bang model stands. However, the high degree of isotropy has long been a puzzle for cosmologists, since studies backwards to the early ages told that patches of sky from which the CMB last scattered should not have been in casual contact at that time. This is the so-called *horizon problem*, which will be explored later. The most promising solution is called *inflation* and it postulates a phase of rapid expansion at early time which separated originally causally connected regions by the vast distances. This scenario is necessary in order to account for the isotropy of the CMB on large scale.

The accuracy of cosmological measurements resulted in the latest cosmological model, the so-called *standard Lambda Cold Dark Matter* model (ΛCDM model), where Λ indicates the Einstein's cosmological constant, associated with the so-called *dark energy* component of the Universe. In the standard cosmological model the dark energy is expected to be almost the 70% of the total energy density of the Universe and it is responsible for the accelerated expansion. The cold dark matter is measured to be almost the 25% and it is

called *cold* to indicate that it was non-relativistic at the time of its decoupling, while *dark* stands for the fact that it does not emit light [16–18]. It is noteworthy that the baryonic matter, all galaxies, stars, so all visible matter in general, constitute only a very small percentage of the total composition of the Universe, about 5%.

The notable feature of the ΛCDM model is that it is characterized by just six parameters. They are the baryon density $\Omega_{\rm b}$, the CDM density $\Omega_{\rm c}$, the value of the sound horizon at recombination time $\theta_{\rm MC}$, the reionization optical depth τ, the curvature fluctuation amplitude $A_{\rm s}$, which is the normalization of the power spectrum of the primordial density perturbations, and the spectral index $n_{\rm s}$ (which describes the shape of the scalar power spectrum) [17].

The main observational successes of the ΛCDM model are a very good account of the properties of the Universe on cosmological scales, as the accelerating expansion of the Universe, the temperature and polarization anisotropies of the CMB, the abundances of light elements and the Large-Scale Structures (LSS). All the structures of the Universe arise from the initial conditions of the ΛCDM model and the inflation provides an explanation for the generation of the primordial density perturbations, which are precisely the initial conditions. This model includes accurate testable hypotheses in each of these areas, supported by an incredible agreement with the observational data. For that reason, new generations are very optimistic about the power of studies in cosmology.

In this Chapter, we will go through the basics of the modern standard cosmological model, dealing with some of its main problems. Then, as a solution of them, the theory of inflation will be presented and a briefly description of primordial scalar perturbations will be given (the reader can find these basic concepts covered in more detail in any textbook, e.g. [19, 20]). We will conclude providing a description of the power spectrum and bispectrum (the two- and three-point correlation function in Fourier space) which are important statistical tools used to extract cosmological information.

1.1 The homogeneous and isotropic Universe

In order to study the properties and the dynamics of the Universe, we need some theoretical assumptions, which are backed by experimental evidence, about the background properties of the Universe. According to the Hot Big Bang model, the Universe originates about 14 billions years ago and it is still expanding.

A staple of the Standard Model of cosmology is the *Cosmological Principle*, which assumes that for any cosmological observer the Universe is homogeneous and isotropic on large scale at fixed time. The last two adjectives are referred to mass-energy distribution on large scale[1]. In particular, homogeneity means that there are no preferred locations,

[1]Nowadays, the Universe is considered to be homogeneous and isotropic when observed on scales greater than a hundred Mpc.

thus there are no privileged points of observation with respect to all the other points of the Universe. Isotropy means that the Universe looks the same on different directions of lines-of-sight for an observer[2]. The best evidence for the isotropy of the observed Universe is related to the uniform value of the temperature of the CMB radiation: in fact, intrinsic temperature anisotropies are of the order of one part in 10^5 [21].

The most general expression of the metric for a Universe in which the Cosmological Principle holds is the Friedmann-Lemaître-Robertson-Walker (FLRW) metric, which can be written in polar coordinates in the form [3]

$$ds^2 = g_{\mu\nu}dx^\mu dx^\nu = -c^2dt^2 + a^2(t)\left[\frac{dr^2}{1-kr^2} + r^2d\theta^2 + r^2\sin^2\theta d\phi^2\right], \tag{1.1}$$

where $g_{\mu\nu}$ is the metric, t is the cosmic time, r, θ, ϕ are the comoving adimensional coordinates and $a(t)$ is the scale-factor of the Universe. The latter is a key parameter and it encodes information about the expansion of the Universe. k is the curvature parameter of 3-dimensional hypersurfaces at constant time t and it can assume only the values $k = 0, \pm 1$, depending on the geometry of the Universe ($k = +1$ for a curved and closed Universe, $k = 0$ for a spatially flat Universe and $k = -1$ for a curved and open Universe). Observations show that the Universe is very close to being flat, then compatible with the solution $k = 0$ [17, 22]. Moreover, the FLRW metric can be rewritten by introducing the *conformal time*

$$d\eta = \frac{dt}{a(t)} \tag{1.2}$$

such as

$$ds^2 = a^2(\eta)\left[d\tau^2 - \left(\frac{dr^2}{1-kr^2} + r^2d\Omega^2\right)\right], \tag{1.3}$$

where it has been set $c = 1$.

The *Einstein equation* links the space-time described by the metric with the matter and the energy contained in the Universe,

$$G_{\mu\nu} = 8\pi G T_{\mu\nu}\,, \tag{1.4}$$

where G is the Newtonian gravitational constant and $T_{\mu\nu}$ is the energy-momentum tensor of the fluid which describes the energy content of the Universe. It is possible to describe the latter as a perfect fluid with matter energy density ρ, isotropic pressure P and 4-velocity $u_\mu = dx_\mu/d\lambda$, λ being some affine parameter so that $g_{\mu\nu}u^\mu u^\nu = -1$. In the case of a

[2] As already pointed out, this refers to scales of the order of 100 Mpc, larger than the dimensions of structures such as galaxies and galaxy-clusters.

[3] This metric is written from the point of view of a comoving observer. In general, normal and comoving distances are related by $\lambda_{\rm phys} = a(t)\lambda_{\rm com}$, where the comoving distance between two points measures the difference between coordinates in the space and thus remains constant while space expands uniformly as time evolves [19].

perfect fluid the energy-momentum tensor can be written as [20]

$$T_{\mu\nu} = (\rho + p)u_\mu u_\nu - p g_{\mu\nu} \,. \tag{1.5}$$

Here, $\rho = \rho(t)$ and $p = p(t)$ because of homogeneity and isotropy. $G_{\mu\nu}$ in Eq. (1.4) is a symmetric tensor defined as

$$G_{\mu\nu} = R_{\mu\nu} - \frac{1}{2} g_{\mu\nu} R \,, \tag{1.6}$$

where $R_{\mu\nu}$ is the Ricci tensor and R is the Ricci scalar, defined, respectively, as (see e.g. [20])

$$R_{\mu\nu} = R^{\rho}_{\mu\rho\nu} = g^{\rho\sigma} R_{\mu\rho\nu\sigma} \tag{1.7a}$$

$$R = g^{\mu\nu} R_{\mu\nu} \,, \tag{1.7b}$$

and

$$R^{\rho}_{\mu\rho\nu} = \partial_\sigma \Gamma^{\rho}_{\mu\nu} - \partial_\nu \Gamma^{\rho}_{\mu\sigma} + \Gamma^{\alpha}_{\mu\nu}\Gamma^{\rho}_{\sigma\alpha} - \Gamma^{\alpha}_{\mu\sigma}\Gamma^{\rho}_{\nu\alpha} \,, \tag{1.8}$$

with $\Gamma^{\rho}_{\mu\nu}$ indicating the Christoffel symbol.

With some algebraic manipulation, plugging this tensor and the Eq. (1.1) into the Einstein equations (1.4), one ends up with the so-called *Friedmann equations*

$$H^2 = \frac{8}{3}\pi G \rho - \frac{k}{a^2} \tag{1.9}$$

$$\frac{\ddot{a}}{a} = -\frac{4\pi G}{3}(\rho + 3p) \,, \tag{1.10}$$

where $H \equiv \dot{a}/a$ is the *Hubble rate* and the dots indicate the derivative with respect to the time t. In addition, using the continuity equation for the energy-momentum tensor,

$$\nabla_\mu T^{\mu\nu} = 0 \,, \tag{1.11}$$

one obtains

$$\dot{\rho} + 3H(\rho + p) = 0 \,. \tag{1.12}$$

Notice that these three equations are not independent. To close the system of equations (since in this system there are three independent variables, i.e., a, ρ and p, but the independent equations are two), the equation of state, which relates the pressure to the energy density, i.e., $p = p(\rho)$, is added. In the case of perfect fluids, it takes the form

$$p = w\rho, \qquad \text{with} \begin{cases} w = 0 & \text{matter} \\ w = \frac{1}{3} & \text{radiation} \\ w = -1 & \text{dark energy} \,. \end{cases} \tag{1.13}$$

Substituting it in Eq. (1.12), one obtains

$$\dot{\rho} + 3\frac{\dot{a}}{a}\rho(1+w) \qquad \Longrightarrow \qquad \rho \propto a^{-3(1+w)}. \tag{1.14}$$

Therefore, depending on the value of w, one can understand how the energy density ρ evolves with respect to the expansion of the Universe.

In the case of ordinary matter, in which $w = 0$, the pressure is null or negligible and $\rho \propto a^{-3}$. The case of a radiation-dominated Universe, in which $w = 1/3$, is characterized by $\rho \propto a^{-4}$ and $p = (1/4)\rho$. The case in which $w = -1$ corresponds to a Universe dominated by a fluid with constant energy density, due to a cosmological constant, and negative pressure $p = -\rho$.

Nevertheless, the real Universe is not composed by a single fluid, but it is made up of several components (radiation, matter, etc.). As a first approximation, each fluid obeys its own equation of state and has its own energy density. However, the various contributions change over time in a different way. The Universe, during its evolution, went through various phases, during each of which its composition was dominated by a specific component. By evaluating the energy densities of the different components of the Universe as a function of the scale factor, one finds that at early times, i.e., for small values of the scale factor, radiation dominates. Subsequently, the predominant component becomes matter and then, at late times, i.e. for large values of the scale factor, dark energy dominates, since it is the only one not decaying.

Before concluding this Section, let us define some other fundamental parameters.

PARTICLE HORIZON: it is the distance that the light travel between points in the space-time and it is defined as

$$d_{\rm H} = a(t) \int_0^t \frac{dt'}{a(t')}\,. \tag{1.15}$$

It marks the limit of how far, in principle, one can see in the Universe. It sets the radius of a sphere, centered around an observer, within which there are regions of the Universe in causal contact with the observer. This means that, if two point are separated by a distance grater than the particle horizon, then they have never been in causal contact. In a standard FLRW Universe, the scale factor scales as

$$a(t) \propto t^{\frac{2}{3(1+w)}}\,, \tag{1.16}$$

and then $d_{\rm H}(t)$ takes the form

$$d_{\rm H}(t) = \frac{3(1+w)}{3w+1} t\,. \tag{1.17}$$

HUBBLE RADIUS: it represents the distance travelled by light in a Hubble time, defined as

$$R_{\rm H} = \frac{1}{H(t)} = \tau_{\rm H}\,, \tag{1.18}$$

where $\tau_{\rm H}$ is the *Hubble time*.

COMOVING HUBBLE RADIUS: it is defined as

$$r_{\rm H}(t) = \frac{R_{\rm H}(t)}{a(t)} = \frac{1}{a(t)H(t)} = \frac{1}{\dot{a}(t)}\,. \tag{1.19}$$

In particular,

$$\begin{aligned} &\text{radiation dominance} && a(t) \propto t^{1/2} \longrightarrow r_{\rm H}(t) \propto t^{1/2} \propto a \\ &\text{matter dominance} && a(t) \propto t^{2/3} \longrightarrow r_{\rm H}(t) \propto t^{1/3} \propto a^{1/2}\,. \end{aligned}$$

Thanks to this quantity, it is possible to explain a solution for the horizon problem. In fact, during inflation the comoving length scales, which are at the beginning causally connected, gradually become larger than $r_{\rm H}$ and then cross the horizon. Subsequently, during radiation and matter dominated eras, $r_{\rm H}$ increases in time, allowing these scales to reconnect themselves (see Section 1.3.4).

COMOVING PARTICLE HORIZON it is defined as

$$\frac{d_{\rm H}(t)}{a} = \int_0^t \frac{dt'}{a(t')} = \int_0^a \frac{da'}{a'\dot{a}'} = \int_0^a \frac{da'}{a'}\frac{1}{a'H} = \int_0^a \frac{da'}{a'} r_{\rm H}\,. \tag{1.20}$$

Today, the dominant energy component of the Universe is the dark energy. It is a form of energy that has a constant density throughout the Universe. The most natural form of dark energy is the cosmological constant, Λ, which causes the expansion of the Universe to accelerate.

1.2 Brief history of the Universe

About 13.7 billion years ago, the Universe began in a gigantic explosion, the Hot Big Bang. Its subsequent evolution, from one hundredth of a second up to the present day, can be described by the Big Bang model. The latter includes a description for the expansion of the Universe, the origin of light elements and the relic radiation, for understanding the formation of large-scale structure.

Cosmologists are currently working to shed light on the history of the Universe, especially to outline the features of the early stages of its evolution. This is the task of the standard cosmology, which focuses on the time between about one hundredth of a second

after the Big Bang through until today. The standard model of cosmology has been supported by numerous observational tests, even if, it still has a number of unresolved issues (see Section 1.3). Moreover, cosmologists are also interested in the picture prior to this, at higher temperature regimes. This is the search field of particle cosmology, which tests physical models for processes which would occur only very small fractions of seconds after the Big Bang [4]. Lastly, great interest is addressed to questions about the origin of the Universe itself, describing quantum processes at the earliest conceivable times, the Planck epoch [5]. This is the branch of quantum cosmology.

In order to explore the history of the Universe, one needs to study the evolution of the scale factor with cosmic time, determined by the energy density in the Universe. At early time, the dominant component was the radiation, hence for primordial times the fluid was ultra-relativistic, while, at later times, non-relativistic matter accounts for most of the energy density. Initially, the latter was in a thermodynamic equilibrium, in the sense that the rate of interactions between the particles was much greater than the rate of expansion of the Universe. Considering the conservation of the entropy in an expanding Universe, condition valid as long as the particle species are in thermal equilibrium with each other, one can find the following relation between the temperature and the scale factor,

$$T \propto a^{-1} \,. \tag{1.21}$$

Analogously, in term of the redshift [6],

$$T \propto 1 + z \,. \tag{1.23}$$

In particular, from Eq. (1.21) one can notice that the Universe becomes colder as time passes. This is why the evolution of the Universe can be described through its thermal history. The study of the history of the Universe as its temperature varies is of great interest, especially in order to explain the observed abundance of some elements.

At early times, all particle species were in thermal equilibrium and then there has been a phase during which the symmetry between matter and anti-matter (particles sharing the same mass as their matter counterparts, but qualities such as electric charge are opposite) was broken. In fact, if matter and anti-matter come in contact, annihilate each other, but today everything we see, from the smallest life forms to the largest cosmic objects, is

[4] High energy particle accelerators studies at CERN and Fermilab are dedicated to these purposes.

[5] This is the earliest period of time, 10^{-43} seconds after the beginning of time.

[6] Recall the definition of the cosmic redshift,

$$1 + z = \frac{\lambda_0}{\lambda_\mathrm{e}} = \frac{a_0}{a_\mathrm{e}} = \frac{1}{a_e} \,, \tag{1.22}$$

where λ_0 and λ_e are, respectively, the observed wavelength at the present time and the emitted wavelength at the time of emission.

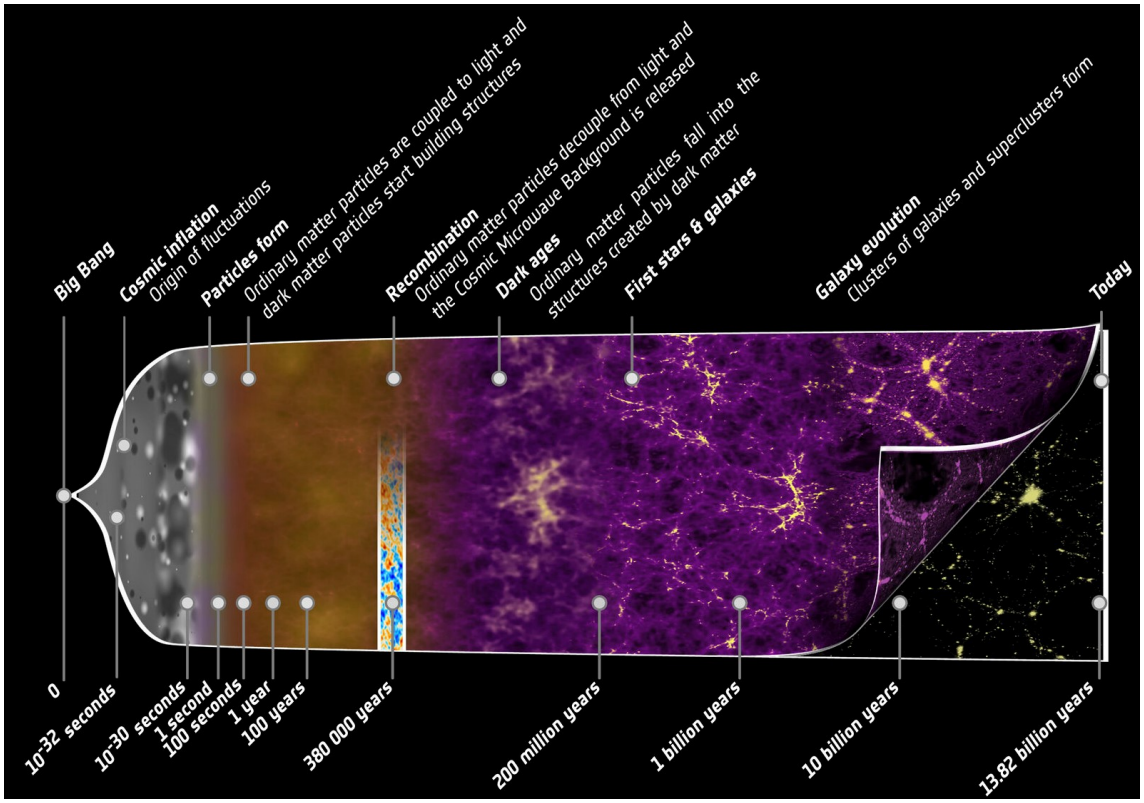

Figure 1.1: Timeline of the history of the universe according to Standard Model of cosmology.

made almost entirely of matter: something must have happened to break the equilibrium. A number of theoretical mechanisms have been proposed to account for this discrepancy, namely identifying conditions that favoured symmetry breaking and the creation of normal matter. This epoch is known as *baryogenesis*, a process that gave rise to the formation of baryons in the period immediately following cosmic inflation [23–27]. The so-called *baryon asymmetry* was very tiny (about $10^9 + 1$ baryons every 10^9 anti-baryons); after most of the matter and antimatter was annihilated, what remained was all the baryonic matter in the current Universe. The reason for this asymmetry and figuring out what happened to the antimatter is one of the greatest challenges in physics.

The high temperature of the radiation prevented all nuclear bonds from forming all nucleus into protons and neutrons. As the temperature decreased, there was a moment in which the boundary nuclear energies became higher than the their kinetic energies, leading to the formation of the first nucleus: this phase is called *nucleosynthesis* (see e.g. [28]). It is a fundamental component of the Big Bang theory. Historically, this mechanism was proposed to explain the observed abundance of Helium, which was not justified considering only the elements produced in the stellar nuclear reactions. The observation of the abundance of chemical elements in accordance with the nucleosynthesis prediction is one of the main successes of the Big Bang model.

	Time	Energy	
Planck Epoch?	$< 10^{-43}$ s	10^{18} GeV	
String Scale?	$\gtrsim 10^{-43}$ s	$\lesssim 10^{18}$ GeV	
Grand Unification?	$\sim 10^{-36}$ s	10^{15} GeV	
Inflation?	$\gtrsim 10^{-34}$ s	$\lesssim 10^{15}$ GeV	
SUSY Breaking?	$< 10^{-10}$ s	> 1 TeV	
Baryogenesis?	$< 10^{-10}$ s	> 1 TeV	
Electroweak Unification	10^{-10} s	1 TeV	
Quark-Hadron Transition	10^{-4} s	10^{2} MeV	
Nucleon Freeze-Out	0.01 s	10 MeV	
Neutrino Decoupling	1 s	1 MeV	
BBN	3 min	0.1 MeV	
			Redshift
Matter-Radiation Equality	10^{4} yrs	1 eV	10^{4}
Recombination	10^{5} yrs	0.1 eV	1,100
Dark Ages	$10^{5} - 10^{8}$ yrs		> 25
Reionization	10^{8} yrs		$25 - 6$
Galaxy Formation	$\sim 6 \times 10^{8}$ yrs		~ 10
Dark Energy	$\sim 10^{9}$ yrs		~ 2
Solar System	8×10^{9} yrs		0.5
Albert Einstein born	14×10^{9} yrs	1 meV	0

Table 1.1: Main events in the thermal history of the Universe. Table credit [30].

Later, at energies of order of 1 MeV, the interaction rate for the electroweak processes became smaller than the Hubble rate and so the neutrinos ceased to interact with the photons. Subsequently, the energy density of the radiation became smaller than the one of the matter: this moment is known as *radiation-matter equivalence* and marks the beginning of the matter dominated epoch of the Universe, during which the large-scale structure observed today started to form through gravitational instability.

After the equivalence moment, the epoch of *recombination* occurred. When the Universe was almost 4×10^5 years old, it was ionized and opaque to the radiation; the photons were not free to stream due to the interaction with the electron through the Compton scattering. When the temperature decreased, in particular becoming less than the boundary energy of the Hydrogen, the electrons interacted with the protons, creating the first atoms of Hydrogen. This corresponds to the last scattering surface and the radiation which leaves it then cooled due to the expansion of the Universe until it reaches the temperature of about 2.725 K. This constitutes the Cosmic Microwave Background radiation observable today [29]. Fig. 1.1 shows the timeline of the entire history of the Universe, while in Table 1.1 a list of the most important events characterizing the thermal history is reported. For a more accurate description and more details about the Hot Big Bang model see, for instance, [19, 20, 27].

1.3 Shortcomings of the Hot Big Bang model

Despite the self-consistency and remarkable success of the standard Hot Big Bang model in describing the evolution of the Universe, a number of questions regarding the initial state of the Universe remain unanswered. For instance, why does the Universe looks the same in all directions if different patches evolved from causally disconnected regions? What is the primordial origin of the perturbations which gravitationally collapsed to form galaxies? Furthermore, phase transitions in the early Universe inevitably give rise to topological defects, such as monopoles and exotic particles. Why are they not visible today? These and many others constitute the shortcomings of the Hot Big Bang model: they do not highlight inconsistencies in the theory but extremely finetuned initial conditions are needed to explain results.

In particular, there are two remarkable aspects: the fact that the Universe is practically flat and that even regions far off in different directions, as observed from Earth, have roughly the same temperature, although in an expanding Universe there would not have been time for heat to pass between them to even things out. For these reasons, the theory of inflation was introduced. According to that, the early Universe expanded exponentially fast for a fraction of a second after the Big Bang; this condition can solve the previous issues, as we will see below.

1.3.1 Horizon problem

Looking at the Universe, one finds that distant regions, in opposite directions, which seem to never have been in causal contact with each other, seems to share same properties. In particular, to have the same temperature. Let us consider a region with a comoving characteristic size λ: the region is causally connected only when λ is less than the comoving Hubble horizon, i.e., $\lambda < r_{\rm H}$ or, analogously, at time $t > \tau_{\rm H}$. This means that, for very large cosmological scales, the corresponding regions were causally disconnected for most of their past history, getting in causal connection only recently. However, this is not what we observe, for instance, looking at the CMB. Since COBE flew, we have been able to observe regions that have become causally connected only in recent times [31]: it showed that the background radiation is nearly homogeneous ad isotropic, all the points have the same temperature up to small fluctuations of the order 10^{-5}. Thus, photons from opposite directions must have communicated somehow, because the CMB has almost exactly the same temperature in all directions over the sky, about 2.725 K, irrespective of the direction. The natural question is how this is possible. This problem can be solved by the idea that the Universe expanded exponentially for a short time period after the Big Bang. Before this period, the observable Universe could have been in causal contact, sharing a common temperature. Regions that are widely separated today were actually very close together in

the early epochs, explaining why photons from these regions have almost exactly the same temperature.

1.3.2 Flatness problem

From observations on the CMB [17, 22, 32] the Universe seems to be spatially flat or close to spatially flat. In order to understand why this turns out to be a problem, let us recall the Eq. (1.9) and define the *critical density* ρ_c as the value of density setting the spatial curvature k equal to zero. Then, it follows $\rho_c = 3H^2/(8\pi G)$. Moreover, it is possible to define the *curvature parameter* as [30]

$$\Omega(t) = \frac{\rho(t)}{\rho_c}\,. \tag{1.24}$$

From Eq. (1.9) and Eq. (1.24), one obtains

$$\Omega(t) - 1 = \frac{k}{a^2H^2} = kr_H^2(t)\,. \tag{1.25}$$

One can notice that if the Universe is perfectly flat, then $\Omega = 1$. The actual measurements on spatial curvature are consistent with a flat Universe, $\Omega_K = 0.001 \pm 0.002$ [17] (68% CL). However, as seen above, r_H increases over time, implying $\Omega \neq 1$ and only going backwards in time the density parameter was closer to 1. This means that at the beginning of the Universe the curvature parameter was much closer to 1 than today. Taking as primordial reference time the Planck time $t_{Pl} \simeq 10^{-44}$ s after the Big Bang, one can find that [30]

$$|\Omega(t_{Pl}) - 1| < 10^{-62}\,. \tag{1.26}$$

This is a problem since it means that in the early epoch the curvature parameter needed to be very close to 1 with a precision of one part over 10^{62}. This issue is known as *fine tuning problem*.

1.3.3 Unwanted relics

Referring to [33], let us briefly mention the topological defects and unwanted relics associated with spontaneous symmetry breaking in unified theories. The physics of the Universe at early times is described by particle theory. Many of these theories predict the creation of topological *defects*, which arise when phase transitions occur in particle models. Because of the decrease in temperature of the Universe due to its expansion, these phase transitions are a consequence of symmetry breaking typical of particle models. These phase transitions may have had profound implications on the evolution of our Universe and its contents. Some types of defects are the following:

Monopoles: the field points radially away from the defect, which has a magnetic field configuration at infinity that makes them analogous to that of the magnetic monopole.

Cosmic strings: they can be visualized as large strings stretched in space that possibly cause galaxies to form into groups and they are an alternative proposal to inflation to explain the large-scale structure of the Universe.

Domain Walls: the space is divided into connected regions; one region exhibit a phase, the other region the opposite phase. These regions are separated by walls of discontinuity described by a certain energy per unit area.

Textures: they can be considered as a combination of all the other defects; they are hard to visualize and are not expected to form in most theories.

Among all these defects, monopoles are the most prevalent in different theories. They constitute a shortcoming of the Hot Big Bang model since, if one calculates the number of monopoles produced in events such as in the electroweak symmetry breaking case, it results that they would be the dominant component in the Universe. However, no monopole has ever been observed, directly or indirectly. These monopoles would effect the curvature parameter and in turn the Hubble parameter, galaxy formation, etc. Therefore, unwanted relics remain an anomalous component of the Hot Big Bang theory [33, 34].

1.3.4 Inflationary solution

Flatness and horizon problems are not strictly inconsistencies of the standard cosmological model. By assuming that the Universe was homogeneous on superhorizon scales (but with the right level of inhomogeneity able to explain structure formation) and that the initial value of Ω was extremely close to 1, then the Universe could evolve in agreement with actual observations [30]. These specific initial conditions are needed in order to explain results: the flatness of the early Universe and large-scale homogeneity must simply be assumed. In this context, a theory able to explain these initial conditions seems to be very interesting.

The idea is based on the the existence of a period, before the standard radiation-dominated epoch, in which the comoving Hubble radius decreased, instead of increasing. Then, let us consider a region of the Universe of typical comoving distance λ and assume that $\dot{r}_{\rm H} < 0$ before the radiation-dominated era. In this way, this region that entered the horizon only recently was already causally connected during the initial phase. Therefore, one finds

$$\dot{r}_{\rm H} = -\frac{1}{\dot{a}^2}\ddot{a} < 0 \qquad \Longrightarrow \qquad \ddot{a} > 0\,. \tag{1.27}$$

In full generality, the *inflationary phase* refers to a period in the early Universe, before the radiation-dominated epoch, characterized by an accelerated expansion of space.

Notice that, imposing this condition in Eq. (1.10), this leads to a fluid component with an effective pressure given by

$$p < -\frac{1}{3}\rho \qquad \left(w < -\frac{1}{3}\right), \tag{1.28}$$

which corresponds to a negative pressure, if ρ is assumed to be positive. As already seen, this is compatible with the case of a Universe dominated by an exotic component with constant energy density and $w = -1$. In this case the Universe is exponentially expanding. However, the condition of an accelerated expansion period is not sufficient to solve the problems: it is also necessary a condition on the duration of this accelerated expansion. It is possible to give an estimate of the duration of the inflationary epoch: it is necessary to impose that inflation lasted a sufficiently long period such that all the observed comoving scales exited the Hubble horizon during inflation. In fact, the beginning of the inflation period must be set at a time, $t_{\rm i}$, such that the comoving Hubble horizon at that time was larger than today, t_0. This means

$$r_{\rm H}(t_{\rm i}) \gtrsim r_{\rm H}(t_0)\,. \tag{1.29}$$

In this way, the observed regions were already causally connected, then they exited the comoving Hubble horizon, since the latter decreased during inflation, and finally they re-entered the horizon after inflation. This explains the homogeneity and isotropy.

Accordingly, let us define the *number of e-foldings*

$$N = \ln\left(\frac{a_{\rm f}}{a_{\rm i}}\right) = \ln\left(\frac{a(t_{\rm f})}{a(t_{\rm i})}\right) = \int_{t_{\rm i}}^{t_{\rm f}} H(t)dt\,, \tag{1.30}$$

where $t_{\rm i}$ and $t_{\rm f}$ are, respectively, the time at which inflation began and ended. N provides an evaluation of the duration of inflation. In order to solve the horizon problem, it must occur that $N \gtrsim 50 - 60$ [35, 36].

Thanks to the expansion of the Universe, one can infer the properties about quantum fluctuations that were created at the beginning of inflation, which leave imprints in the CMB, through hotter and colder regions. Moreover, these fluctuations act as seeds for structure formation: after the inflationary epoch, the fluctuations are amplified, the density of matter varies slightly from region to region and gravity causes the more dense regions to start contracting, leading to the formation of structures. According to the model of inflation and current observations of the accelerating Universe, today we seem to again enter in a de-Sitter phase due to the cosmological constant Λ.

1.4 Dynamics of inflation

The first models of inflation, proposed around the 80s, tried to solve the problem of cosmic relics in the context of the spontaneous symmetry breaking of *Grand Unified Theories* (GUTs), well motivated extensions of the Standard Model of particle physics [37–42]. The theory of cosmic inflation was then studied and improved, until it became the standard model for cosmological inflation, with specific observable predictions, investigated in recent decades and still subject of current research. In particular, inflation is believed to have occurred at very high energy scale, even of the order of 10^{15} GeV, which roughly corresponds to the GUT scale (the energy level above which it is believed the electromagnetic force, weak force and strong force become equal in strength and unify to one force). While GUTs exploit the power of symmetries and group theory to unify the electroweak and strong interactions into a single force and they are successful in addressing several of outstanding issues of the Standard Model, the microscopic origin of inflation is still a mystery: there are still unanswered questions, for instance, about what the inflaton is and what the shape of its potential is. In the following the dynamics of standard *slow-roll* models of inflation will be deepened. These are the simplest models of inflation (see e.g. [30] for more details). However, inflation is a paradigm, but it is not the unique theory. A large number of phenomenological models has been proposed with different theoretical motivations and observational predictions. For instance, there exist scenarios involving several scalar fields, non-standard kinetic terms, or both (see e.g. [30, 43, 44]).

The definition of an inflationary model amounts to a specification of the inflaton action and its coupling to gravity. The simplest models of inflation involve a single scalar field φ, called *inflaton*, which can parameterize the time-evolution of the inflationary energy density. Assuming that it is minimally coupled to gravity, the action takes the form [30]

$$\begin{aligned} S &= \frac{1}{2}\int d^4x\sqrt{-g}R + \int d^4x\sqrt{-g}\mathcal{L}_\varphi(\varphi, g_{\mu\nu}) \\ &= \int d^4x\sqrt{-g}\left[R - \frac{1}{2}g^{\mu\nu}\partial_\mu\varphi\partial_\nu\varphi - V(\varphi)\right] = S_{\rm HE} + S_\varphi\,, \end{aligned} \tag{1.31}$$

which is the sum of the gravitational Einstein-Hilbert action, $S_{\rm HE}$, and the action of a scalar field with canonical kinetic term, S_φ. The potential $V(\varphi)$ describes the self-interactions of the scalar field. Moreover, the energy-momentum tensor for the scalar field is defined as

$$T^\varphi_{\mu\nu} = -\frac{2}{\sqrt{-g}}\frac{\delta S}{\delta g^{\mu\nu}} = \partial_\mu\varphi\partial_\nu\varphi + g_{\mu\nu}\left[-\frac{1}{2}g^{\alpha\beta}\partial_\alpha\varphi\partial_\beta\varphi - V(\varphi)\right]. \tag{1.32}$$

Now let us look at the equation of the motion of the scalar field, corresponding to the Klein-Gordon equation,

$$\Box\varphi = \frac{\partial V}{\partial\varphi}\,, \tag{1.33}$$

where the covariant D'Alembert operator is defined as

$$\Box = \frac{1}{\sqrt{-g}}\partial_\nu\left(g^{\mu\nu}\sqrt{-g}\partial_\mu\right). \tag{1.34}$$

This leads to

$$\ddot{\varphi} + 3H\dot{\varphi} - \frac{\nabla^2\varphi}{a^2} = -\frac{\partial V}{\partial\varphi}. \tag{1.35}$$

Notice that the term $3H\dot{\varphi}$ is typical of a curved space-time (it is not present in the the Klein-Gordon equation for a flat space-time) and it can be interpreted as a sort of friction term which act on the inflaton during its motion in the expanding background.

In general, the inflaton field can be written as

$$\varphi(\mathbf{x}, t) = \varphi_0(t) + \delta\varphi(\mathbf{x}, t), \tag{1.36}$$

where $\varphi_0 \equiv \langle\varphi\rangle$ indicates the classical background motion of φ, while $\delta\varphi$ indicates the quantum fluctuations around φ_0. It is important to guarantee that these fluctuations are small, i.e., $\langle\delta\varphi^2\rangle \ll \varphi_0^2$. From an observational point of view, this property needs to be satisfied to end up with a Universe where the temperature anisotropies of the CMB are very small, $\Delta T/T \simeq 10^{-5}$.

For the moment, let us restrict to the case of a homogeneous field $\varphi(\mathbf{x}, t) \equiv \varphi_0(t)$, i.e., to study the background dynamics, and assume the FLRW metric with null spatial curvature,

$$ds^2 = -dt^2 + a^2(t)\delta_{ij}dx^i dx^j. \tag{1.37}$$

The analysis of the perturbations will be given in the next Section. Neglecting the subscript 0 of the filed for simplicity, the energy-momentum tensor takes the form

$$T^0{}_0 = -\left[\frac{1}{2}\dot{\varphi}^2 + V(\varphi)\right] = -\rho_\varphi \tag{1.38a}$$

$$T^i{}_j = \left[\frac{1}{2}\dot{\varphi}^2 - V(\varphi)\right]\delta^i{}_j = p_\varphi\delta^i{}_j. \tag{1.38b}$$

Notice that such a energy-momentum tensor allows us to realize an inflationary epoch. In fact, as said before, having a negative pressure ensures the condition of an accelerated expansion (see Eq. (1.28)). This condition translates in the following

$$\frac{1}{2}\dot{\varphi}^2 \ll V(\varphi) \quad \Longrightarrow \quad p_\varphi \simeq -\rho_\varphi \quad (\Longleftrightarrow w_\varphi \simeq -1). \tag{1.39}$$

From this equation one can understand that the field is moving very slowly with respect to its potential: this kind of motion is characterized the so-called *slow-roll* condition and it is satisfied for an almost flat potential for all the duration of the inflation (see Fig. 1.2). Therefore, neglecting the curvature contribution, Eq. (1.9) becomes

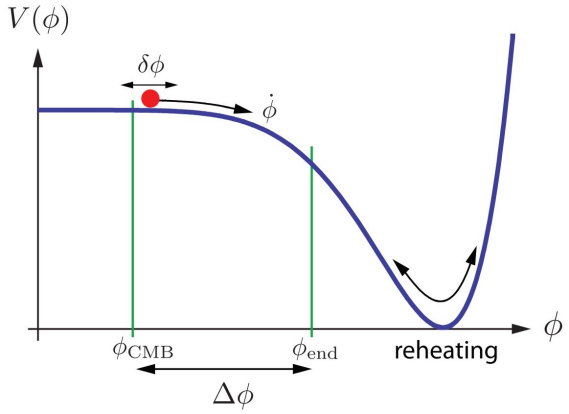

Figure 1.2: Cartoon of inflationary potential, taken from [30].

$$H^2 = \frac{8}{3}\pi G\rho_\varphi \simeq \frac{8}{3}\pi G V\,. \tag{1.40}$$

Moreover, under the slow-roll dynamics, it results

$$\dot{\varphi} \simeq -\frac{V'}{3H}\,, \tag{1.41}$$

where $V' = \partial V/\partial\varphi$. This is known as second slow-roll condition.

It is important to underline that the potential is almost constant, but not exactly. This ensures that the inflationary epoch eventually ends. In order to test the features of the slow-roll dynamics, the so-called *slow-roll parameters* are introduced,

$$\epsilon \equiv -\frac{\dot{H}}{H^2} \simeq \frac{3}{2}\frac{\dot{\varphi}^2}{V} \tag{1.42a}$$

$$\eta \equiv -\frac{\ddot{\varphi}}{H\dot{\varphi}}\,. \tag{1.42b}$$

These quantities are useful to compare observations with the theoretical predictions of different infationary models. As one can see, in order to have inflation, it must occur that $\epsilon, |\eta| < 1$: this condition holds for the duration of the inflation; inflation ends when they reach the unity. Moreover, it is also possible to define other two parameters, $\epsilon_{\rm V}$ and $\eta_{\rm V}$, as follows [30]

$$\epsilon_{\rm V} = \frac{M_{\rm Pl}^2}{2}\left(\frac{V'}{V}\right)^2 \tag{1.43a}$$

$$\eta_{\rm V} = M_{\rm Pl}^2\frac{V''}{V}\,. \tag{1.43b}$$

The parameters $\epsilon_{\rm V}$ and $\eta_{\rm V}$ are called *potential slow-roll parameters* to distinguish them from the *Hubble slow-roll parameters*, ϵ and η. In the slow-roll approximation they are are

related to each other as follows

$$\epsilon \simeq \epsilon_{\rm V}, \qquad \eta \simeq \eta_{\rm V} - \epsilon_{\rm V}\,. \tag{1.44}$$

The experimental bounds on these parameters are given by Planck satellite [29].

Reheating phase To conclude this discussion, let us point out that it is necessary to have a mechanism which could allow the transition from the inflationary era to a radiation-dominated Universe. This transition is called *reheating*. The idea is that when the field φ leaves the slow-roll regime, it starts to fall a non-vanishing curvature of the potential (see Fig. 1.2). This means that $\varepsilon, |\eta|$ are no longer smaller than one and φ starts to oscillate around the minimum of its potential. Due to these oscillations, the inflaton starts to decay in lighter particles, which will constitute the content of the radiation-dominated epoch. Referring to a potential like the one in the Fig. 1.2, the equation of motion of the scalar field becomes

$$\ddot{\varphi} + (3H + \Gamma_\varphi)\dot{\varphi} = -V'(\varphi)\,, \tag{1.45}$$

where Γ_φ represents the decay rate of the inflaton field. From here, using Eq. (1.38a), since the potential is almost flat, one can derive the equation of the decay of the inflaton energy [27],

$$\dot{\rho}_\varphi + (3H + \Gamma_\varphi)\rho_\varphi = 0\,. \tag{1.46}$$

Γ_φ depends on model-dependent physical processes. In general, reheating is a more involved topic which will not be explored in this work. A more detailed study of the reheating can be found, for instance, in [45, 46].

1.5 Cosmological perturbations from inflation

It is important to discuss the evolution of the quantum fluctuations of the inflaton field since they are at the origin of structures in the Universe. The idea is that these fluctuations are generated on scales much smaller than the comoving Hubble radius, and later, during inflation, are stretched to scales bigger than the horizon. On such scales the fluctuations are not causally connected and they remains almost constant in time, since in this regime microscopic physics does not affect their evolution. The quantum fluctuations of the scalar field are strictly connected with the density perturbations which causes the observed anisotropy in the CMB temperature. When these perturbations gradually re-enter the horizon, cause the collapse at the origin of the large-scale structure in the Universe. A complete and more accurate derivation of the following results can be found in the literature, see e.g. [21, 30]. Here, we will present the main results that provide us the background useful for our work.

To describe the evolution of the quantum fluctuations, one can perturb the equation of motion of the field, Eq. (1.35) and, at first order, get

$$\delta\dot{\varphi} + 3H\delta\dot{\varphi} - \frac{\nabla^2\delta\varphi}{a^2} = -\frac{\partial V}{\partial\varphi}\,. \tag{1.47}$$

Using the rescaling $\delta\hat{\varphi} = a\delta\varphi$ and expressing the quantum fluctuation as a function of the conformal time $d\eta = dt/da$, in Fourier space one can write

$$\begin{aligned}\delta\hat{\varphi}(\mathbf{x},\eta) &= \int \frac{d^3k}{(2\pi)^3} e^{-i\mathbf{k}\cdot\mathbf{x}}\delta\hat{\varphi}(\mathbf{k},\eta) \\ &= \int \frac{d^3k}{(2\pi)^3}\left[u_k(\eta)a_{\mathbf{k}}e^{-i\mathbf{k}\cdot\mathbf{x}} + u_k^*(\eta)a_{\mathbf{k}}^\dagger e^{i\mathbf{k}\cdot\mathbf{x}}\right],\end{aligned} \tag{1.48}$$

where $a_{\mathbf{k}}$ and $a_{\mathbf{k}}^\dagger$ are the usual creation and annihilation operators,

$$a_{\mathbf{k}}\,|0\rangle = 0 \qquad \forall\mathbf{k} \tag{1.49a}$$

$$\langle 0|\,a_{\mathbf{k}}^\dagger = 0 \qquad \forall\mathbf{k} \tag{1.49b}$$

obeying the algebra

$$[a_{\mathbf{k}}, a_{\mathbf{k'}}^\dagger] = \delta^{(3)}(\mathbf{k}-\mathbf{k}') \tag{1.50a}$$

$$[a_{\mathbf{k}}, a_{\mathbf{k'}}] = 0\,, \tag{1.50b}$$

and u_k are the wave functions associated to $\delta\hat{\varphi}$, with the normalization condition

$$u_k^* u_k' - u_k u_k^{*'} = -i\,. \tag{1.51}$$

$|0\rangle$ in Eq. (1.49) defines the free vacuum state of the system. In an expanding Universe, there is an ambiguity in the choice of the vacuum state due to the expansion of the background space-time. In fact, in the flat space-time, the solution of the Klein-Gordon equation is given by

$$u_k \simeq \frac{e^{-i\omega_k t}}{\sqrt{2k}}, \qquad \text{with } \omega_k^2 = k^2 + m^2\,. \tag{1.52}$$

This means that, in an expanding Universe, as the field evolves, the background space-time itself varies. However, due to the equivalence principle, if we consider small scales and short intervals of time [7], we expect the solution to reproduce the behaviour in the flat Minkowski space-time (which are of the plane wave form), since we can locally approximate our space-time to the flat one (see e.g. [20]). Therefore, we require

$$u_k(\eta) \overset{k\gg aH}{\longrightarrow} \frac{e^{-i\omega_k t}}{\sqrt{2k}}\,. \tag{1.53}$$

[7] Here, with short we mean much shorter than the characteristic expansion time.

This is called *Bunch-Davies vacuum choice*: for a scalar field on a curved space-time we demand that the flat case is restored on very small scales.

Therefore, after some algebra, one obtains

$$u_k'' + \left[k^2 - \frac{a''}{a} + a^2 \frac{\partial^2 V}{\partial \varphi^2}\right] u_k = 0\,. \tag{1.54}$$

Let us solve this equation by considering the de-Sitter stage ($H \simeq const$) and a massless scalar field, which simplifies the previous expression since the term $m_\varphi^2 = \partial^2 V/\partial\varphi^2$ corresponds to the effective mass of the inflaton. Since H is almost constant,

$$d\eta = \frac{dt}{a} = dt\, e^{-Ht} \quad \Longrightarrow \quad \eta = -\frac{1}{aH} \tag{1.55}$$

and then, the term a''/a in Eq. (1.54) becomes $a''/a = 2/\eta^2 = 2r_{\rm H}^2$. So it is possible to distinguish two regimes:

SUB-HORIZON REGIME: the comoving wavelength k^{-1} of the fluctuation is smaller than $r_{\rm H}$. Then,

$$k \gg aH \quad \Longrightarrow \quad u_k'' + k^2 u_k = 0\,, \tag{1.56}$$

i.e., the final equation is a simple harmonic oscillator equation, whose solution takes the form

$$u_k(\eta) = \frac{e^{-ik\eta}}{\sqrt{2k}}\,. \tag{1.57}$$

This result is not surprising, since in the small scale limit one should reproduce the behaviour of the solution in the flat spacetime, which takes the plane wave form.

SUPER-HORIZON REGIME: the comoving wavelength k^{-1} exits the horizon,

$$k \ll aH \quad \Longrightarrow \quad u_k'' - \frac{a''}{a} u_k = 0\,. \tag{1.58}$$

This is a second order differential equation whose solution corresponds to a combination of a growing and decaying mode,

$$u_k(\eta) = B(k) a(\eta) + C(k) a^{-2}(\eta)\,, \tag{1.59}$$

and since the decaying mode becomes negligible very quickly, the interesting mode is the growing one. In particular, one can fix the initial amplitude by matching the amplitude of the plane wave solution with the solution Eq. (1.59) at the time in which the mode k leaves the horizon [47],

$$|B(k)|a(\eta) = \left|\frac{e^{-ik\eta}}{\sqrt{2k}}\right| = \left.\frac{1}{\sqrt{2k}}\right|_{k=aH} \quad \Longrightarrow \quad |\delta\varphi(\mathbf{k})| = |B(k)| = \frac{H}{\sqrt{2k^3}}\,. \tag{1.60}$$

In conclusion, in the super-horizon regime, the scalar fluctuations remain constant, frozen at the constant value in Eq. (1.60).

1.5.1 Power spectrum of cosmological perturbations

A very important challenge of cosmology is to understand how to characterize the distribution of the CMB and the large-scale structure, so that the theory can be compared to experiments. To make quantitative tests of cosmological models, it is often useful to take the Fourier transform of the distributions. The most important statistic in the case of both CMB and large-scale structure is the two-point function, called *power spectrum* in Fourier space [19]. It represents a statistical tool to quantify the amplitude of cosmological perturbations generated from inflation. From Eq. (1.36), let us recall that the vacuum expectation value of the fluctuations is zero. However, in general $\langle \delta\varphi^2 \rangle \neq 0$. Moreover, assuming that the fields are described by a Gaussian statistics, they are completely described by their mean value, zero in this case, and the covariance, that is the two-point correlation function. The latter is defined as

$$\langle \delta(\mathbf{x}+\mathbf{r})\delta(\mathbf{x}) \rangle \equiv \xi(r)\,, \tag{1.61}$$

where angle brackets denote the ensemble average over the whole distribution and δ the generic perturbation field. Due to isotropy and homogeneity hypothesis, ξ is a function only of the modulus of $\mathbf{r}$. Expanding the field in Fourier space,

$$\delta(\mathbf{x}) = \frac{1}{(2\pi)^3} \int d^3k e^{i\mathbf{k}\cdot\mathbf{x}} \delta(\mathbf{k})\,, \tag{1.62}$$

the power spectrum of $\delta(\mathbf{x})$ is defined as the Fourier transform of the two-point correlation function in the real space,

$$\langle \delta(\mathbf{k})\delta(\mathbf{k}') \rangle = (2\pi)^3 \delta^{(3)}(\mathbf{k}+\mathbf{k}') P(k)\,. \tag{1.63}$$

Notice that the power spectrum $P(k)$ is a function of the modulus of the momentum because of the isotropy of the background, while the presence of the Dirac delta ensures the homogeneity, constraining $\mathbf{k} = \mathbf{k}'$.

It is also possible to define the *dimensionless power spectrum* as [47]

$$\Delta^2_\delta(k) = \frac{k^3}{2\pi^2} P(k) \tag{1.64}$$

and then another interesting statistical quantity is the *variance*, defined as

$$\langle \delta(\mathbf{x})^2 \rangle = \int_0^\infty \frac{dk}{k}\, \Delta^2(k)\,. \tag{1.65}$$

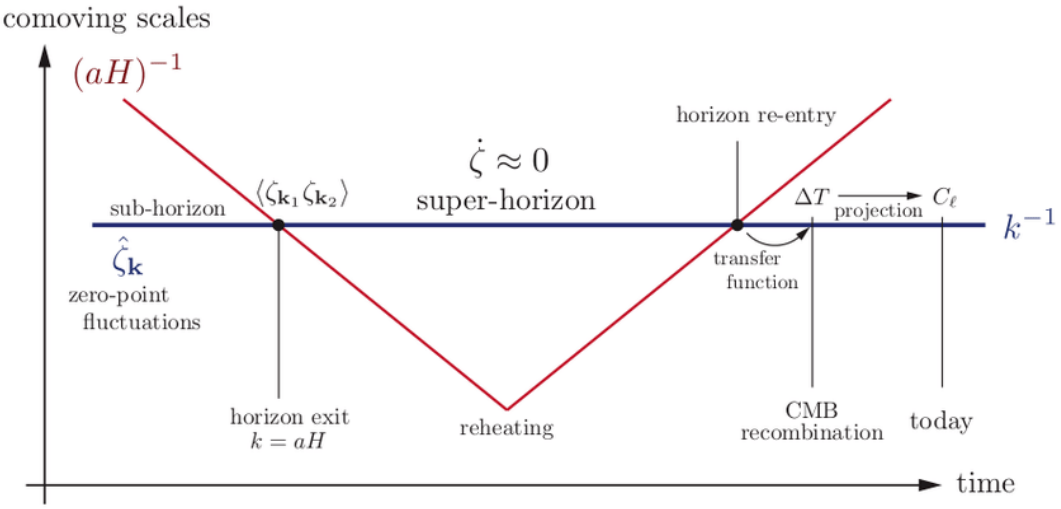

Figure 1.3: Evolution of curvature perturbations during and after inflation [30].

In order to better study the shape of the power spectrum $\Delta(k)$, it is customary to introduce the *spectral index* $n_{\rm s}$, defined as

$$n_{\rm s} - 1 \equiv \frac{d \ln \Delta^2(k)}{d \ln k} \,. \tag{1.66}$$

Here, the subscript s stands for scalar, since $n_{\rm s}$ is usually used for primordial density fluctuations which are classified as scalar perturbations. If $n_{\rm s}$ is constant, which means it does not depend on k, the power spectrum is simply a power law

$$\Delta^2(k) = \Delta^2(k_0) \left(\frac{k}{k_0} \right)^{n_{\rm s}-1} \,, \tag{1.67}$$

where k_0 indicates a common pivot scale (e.g., $k_0 = 0.002$ Mpc^{-1} was the one used by WMAP [48, 49], while $k_0 = 0.05$ Mpc^{-1} the one used by Planck [36]). In particular, if $n_{\rm s} = 1$, the power spectrum is the so-called *Harrison-Zel'dovič spectrum* and it does not depend on k: this means that the amplitude of the perturbation is the same for each cosmological scale. The actual bound on the spectral index of scalar perturbations is $n_{\rm s} = 0.9649 \pm 0.0042$ at 68 % CL [36].

To conclude, let us briefly mention that it is possible to make use of the so-called δN *formalism* in order to understand how quantum fluctuations $\delta\varphi$ in an expanding Universe give rise to primordial energy density perturbation $\delta\rho/\rho$. It can be shown that every region in the Universe, on large scale, experience the same history but at slightly different times. Thus, it turns out to be [30]

$$\zeta = \delta N = -H \frac{\delta\varphi}{\dot{\varphi}} \simeq -H \frac{\delta\rho}{\dot{\rho}} \,. \tag{1.68}$$

Since $\zeta \simeq const$ on super-horizon scales (see Fig. 1.3), it can be easily proved that the inhomogeneities generated by quantum fluctuations $\delta\varphi$ generate anisotropies $\delta T/T$ in the CMB. Basing on previous relation, it is possible to determine an expression for the power spectrum for the curvature perturbations, which results

$$\Delta_\zeta(k) \simeq \frac{H^2}{\dot{\varphi}^2}\Delta_{\delta\varphi}(k)\bigg|_{t_{\rm H}(k)} = \left(\frac{H^2}{2\pi\dot{\varphi}}\right)^2\bigg|_{t_{\rm H}(k)}, \tag{1.69}$$

where $t_{\rm H}(k)$ indicates the time at which the mode k exits the horizon. On super-horizon scales and to lowest order in the slow-roll parameters, the inflaton fluctuations amplitude is given by [30, 47]

$$|\delta\varphi_k| = \frac{H}{\sqrt{2k^3}}\left(\frac{k}{aH}\right)^{\frac{3}{2}-\nu}, \tag{1.70}$$

where it has been defined $\nu \simeq 3/2 + 3\epsilon - \eta$. Therefore,

$$\Delta_{\delta\varphi}(k) = \frac{k^3}{2\pi^2}|\delta\varphi_k|^2 = \left(\frac{H}{2\pi}\right)^2\left(\frac{k}{aH}\right)^{3-2\nu}. \tag{1.71}$$

and this allows to compute the spectral index at the lowest order,

$$n_{\rm s} - 1 = \frac{d\ln\Delta^2_\zeta(k)}{d\ln k} = 3 - 2\nu = 2\eta - 6\epsilon\,. \tag{1.72}$$

It is worth pointing out that inflation also generates primordial GWs and therefore, it is possible to define the tensor power spectrum similarly to the scalars (for more details see Section 4.2.

1.5.2 Bispectrum of cosmological perturbations

It is known that observations are compatible with a scale invariant spectrum of adiabatic perturbations characterized by an almost Gaussian statistics [47, 50–53]. The primordial power spectrum is basically insensitive to the interactions that affected the inflaton. However, *non-Gaussianity* of the primordial perturbations, which means deviations from a pure Gaussian statistics, arises from interactions of the field driving inflation and thus, it contains important information about the physics at early time. Detecting primordial non-Gaussianity would be one the most powerful probe of the physics during inflation [47, 54–57].

In the single-field slow-roll inflation as described before, the perturbations are very close to be Gaussian. However, models which deviate from this minimal configuration contemplate the possibility of generating an amount of non-Gaussianity detectable by measuring higher order correlators (see e.g. [54, 55]). If observed, deviations from a purely Gaussian statistics of density perturbations could provide important constraints on models

describing the early times, leading to a departure from the simplest picture.

In order to evaluate the amount of non-Gaussianity, one can look at the predictions of the *bispectrum*, which is the Fourier transform of the three-point correlation function of the primordial perturbations generated during inflation, given that it would vanish in the Gaussian case. A perturbation with a Gaussian statistics is completely defined by its two-point correlation function: the expression for the even-point correlators can be rewritten in terms of the two-point correlator, while all the odd-point correlation functions are vanishing [58]. If the fluctuations are not Gaussian, then higher-order correlation functions are necessary in order to determine the statistical properties. Moreover, since the CMB seems to be rather Gaussian, this means that the non-Gaussian component must be rather small [59, 60].

Primordial Bispectrum Deviations from Gaussianity in the initial fluctuations are most easily measured through their effect on the bispectrum, the Fourier transform of the three-point correlation function. The adjective *primordial* is related to considering the non-Gaussianity, which means non-linearity, in the primordial curvature perturbation ζ generated in the very early stages of the Universe. Denoting $\zeta(\mathbf{k})$ the density fluctuation in Fourier space, the three-point correlation function is defined as

$$\langle \zeta(\mathbf{k}_1)\zeta(\mathbf{k}_2)\zeta(\mathbf{k}_3)\rangle = (2\pi)^3\delta^{(3)}(\mathbf{k}_1+\mathbf{k}_2+\mathbf{k}_3)B_\zeta(k_1,k_2,k_3)\,. \tag{1.73}$$

Here, the Dirac delta reflects the translation invariance, while $B_\zeta(k_1,k_2,k_3)$ represents the bispectrum. A measure of the amplitude of the bispectrum is typically given in terms of the non-linearity parameter $f_{\rm NL}$. The functional form and shape of the bispectrum are model dependent and, therefore, provides constraints on different inflationary scenarios through the predictions of the corresponding amplitude parameters $f_{\rm NL}$.

By homogeneity and isotropy, the bispectrum is a function of the norm of the spatial momenta $\mathbf{k}_1$, $\mathbf{k}_2$, $\mathbf{k}_3$, which combine to form a closed triangle [53, 59]. Generally, bispectra are most easily visualized according to the contributions in three distinct shapes [47, 55, 56, 61–63]:

EQUILATERAL: $k_1 \simeq k_2 \simeq k_3 = k$

FOLDED: $k_3 \simeq k_1 + k_2$

SQUEEZED: $k_3 \ll k_1 \simeq k_2$

Another considered shape is the *orthogonal* one, called in this way since this shape of non-Gaussianity is orthogonal to both the local and equilateral types [64, 65].

Among the models that predict sizable non-Gaussianity, a first model of primordial non-Gaussianity which is often considered in the literature is the so-called *local model*,

characterized by the following ansatz in real space [66]

$$\zeta(\mathbf{x}) = \zeta_{\rm g}(\mathbf{x}) + \frac{3}{5} f_{\rm NL}^{\rm loc}\left[\zeta_{\rm g}^2(\mathbf{x}) - \langle\zeta_g^2(\mathbf{x})\rangle\right] . \tag{1.74}$$

This is the simplest weakly non-linear coupling case: the curvature perturbation is a non-linear function, local in real space, of a Gaussian perturbation $\zeta_{\rm g}$. The coefficient 3/5 is due to the fact that at linear order during the matter-dominated epoch and on large scale $\zeta = (5/3)\varphi$. In local non-Gaussianity model, the bispectrum takes the form [67]

$$B_\zeta^{\rm loc}(k_1, k_2, k_3) = -\frac{6}{5} f_{\rm NL}^{\rm loc}[P_\zeta(k_1)P_\zeta(k_2) + P_\zeta(k_2)P_\zeta(k_3) + P_\zeta(k_1)P_\zeta(k_3)] , \tag{1.75}$$

where P_ζ is the scalar primordial power spectrum. The signal of the local non-Gaussianities peaks, which means that the bispectrum is then largest, in the so-called *squezeed configuration* of the triangle (namely when one wavenumber in Fourier space is much smaller than the other two involved in the bispectrum) and it can arise, for instance, in the case of multi-fields models of inflation [47, 53, 55].

Squeezed limit In the limit in which one of the sides of the triangle, for instance $\mathbf{k}_3$, goes to zero, the other two modes become equal and opposite ($\mathbf{k}_1 \simeq -\mathbf{k}_2$), due to momentum conservation, and the triangle becomes *squeezed*. In general, k_3 is referred to as the long mode $k_{\rm L}$, while $k_1 \simeq k_2 = k_{\rm s}$ as the short modes. In this limit, if ζ is characterized by an almost scale-invariant power spectrum, $P(k) \propto k^{-3}$ (see Eq. (1.64)), the first term in the square brackets of Eq. (1.75) is sub-dominant with respect to the other two and so

$$\lim_{\mathbf{k}_3 \longrightarrow 0} B_\zeta^{\rm loc}(k_1, k_2, k_3) \simeq -\frac{12}{5} f_{\rm NL}^{\rm loc} P(k_1)P(k_3) . \tag{1.76}$$

Therefore,

$$\lim_{\mathbf{k}_3 \longrightarrow 0} \langle\zeta_{\mathbf{k}_1}\zeta_{\mathbf{k}_2}\zeta_{\mathbf{k}_3}\rangle \simeq (2\pi)^3\delta^3(\mathbf{k}_1 + \mathbf{k}_2 + \mathbf{k}_3)\frac{12}{5} f_{\rm NL}^{\rm loc} P(k_1)P(k_3) . \tag{1.77}$$

Following [51, 68], it results that the three-point function is proportional to the two-point function of the long wavelength modes multiplied by the two point function of the short wavelength mode times its deviation from scale invariance, that is

$$\lim_{\mathbf{k}_3 \longrightarrow 0} \langle\zeta_{\mathbf{k}_1}\zeta_{\mathbf{k}_2}\zeta_{\mathbf{k}_3}\rangle \simeq -(2\pi)^3\delta^{(3)}(\mathbf{k}_1 + \mathbf{k}_2 + \mathbf{k}_3)(n_{\rm s} - 1)P_\zeta(k_3)P_\zeta(k_1) . \tag{1.78}$$

Indeed, comparing Eq. (1.78) with Eq. (1.77), one can notice that $f_{\rm NL}^{\rm loc} \simeq n_{\rm s} - 1$. This implies that these models predict very small local non-Gaussianity. The most stringent constraints on the primordial non-Gaussianity parameters $f_{\rm NL}$ come from *Planck* measurements of the CMB, combining temperature and polarization analysis [69]. The obtained

results are $f_{\rm NL}^{\rm loc} = -0.9 \pm 5.1$, $f_{\rm NL}^{\rm equil} = -26 \pm 47$ and $f_{\rm NL}^{\rm ortho} = -38 \pm 24$ (at 68% CL). Let us emphasize that, if a large local non-Gaussian component in the bispectrum were detected, this could exclude single field inflation models [68]. In this sense, local non-Gaussianity can be used to distinguish between different inflationary models.

Chapter 2

The Cosmic Microwave Background

The Cosmic Microwave Background (CMB) is the electromagnetic radiation permeating the space, coming from the early stages of the Universe. It contains a large amount of physical information and it is a fundamental source of data about the early time, since it is the oldest electromagnetic radiation, dating to the epoch of the recombination (about 370000 years after the Big Bang, corresponding to a redshift $z \simeq 1100$). The CMB was first predicted by Gamow, Alpher and Herman in 1948 [28, 70], while the first detection of the CMB dates back to 1965, thanks to Penzias and Wilson [15], who detected it by chance as they were conducting some experiments about radio astronomy and satellite communications. This marked a fundamental turning point in modern cosmology, definitely growing the interest in the field of the origins and evolution of the Universe. Later, Harrison, Peebles, Yu and Zel'dovich realized that the early Universe had inhomogeneities at the level of 10^{-5} [71–73]. Starting from the 80s, increasingly stringent limits on the anisotropy of the CMB were set from experiments. In particular, a first precise measurement of the CMB spectrum was given by the COBE satellite [31, 74], launched in 1989. It revealed that such spectrum corresponds to a blackbody thermal spectrum at the temperature of nearly $T_0 \simeq 2.725$, with temperature fluctuations at the level of the order 10^{-5} [1, 2, 31, 75]. Anisotropies in the temperature of the CMB radiation are a powerful tool to measure cosmological parameters, but also to get information on the formation of structures in the Universe. For that reason, these anisotropies have been the target of many space and ground-based missions over the last fifty years.

The Big Bang model predicts a Universe initially very hot and dense which then cooled down, due to its expansion. In the pre-recombination era, photons were coupled to electrons and protons, strongly interacting forming the ionized plasma. All together described a single fluid, the so-called *baryon-photon* fluid [19, 76]. The early Universe was sufficiently hot for all the matter in it to be completely ionized. Under these conditions, the photons were scattered very efficiently by matter such that they could not travel very far without interacting with matter, coupling to it. This kept the Universe in a state of thermal

equilibrium and the Universe could be considered practically opaque to radiation [19, 76]. However, during the expansion of the Universe its thermal energy decreased, which means that the radiation gradually became less energetic until the photons were no longer able to ionize neutral atoms. In particular, when the temperature went down the boundary energy of Hydrogen (13.6 eV), the electrons could interact with the protons through the following interaction,

$$p + e^- \longrightarrow H + \gamma\,,$$

and then the first atoms of Hydrogen were created. This corresponds to the moment of the recombination. Then, the photons decoupled by the rest of the components of the Universe (their interaction rate became lower than the rate of the expansion of the Universe) and they were free to travel, suffering only the effects of the cosmological redshift. These photons travelled to us until today and constitute the Cosmic Microwave Background radiation with its observed anisotropies. This radiation appears to come from a spherical surface around the observer such that the radius of the shell is the distance each photon has travelled since it was last scattered at the epoch of recombination. This surface is what is called *last scattering surface*.

In this Chapter, after a brief reference to the discovery and detection of the CMB, we will go through the main features of the CMB, by studying the formation and characterization of the anisotropies and presenting its angular power spectrum. This will allow us to compute the cross-correlation signal between the CMB temperature anisotropies and the μ-distortion (in Chapter 3).

2.1 Detection of the CMB

After the discovery of the CMB, deviations from the blackbody shape and isotropy became the next target for both theorists and observers. These deviations are referred to as spectral distortion and anisotropies, respectively. Gravitational redshift (Sachs and Wolfe in 1967 [77]) and diffusion damping (Silk in 1968 [78]) were some proposed processes to generate anisotropies, while a discussion of the evolution of density perturbations through the treatment of acoustic oscillations of the photon-baryon fluid was given by Peebles and Yu (1970) [72] and by Zeldovich and Sunyaev (1970) [79, 80]. Furthermore, studies about the thermal history of the Universe and their consequences on CMB were carried out by Sunyaev and Zeldovich [79, 81–83]. These are just some of the pioneering works.

However, since these theoretical predictions were far beyond the reach of any experiment already running at that time, the *Cosmic Background Explorer* (COBE) satellite was proposed in 1974 and it represented an important step for CMB research. The COBE satellite was developed by NASA to measure the diffuse infrared and microwave radiation from the early Universe. It was launched in 1989 and carried three instruments, the *Diffuse*

Infrared Background Experiment (DIRBE) to search for the cosmic infrared background radiation, the *Differential Microwave Radiometer* (DMR) to map the angular distance of cosmic microwave radiation and the *Far Infrared Absolute Spectrophotometer* (FIRAS) to compare the spectrum of the CMB radiation with a precise reference blackbody. Thanks to COBE, for the first time the CMB was found to have intrinsic anisotropies [31], at a level of a part in 10^5 and to have a nearly perfect blackbody spectrum with a temperature of 2.725 ± 0.002 K. In particular, the measure of the degree of isotropy of the radiation was possible thanks to the DMR instrument, which achieved an angular resolution of 7°, corresponding to an order of multipole $\ell \simeq 30$. Thus, COBE measured the dipole anisotropy due to the Earth's motion with respect to the reference frame of the radiation. In addition, thanks to FIRAS, COBE gave a stringent constraint on the spectral distortions [1, 2, 4]. This observation is remarkably in agreement with the predictions of the hot Big Bang theory.

In 2001, NASA launched a second CMB space mission, that was the *Wilkinson Microwave Anisotropy Probe* (WMAP) mission, in order to make much more precise measurements of the large scale anisotropies over the full-sky. It achieved a much greater angular resolution than COBE, reaching $\ell \simeq 1000$, leading to a large amount a of information on small-scale anisotropies of radiation [49, 84]. Afterwards, the ESA *Planck* mission (launched in 2009) has exceeded this result further, leading to an angular resolution of $\ell \gtrsim 2000$, increasing also the sensitivity of the measurements and the number of frequencies observed. The *Planck* team submitted a series of papers about the results, starting from 2013 [85, 86].

2.2 Anisotropies in the CMB

The purpose of this Section is to review the underlying physical mechanisms behind theoretical predictions of the anisotropy. The fluctuations in the total density of matter are responsible for the formation of CMB anisotropies and create gravitational potential wells, which can grow due to instability until forming the structures on large scales.

Before the recombination epoch, the Compoton scattering between photons and electrons and Coulomb interaction between electrons and protons strongly couple the photons to the baryons, establishing a photon-baryon fluid. While regions of overdensity gravitationally attracts matter towards it, the heat of photon-matter interactions creates a large amount of outward pressure. Photon pressure resists compression of the fluid by gravitational infall, setting up oscillations, analogous to sound waves created in air by pressure differences. [76]. These fluctuations in the density of the visible baryonic matter are called *acoustic oscillations*. Physically these oscillations are compressions and rarefactions of the fluid, which therefore involve the local heating and cooling. These differences in temper-

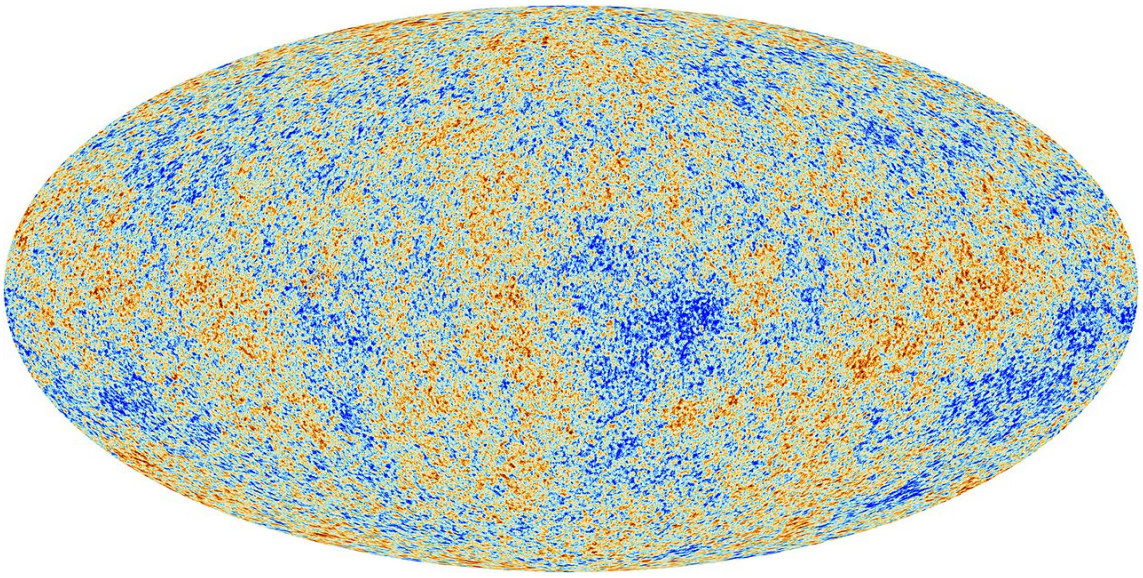

Figure 2.1: The anisotropies map of the Cosmic Microwave Background as observed by Planck, [85].

ature and density represent the anisotropies. Regions of compression represent hot spots, while rarefaction regions represent cold spots (see Fig. 2.1): thus, there will be a harmonic series of peaks in wavelength associated to the acoustic oscillations (see Fig. 2.2). The features of these peaks provide us with a series of cosmological tests.

During the recombination epoch, the Universe cooled rapidly as free electrons were captured by atomic nuclei and it became transparent: the amount of photon scattering decreased dramatically. Scattering less, photons could travel, diffuse, much greater distances. This caused the temperatures and densities of the hot and cold regions to be averaged and the Universe became less anisotropic. This reduction in anisotropy is the *diffusion damping*. The latter is also called Silk damping, from the name of who first studied this effect, J. Silk [78]. Thus, diffusion damping adiabatically damps temperature and density anisotropies in the early Universe, resulting in decline of the amplitude of acoustic waves. Two fundamental quantities that can be defined, which will be useful for our discussion, are the *diffusion length* and the *diffusion damping scale* or *effective diffusion scale*. The diffusion length relates how far photons travel during diffusion and includes a finite number of short steps in random directions. The effective diffusion scale represents the thickness of the last scattering surface providing a cut off in the anisotropy spectrum [76].

First we evaluate the diffusion length. Consider the path of a single photon as it scatters off a sea of electrons. It travels a mean comoving distance $\lambda_{\rm C}$ in between each scatter. In our case this distance is $(n_{\rm e}\sigma_{\rm T}a)^{-1} = -1/\tau'$, where τ is the optical depth, defined as

$$\tau(\eta) = \int_{\eta}^{\eta_0} d\eta'\, n_{\rm e}\sigma_{\rm T}a\,, \tag{2.1}$$

where $\sigma_{\rm T}$ is the Thomson cross section, $n_{\rm e}$ is the electron number density and η indicates the conformal time [19, 76, 78]. If the density $n_{\rm e}$ of electrons is very large, then the mean free path is small. During a Hubble time, H^{-1}, a photon scatters of order $n_{\rm e}\sigma_{\rm T}H^{-1}$ times, performing a random walk. The total distance traveled in the course of a random walk is the mean free path times the square root of the total number of steps. Thus, in a Hubble time, a cosmological photon moves a mean comoving distance equal to

$$\lambda_{\rm D} \simeq \lambda_{\rm C}\sqrt{n_{\rm e}\sigma_{\rm T}H^{-1}}\,. \tag{2.2}$$

Any perturbation on scales smaller than $\lambda_{\rm D}$ can be expected to be washed out, because the many photons diffusing over a region of order $\lambda_{\rm D}$ will have restored the region to a single mean temperature [19]. Notice that we have been implicitly assuming that nothing happens to the photons while traveling from the last-scattering surface to Earth. However, while gravitational potentials are constant deep in matter domination, they evolve right after recombination (due to the presence of radiation) and at late times (due to dark energy), producing additional perturbations to the photons [19].

The second quantity is the damping scale $k_{\rm D}(z)$, defined as

$$\frac{1}{k_{\rm D}^2(\eta)} \equiv \int_0^\eta \frac{d\eta'}{6(1+R)n_{\rm e}\sigma_{\rm T}a(\eta')}\left[\frac{R^2}{(1+R)}+\frac{16}{15}\right], \tag{2.3}$$

with $R \equiv 3\rho_{\rm B}/4\rho_\gamma \ll 1$. Here, ρ_B is the baryon energy density and ρ_γ the photon energy density. In particular, since this scale is sensitive to the baryon content and the thermal history while being almost entirely independent of the model for structure formation, it provides a valuable tool for measuring these cosmological quantities.

Another effects that has to be considered to accurately describe the CMB spectrum is the *Sachs-Wolfe effect* (SW) [77]. After the decoupling and before they freely propagate in the Universe, the photons need to climb out of the potentials on the last scattering surface. This generates gravitational redshifts which stretch the wavelength of the photons. In addition, also the *Doppler effect* has to be considered in order to account for the relative motion of the fluid with respect to the observer. Moreover, another effect is the *Integrated Sachs-Wolfe effect* (ISW), which takes into account the variation of the energy of the photons freely propagating in the Universe, after interacting with the gravitational potentials. The main difference between the SW and the ISW effect is that the SW effect is imprinted at the last scattering, while the ISW during the propagation and then, in this case, it is necessary to evaluate the time-evolution of the gravitational potentials for the whole path from last scattering to us. This effect can be understood as follows. Let us consider a photon which propagates in the Universe at a given frequency. At some point, it enters in a potential well between the last scattering surface and the observer, being gravitationally blueshifted. As it climbs out the potential, one should expect that the final and the initial

frequency are equal. However, if the depth of the potential well changes as the photons cross it, the blueshift from falling in and the redshift from climbing out no longer cancel, leading to a residual temperature shift and thus inducing further anisotropies in the CMB. Since the overall effect is obtained by integrating the variation of gravitational potential over the line of sight, this is why it is referred to as *integrated* SW [77, 87].

The CMB anisotropies are essentially divided into two types, called, respectively, *primary* and *secondary* anisotropies [76]. In general, the primary fluctuations are imprinted on the surface of the last scattering and they reflect density inhomogeneities which are the seeds for the evolution of the large-scale structures; they are originated by random quantum fluctuations in the very early Universe. Secondary fluctuations are due to the interaction of CMB photons with hot gas (e.g. Sunyaev-Zel'dovich effect [82] or Ostriker-Vishniac effect [88, 89]) or gravitational potential (e.g. integrated Sachs-Wolfe effect [77] or Rees-Sciama effect [90]), travelling from the surface of the last scattering to the nearby Universe (the observer). Among all these secondary anisotropies, the dominant effect is the Sunyaev-Zel'dovich (SZ) effect, which represents the inverse Compton scattering of the CMB photons by the free electrons of the ionized and hot intra-cluster gas. There are two types of SZ effect: the *thermal* and *kinetic* effects. The most interesting effect for applications in astrophysics is the thermal effect, able to provide information on the clusters that cause it. The thermal SZ (TSZ) effect has an amplitude characterized by the Compton parameter y (see Chapter 3) and depends on the cluster electron temperature and density distribution. The inverse Compton effect causes a shift in the spectrum, such as there is a lowering of the temperature of the photons when observed at low frequencies or an increasing when observed at high frequencies. When the galaxy cluster moves with respect to the CMB rest frame with a specific peculiar radial velocity, the Doppler shift induces an additional effect called the kinetic SZ (KSZ) effect (for more details, see e.g. [19, 76]).

The CMB anisotropies must be analyzed statistically. For Gaussian fluctuations, the statistical content is embedded in the the two-point correlation function, C_ℓ. It is possible to obtain predictions for C_ℓ by tracking the evolution of temperature fluctuations [76]. In the following Section we will see how to compute the C_ℓ.

2.3 Angular Power Spectrum

In order to compare theoretical predictions of CMB temperature anisotropies with observational data, it is convenient to evaluate them as a function of frequency and direction on the celestial sphere $\hat{\mathbf{n}}$. Moreover, as already pointed out, the spectrum of the radiation is close to a black body spectrum with a temperature almost constant on the plane of the sky [1]. This spectrum is generally described in terms of the fluctuations of the temperature

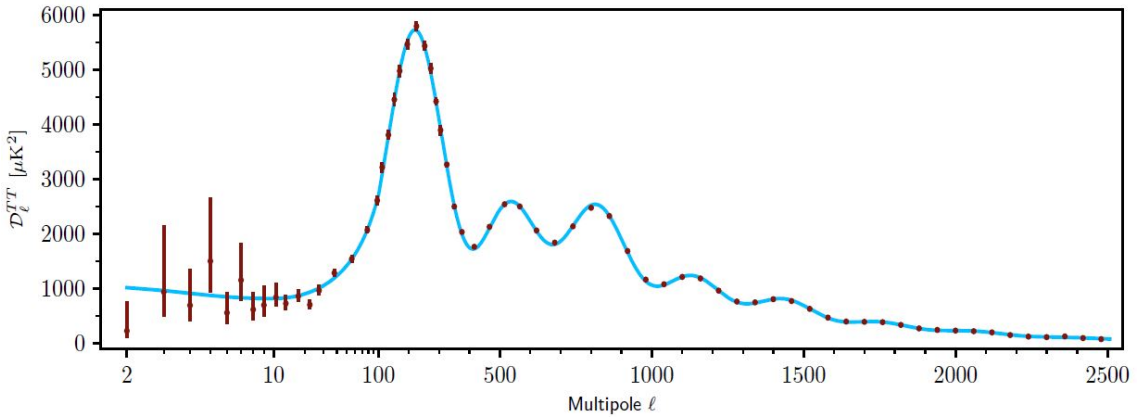

Figure 2.2: The latest plot for the temperature multipoles power spectrum, edit from [29]. Here, it is plotted $D_\ell^{TT} = \ell(\ell+1)C_\ell/(2\pi)$ and not exactly C_ℓ. This is because for large scale, corresponding to small values of ℓ, the dominant effect is the so called Sachs-Wolfe effect, which predicts $\ell(\ell+1)C_\ell \simeq const$ for small multipoles.

[19]

$$T(\mathbf{x}, \hat{\mathbf{n}}, \eta) = T(\eta)\left[1 + \frac{\Delta T}{T}(\mathbf{x}, \hat{\mathbf{n}}, \eta)\right], \tag{2.4}$$

where $\hat{\mathbf{n}}$ is the direction of the incoming photons, $T(\mathbf{x}, \hat{\mathbf{n}}, \eta)$ represents the local value of the temperature and $T(\eta)$ the mean value. Notice that, even if in principle the previous expression is defined in all points of space and time, it is possible to observe the temperature field in the present, i.e., for $\mathbf{x}_0$ and η_0, then all that remains is to change the direction of observation $\hat{\mathbf{n}}$ in order to observe variations of the radiation, and therefore anisotropies.

In general the temperature fluctuations are labelled as

$$\frac{\Delta T}{T}(\mathbf{x}, \hat{\mathbf{n}}) = \Theta(\mathbf{x}, , \hat{\mathbf{n}})\,. \tag{2.5}$$

In order to describe the anisotropy of the CMB, let us remember that the surface of last scattering appears as a spherical surface at a redshift $z \simeq 1100$. For this reason, a natural parameterization for the temperaure anisotropies is expanding them into spherical harmonics $Y_{\ell m}$ as follows

$$\Theta(\theta, \phi) = \sum_{\ell=0}^{\infty} \sum_{m=-\ell}^{\ell} a_{\ell m} Y_{\ell m}(\theta, \phi)\,, \tag{2.6}$$

where θ, ϕ are the polar coordinates corresponding to the temperature spots in the sky and $a_{\ell m}$ are the space-time dependent amplitude. To relate these coefficients with the temperature anisotropies, let us take advantage of the orthogonality property of the spherical harmonics,

$$\int d\Omega\, Y_{\ell m}(\hat{\mathbf{n}}) Y^*_{\ell' m'}(\hat{\mathbf{n}}) = \delta_{\ell m}\delta_{\ell' m'}\,, \tag{2.7}$$

where $d\Omega = \sin\theta d\theta d\phi$ is the infinitesimal solid angle spanned by $\hat{\mathbf{n}}$. Hence, Eq. (2.6) can be rewritten multiplying both sides by $Y^*_{\ell' m'}(\hat{\mathbf{n}})$ and indeed integrating, getting

$$a_{\ell m} = \int \frac{d^3k}{(2\pi)^3} e^{i\mathbf{k}\cdot\mathbf{x}} \int d\Omega\, Y^*_{\ell m}(\hat{\mathbf{n}}) \Theta(\mathbf{k}\,, \hat{\mathbf{n}}, \eta), \tag{2.8}$$

where it has been considered the Fourier transform of the temperature perturbation,

$$\Theta(\mathbf{x}, \hat{\mathbf{n}}) = \int \frac{d^3k}{(2\pi)^3} e^{i\mathbf{k}\cdot\mathbf{x}} \Theta(\mathbf{k}, \hat{\mathbf{n}})\,. \tag{2.9}$$

Being the temperature field statistically isotropic, the mean value of all the $a_{\ell m}$ will be zero, but this will not be true for the variance. Therefore, supposing the Gaussianity of the fuctuations,

$$\langle a_{\ell m} a^*_{\ell' m'} \rangle = \delta_{\ell \ell'} \delta_{m m'} C_\ell\,. \tag{2.10}$$

It is interesting to make some observations. First of all, note that, for a given ℓ, all the coefficients $a_{\ell m}$ have the same variance, due to rotation invariance of CMB (isotropy). Secondly, note that for each ℓ there are $2\ell + 1$ values of $a_{\ell m}$: this suggests that for small values of ℓ one will get little information about C_ℓ and vice versa for great values, with the variance that will be known with a little uncertainty [19]. In addition, there is an intrinsic uncertainty that limits the precision with which it is possible to know the variance of this distribution, called *cosmic variance*. The latter is defined as

$$\left(\frac{\Delta C_\ell}{C_\ell} \right)_{\text{c.v.}} = \sqrt{\frac{2}{2\ell + 1}}\,, \tag{2.11}$$

and it is nothing more than the uncertainty scaling as the inverse of the square root of the number of possible samples. The effect of cosmic variance is visible in Fig. 2.2, where one can notice that the error bars become larger when considering small values of ℓ.

From Eq. (2.10) it is possible to understand the meaning of C_ℓ, which represents the quadratic mean of the coefficients $a_{\ell m}$ for a given ℓ. The C_ℓ plotted as a function of the order of multipole ℓ is precisely the power spectrum, useful for characterizing the amplitude of inhomogeneities.

In order to clarify its role of the power spectrum, an expression for C_ℓ in terms of Θ_ℓ will be derived in the following. Referring to Eq. (2.8) and Eq. (2.10), let us take the expected value of the distribution. Keeping the η dependence implicit, one obtains [19]

$$\langle \Theta(\mathbf{k}, \hat{\mathbf{n}}) \Theta(\mathbf{k}', \hat{\mathbf{n}}') \rangle = (2\pi)^{(3)} \delta^3(\mathbf{k} - \mathbf{k}') P(k) \frac{\Theta(k, \hat{\mathbf{k}} \cdot \hat{\mathbf{n}})}{\delta(k)} \frac{\Theta^*(k, \hat{\mathbf{k}} \cdot \hat{\mathbf{n}})}{\delta^*(k)}\,, \tag{2.12}$$

where $P(k)$ is the power spectrum of matter, $\delta(k)$ is the density variation of dark matter, and we used Eq. (1.63) [1]. At this point, expanding the temperature fluctuations into spherical harmonics, writing them in terms of Legendre polynomials and by exploiting the orthonormality property of the spherical harmonics, the final result turns out to be [19]

$$C_\ell = \frac{2}{\pi}\int_0^\infty dk\, k^2 P(k)\left|\frac{\Theta_\ell(k)}{\delta(k)}\right|^2 . \tag{2.13}$$

Thus, for a given ℓ, the C_ℓ are the integral over all Fourier modes of the variance of Θ_ℓ. Solving the Boltzmann equation for all the modes Θ_ℓ, it is possible to plot the anisotropy spectrum today, reported Fig. 2.2.

For the purposes of this Thesis, let us calculate the C_ℓ as follows. Let us consider the following expressions,

$$e^{i\mathbf{k}\cdot\mathbf{x}} = \sum_\ell (2\ell+1) i^\ell P_\ell(\hat{\mathbf{k}}\cdot\hat{\mathbf{x}}) j_\ell(kx) \tag{2.14a}$$

$$P_\ell(\hat{\mathbf{k}}\cdot\hat{\mathbf{x}}) = \frac{4\pi}{2\ell+1}\sum_{m=-\ell}^{\ell} Y^*_{\ell m}(\hat{\mathbf{k}}) Y_{\ell m}(\hat{\mathbf{x}})\,, \tag{2.14b}$$

where P_ℓ are the Legendre polynomials and j_ℓ the spherical Bessel functions. Let us evaluate the $a_{\ell m}$ coefficients on the last scattering surface, that is $\mathbf{x} = r_{\rm LS}\mathbf{n}$, where $r_{\rm LS} \simeq$14 Gpc is the distance from last scattering. Therefore, Eq. (2.8) becomes

$$\begin{aligned} a_{\ell m} &= \int \frac{d^3k}{(2\pi)^3}\sum_\ell \sum_{m=-\ell}^{\ell} (2\ell+1) i^\ell \frac{4\pi}{2\ell+1} Y^*_{\ell m}(\hat{k}) j_\ell(kr_{\rm LS})\Theta(\mathbf{k}) \int d\Omega\, Y_{\ell m}(\hat{n}) Y^*_{\ell' m'}(\hat{n}) \\ &= 4\pi \int \frac{d^3k}{(2\pi)^3}\sum_\ell \sum_{m=-\ell}^{\ell} i^\ell Y^*_{\ell m}(\hat{\mathbf{k}}) j_\ell(kr_{\rm LS})\Theta(\mathbf{k})\delta_{\ell\ell'}\delta_{mm'} \\ &= 4\pi i^\ell \int \frac{d^3k}{(2\pi)^3} j_\ell(kr_{\rm LS})\Theta(\mathbf{k}) Y^*_{\ell m}(\hat{\mathbf{k}})\,. \end{aligned} \tag{2.15}$$

In the SW limit, at first order, $\Theta(\mathbf{k}) \simeq -\zeta(\mathbf{k})/5$, where ζ is the curvature perturbation in Fourier space. Thus [91, 92],

$$\begin{aligned} a_{\ell m} &\simeq -\frac{4\pi}{5} i^\ell \int \frac{d^3k}{(2\pi)^3} j_\ell(kr_{\rm LS})\zeta(\mathbf{k}) Y^*_{\ell m}(\hat{\mathbf{k}}) \\ &\simeq \frac{12\pi}{5} i^\ell \int \frac{d^3k}{(2\pi)^3} \mathcal{T}_\ell(k)\zeta(\mathbf{k}) Y^*_{\ell m}(\hat{\mathbf{k}})\,, \end{aligned} \tag{2.16}$$

where $\mathcal{T}_\ell(k)$ indicates the *radiation transfer function* which, in the SW limit, takes the form $\mathcal{T}_\ell(k) \longrightarrow -(1/3) j_\ell(kr_{\rm LS})$. While in this form the transfer function only accounts for

[1] Note that the ratio Θ/δ only depend on the modulus of $\mathbf{k}$ and on the scalar product between k and the versor $\hat{\mathbf{n}}$. Therefore, different Fourier modes with same k and $\hat{\mathbf{k}}\cdot\hat{\mathbf{n}}$ evolve in the same way, even their initial amplitudes and phases are different.

the SW contribution, the exact one, $\mathcal{T}_\ell$, in principle takes into account all the effects that CMB photons suffered from the decoupling until today.

Then, recalling the definition of the power spectrum,

$$\langle \zeta(\mathbf{k})\zeta^*(\mathbf{k}')\rangle = (2\pi)^{(3)}\delta^3(\mathbf{k}-\mathbf{k}')P_\zeta(k) \tag{2.17a}$$

$$P_\zeta(k) = \frac{2\pi^2\Delta^2_\zeta(k)}{k^3}\,, \tag{2.17b}$$

the C_ℓ becomes

$$\begin{aligned} C_\ell = \langle a_{\ell m} a^*_{\ell m}\rangle &= \frac{144}{25}\pi^2 \int \frac{d^3k}{(2\pi)^3}\mathcal{T}_\ell(k)Y^*_{\ell m}(\hat{\mathbf{k}}) \int \frac{d^3k'}{(2\pi)^3}\mathcal{T}_\ell(k')Y_{\ell m}(\hat{\mathbf{k}}')\langle\zeta(\mathbf{k})\zeta^*(\mathbf{k}')\rangle \\ &= \frac{144}{25}\pi^2 \int \frac{d^3k}{(2\pi)^3}\mathcal{T}^2_\ell(k)Y^*_{\ell m}(\hat{\mathbf{k}})Y_{\ell m}(\hat{\mathbf{k}})P_\zeta(k) \\ &= \frac{144}{25}\pi^2 \int \frac{dk k^2}{(2\pi)^3}\mathcal{T}^2_\ell(k)\frac{2\pi^2\Delta^2_\zeta(k)}{k^3} \\ &= \frac{36}{25}\pi \int \frac{dk}{k}\mathcal{T}^2_\ell(k)\Delta^2_\zeta(k) \\ &= \frac{4}{25}\pi \int \frac{dk}{k} j^2_\ell(kr_{\rm LS})\Delta^2_\zeta(k)\,. \end{aligned} \tag{2.18}$$

By using (see Eq. (1.67))

$$\Delta^2_\zeta(k) \simeq 2.4\times 10^{-9}\left(\frac{k}{0.002\ \mathrm{Mpc}^{-1}}\right)^{n_s-1} \tag{2.19}$$

and assuming a scale-invariant power spectrum ($n_s = 1$), one finds $\Delta^2_\zeta(k) \simeq \Delta^2_\zeta(k_0)$. Moreover, recalling that

$$\int_0^\infty \frac{dx}{x^{2-n}} j^2_\ell(x) = 2^{n-4}\pi\frac{\Gamma(\ell+\frac{n}{2}-\frac{1}{2})\Gamma(3-n)}{\Gamma(\ell+\frac{5}{2}-\frac{n}{2})\Gamma^2(2-\frac{n}{2})}\,, \tag{2.20}$$

in this case ($n = 1$) one gets

$$\int \frac{dk}{k} j^2_\ell(kr_{\rm LS})\Delta^2_\zeta(k) = \frac{\Delta^2_\zeta(k_0)}{2\ell(\ell+1)}\,. \tag{2.21}$$

Therefore, Eq. (2.18) becomes

$$C_\ell = \frac{2\pi}{25}\frac{\Delta^2_\zeta(k_0)}{\ell(\ell+1)}\,. \tag{2.22}$$

This means

$$\ell(\ell+1)C^{\rm SW}_\ell = const\,. \tag{2.23}$$

Just make some observations. For small ℓ, where the approximation works better, there is a plateau (see Fig. 2.2). This is the reason why generally, in order to visualize the power

spectrum, one puts in graph $\ell(\ell+1)C_\ell$. At low ℓ, where the large scale approximation is valid and it is correct to consider only the contribution of the monopole, there will be a plateau (the Sachs-Wolfe plateau precisely). Actually, the effective spectrum is not completely flat due to a dipole contribution which in slightly affect the physics at the recombination. In particular, the small-scale anisotropy spectrum depends not only on the monopole, but also on the dipole and the ISW effect. To be precise, small-scales means cosmological scales which re-entered into the horizon earlier, when the microphysics is able to influence them. Let's briefly see what happens by considering their effects.

The monopole at recombination free-streams to us today creating anisotropies on angular scales $\ell \simeq k\eta_0$. Essentially, adding the small-scale effects, the spectrum shifts slightly to lower ℓ. Accounting for the dipole raises the anisotropy spectrum. Since the dipole is out of phase with the monopole, the difference between maximums and minimus of the monopole becomes less pronunced. Lastly, the early ISW effect enhances the anisotropy on scales comparable to the horizon, since this term accounts for the variation of the potential due to the microphysics acting on sub-horizon scales. In this case, the potential changes near recombination since the Universe is not purely matter-dominated [2]. This effect is particularly important since it is in phase with the monopole (for more details, see e.g. [19]).

[2]The gravitational potential is variable since, immediately after the recombination, the transition between radiation- and matter-dominated Universe is not immediate, and there is still a residue of radiation.

Chapter 3

CMB Spectral Distortions

The energy spectrum of the CMB is a useful tool in order to determine the key cosmological parameters with high extremely precision. However, it is also important since it depends on the thermal history of the Universe at very early stages, when the baryonic matter was tightly coupled to photons through Compton scattering and well before any structure formation. It should be noted that any perturbation to the thermodynamic equilibrium between baryon and radiation in the early epochs leads to distortions in the spectrum of the CMB [93]. There are many types of generation mechanisms for CMB spectral distortions in the standard cosmological model. For instance, one of the sources of the distortions is the Silk damping of small-scale perturbations. Mechanisms beyond the Standard Model can include decay and annihilation of relic particles [94–97] and, e.g, primordial magnetic fields [98–100]; distortions can be imprinted after some energy release due to decaying relic particles or by evaporating primordial black holes [101]. They will be more or less visible depending on the amount of energy transferred to the medium. Therefore, detection or constraints on CMB spectral distortions can provide an important tool in order to understand the physics of the early Universe [102, 103].

The process of erasing these distortions and, therefore, of restoring the equilibrium is called *thermalization*. The thermalization process of the CMB in the early Universe has long been studied. In the early epochs ($z \gtrsim 2 \times 10^6$), a blackbody spectrum is maintained by processes such as Compton scattering, Bremsstrahlung and double Compton scattering. However, due to the expansion of the Universe, these interactions gradually become less efficient. As a result, energy injected at epochs $z \lesssim 2 \times 10^6$ can induce deviations from the blackbody spectrum and CMB spectral distortions are created. The main types of distortions are called μ- and y-distortions and they will be studied in the following sections.

The amount of information derivable from the spectral distortions is very rich and could lead to cover scales not yet explored by other experiments [104]. In particular, in addition to the theoretical framework, it was possible to precisely compute the shape of the distortions for several physical production mechanisms, thanks to the development of

CosmoTherm code [93, 105]. It became possible to find approximate solutions, using the Green's function method, greatly speeding up the calculations [106].

From an experimental point of view, both types of distortions were first constrained by COBE/FIRAS [1, 2, 75, 107]: the current numerical bounds correspond to $|\mu| < 9 \times 10^{-5}$ and $|y| < 1.5 \times 10^{-5}$ (95% CL) [2]. However, another reason for spectral distortions being interesting is due to technological advances. Proposed experimental concepts like PIXIE (*Primordial Inflation Explorer*) [108], PRISM (*Polarized Radiation Imaging and Spectroscopy Mission*) [109, 110], PRISTINE (*Polarized Radiation Interferometer for Spectral disTortions and INflation Exploration*) and SuperPIXIE [111], within the ESA Voyage 2050 Program [7], could extraordinarily improve the current knowledge of the CMB spectrum in the future. These are all designed to reach important milestones towards a detection of CMB distortions (for more details, see e.g. [7] and Refs. therein). These types of experiments could enhance the limits of COBE/FIRAS by more than three orders of magnitude, arriving to constraints $\mu \simeq 10^{-8}$ and $y \simeq 10^{-9}$, providing a unique way to learn about processes. Hence, CMB spectral distortions have an enormous potential which is becoming more and more recognized by the Cosmology community.

3.1 Thermalization problem

If one considers the uniform adiabatic expansion of the Universe, then, neglecting any kind of collision and spatial perturbations, the blackbody shape of the CMB spectrum would be left unchanged at all times [5]. However, if there are processes able to change the number of photons or leading to a release/extraction of energy in the early Universe, this causes distortions in the CMB frequency spectrum. To thermalize the latter, it is necessary that the photon number is readjusted and that photons are redistributed in frequency in order to restore the blackbody shape. The thermalization problem is important since one can learn about different processes characterizing the early stages and the thermal history of the Universe. In general, the thermalization problem can be solved numerically. However, under simplifying assumptions, it is possible to find some analytic solutions[1].

At redshift $z \gtrsim 2 \times 10^6$ the Universe is characterized by a hot photon-baryon plasma and photons very frequently interact with other particles; thus, the thermalization of any distortion is extremely rapid. Any energy release in this era simply causes a change of the temperature of the CMB and it is quickly thermalized by Compton scattering, double Compton scattering and Bremsstrahlung and the distribution of photons is described by a blackbody spectrum. Spectral distortions are created by processes that drive matter and

[1]It should be noticed that these approximated solutions have limitations. For instance, after large injection of energy, non linear-aspects could arise and could no longer be negligible [112]. Instead, for small releases of energy, the shape of the CMB spectral distortions becomes strongly dependent on small temperature difference between electrons and photons [93].

radiation out of equilibrium after thermalization becomes inefficient at redshift $z \lesssim 2\times10^6$. Examples of these processes could be energy-releasing mechanisms that heat the baryonic matter and inject photons. These distortions are classified into two main types: the μ-type distortion, in which case the spectrum of the CMB is a Bose-Einstein distribution with a chemical potential μ, and the y-type distortion, in which the spectral distortion is parameterized by the Compton y-parameter. In particular, y-type distortions formed at late times, i.e., for redshift $z \lesssim 5 \times 10^4$, while μ-distortions determine a tool to investigate processes occurring in the pre-recombination era, i.e., $5 \times 10^4 \lesssim z \lesssim 2 \times 10^6$. Notice that the energy release in the range $10^4 \lesssim z \lesssim 10^5$ is not abrupt: the transition between μ-type and y-type distortions is gradual and at all intermediate stages the signal is given by a superposition of these extreme cases with a small residual (non μ/non y) distortion that contains valuable time-dependent information of the energy-release process. This is the so-called r-type distortion [106, 113].

3.1.1 Photon Boltzmann equation

In order to study the formation and evolution of CMB fluctuations and spectral distortions, it is useful to introduce the photon Boltzmann equation for the photon phase-space distribution $n(t, p)$. Omitting any spatial dependence, the photon Boltzmann equation can be expressed as

$$\frac{\partial n}{\partial t} - Hp\frac{\partial n}{\partial p} = C[n]\,. \tag{3.1}$$

Here, $H(t)$ denotes the Hubble expansion rate, while $C[n]$ the collision term accounting for interactions of photons with other particle-species. In absence of collisions, i.e., setting $C[n] = 0$, the homogeneous photon distribution is constant in time, which means that its shape is conserved by the expansion of the Universe and photon momenta are simply redshifted. Then, one can understand that only the collision term is responsible for changes in the photon distribution, adding or subtracting photons or modifying the momenta of the already existing photons [5, 6]. Notice that if one introduce the variable

$$x = \frac{p}{kT_z(t)} = \frac{h\nu}{kT_z(t)}, \qquad \text{with} \quad T_z(t) = T_z(t_0)\frac{a(t_0)}{a(t)} = T_0(1+z)\,, \tag{3.2}$$

the Boltzmann equation can be rewritten in a more compact way, as $dn/dt = C[n]$ [5, 93]. Here, $T_0 = T_z(t_0)$ can be any temperature as long as it remains constant in time. For that reason, an optimal choice could be the current observed CMB temperature, i.e., $T_0 = 2.725$ K.

In the following the Boltzmann equation will be described by considering the following processes: Compton scattering, double Compton scattering and Bremsstrahlung [5, 93].

Compton scattering The Compton scattering is the process responsible for the energy redistribution of photons. The solution of the collision term has been found in [114] and the result is the famous *Kompaneets equation*,

$$\left.\frac{\partial n}{\partial \tau}\right|_{\rm CS} = \frac{\theta_{\rm e}}{x_{\rm e}^2}\frac{\partial}{\partial x_{\rm e}} x_{\rm e}^4\left[\frac{\partial n}{\partial x_{\rm e}} + n(1+n)\right] = \frac{\theta_{\rm e}}{x^2}\frac{\partial}{\partial x} x^4\left[\frac{\partial n}{\partial x} + \frac{T_z}{T_{\rm e}} n(1+n)\right], \tag{3.3}$$

where $d\tau = dt/t_{\rm C} = \sigma_{\rm T} n_{\rm e} c dt$ is the Thomson optical depth, $\theta_{\rm e} = kT_{\rm e}/m_{\rm e}c^2$ is the dimensionless electron temperature and $x_{\rm e} = h\nu/kT_{\rm e}$ indicates a chosen frequency variable. The previous result can be obtained by computing the collision term in the limit $h\nu \ll kT_{\rm e} \ll m_{\rm e}c^2$, neglecting orders higher than the first in $\theta_{\rm e}$ and $h\nu/m_{\rm e}c^2$ [5]. The Kompaneets equation can be used to describe repeated scattering of photons due to electrons in the isotropic medium.

Double Compton scattering and Bremsstrahlung In the cosmological thermalization problem, the Double Compton scattering and Bremsstrahlung provide an adjustment of the number of photon. The contribution of these two processes to the Boltzmann equation can be written as [5, 93]

$$\left.\frac{\partial n}{\partial \tau}\right|_{\rm DC+BR} = \frac{K_{\rm BR} e^{-x_{\rm e}} + K_{\rm DC} e^{-2x}}{x^3}\left[1 - n(e^{x_{\rm e}} - 1)\right], \tag{3.4}$$

where K are the emission coefficients and take the form, respectively,

$$\begin{aligned} K_{\rm BR} &= \frac{\alpha}{2\pi}\frac{\lambda_{\rm e}^3}{\sqrt{6\pi}\theta_{\rm e}^{7/2}}\left(\frac{T_{\rm e}}{T_\gamma}\right)^3 \sum_i z_{\rm i}^2 N_i \bar{g}_{\rm ff}(z_{\rm i}, T_{\rm e}, T_\gamma, x_{\rm e}) \\ &\simeq 1.4\times 10^{-6}\left[\frac{\bar{g}_{\rm ff}}{3.0}\right]\left[\frac{\Omega_b h^2}{0.022}\right](1+z)^{-1/2} \qquad (3.5a) \\ K_{\rm DC} &= \frac{4\alpha}{3\pi}\theta_\gamma^2 I_{\rm dc} g_{\rm dc}(T_{\rm e}, T_\gamma, x) \\ &\simeq 1.7\times 10^{-20}(1+z)^2\,. \qquad (3.5b) \end{aligned}$$

Here, $\alpha = 1/137$ is the fine structure constant, $\lambda_{\rm e} = h/m_{\rm e}c$ is the Compton wavelength of the electron, $z_{\rm i}$ is the charge, N_i the number density and $\bar{g}_{\rm ff}$ is the Bremsstrahlung Gaunt factor for a nucleus of the atomic species i. As regards $K_{\rm DC}$, $g_{\rm dc}$ is the Double Compton Gaunt factor and $I_{\rm dc} = \int dx\, x^4 n(1+n) \simeq 4\pi^4/15$ [5, 93]. Notice that, due to the presence of the $1/x^3$ factor, the main emission and absorption contribution is at low frequencies. The low-frequency limit is what we are interested in because this is where the distortions are generated.

The Boltzmann equation can be studied in three interesting regimes. For $z = z_{\mu,i} \gtrsim 2\times 10^6$ any energy released into the photon-baryon plasma is quickly thermalized by Compton scattering and double Compton scattering and the result is again a black-body

spectrum with now a higher temperature and a larger total number of photons. For $z_{\mu,f} = 5 \times 10^4 \lesssim z \lesssim z_{\mu,i}$ double Compton scattering and Bremsstrahlung becomes less efficient, causing the number of photons to be almost frozen, but the equilibrium is still achieved after an energy injection due to Compton scattering. However, since this process is not able to change the number of photons, the final result is a Bose-Einstein distribution, characterized by a frequency dependent chemical potential[2] $\mu(x)$. These distortions are defined as μ-type distortions. For $z \lesssim z_{\mu,f}$ even Compton scattering becomes inefficient to establish kinetic equilibrium and the distortion created after this moment is known as y-type distortion. We will delve into the details of these distortions we just introduced.

3.2 Different types of spectral distortions

Before considering the different shapes of the spectral distortions, let us recall some of the main blackbody relations. The blackbody intensity, otherwise called Planckian distribution, is defined as

$$B_\nu(T) = \frac{2h}{c^2}\frac{\nu^3}{e^{h\nu/kT}-1} = \frac{2h\nu^3}{c^2} n_\nu^{\rm BB}(T) = I_0 \frac{x^3}{e^x - 1}\,. \tag{3.6}$$

Here,

$$n_\nu^{\rm BB}(T) = \frac{1}{e^{h\nu/kT}-1} = \frac{1}{e^x - 1} \tag{3.7}$$

is the phase-space distribution of a blackbody (BB) at temperature T, with $x = h\nu/kT$, and $I_0(T) = (2h/c^2)(kT/h)^3$. At early times, for $z \gtrsim 10^6$, the Universe is well described by a hot photon-baryon plasma where the number density of photons n_ν per frequency interval is given, with very high accuracy, by the blackbody spectrum. Notice that the limiting behaviours correspond to

$$B_\nu(T) \simeq \begin{cases} \frac{2\nu^2}{c^2}kT & \text{for } h\nu \ll kT \quad \text{Rayleigh-Jeans limit} \\ \frac{2h\nu^3}{c^2}e^{-h\nu/kT} & \text{for } h\nu \gg kT \quad \text{Wien law}\,. \end{cases} \tag{3.8}$$

Then, one can also define the number density and energy of photons as

$$N_\gamma^{\rm Pl} = \frac{2}{c^3}\int d\nu d\Omega\, \frac{\nu^2}{e^x-1} = \frac{8\pi}{c^3}\left(\frac{kT}{h}\right)^3 \int dx \frac{x^2}{e^x-1} = \frac{16\pi(kT)^3\zeta_3}{c^3h^3} = b_R T^3 \tag{3.9a}$$

$$\rho_\gamma^{\rm Pl} = \frac{2h}{c^3}\int d\nu d\Omega\, \frac{\nu^3}{e^x-1} = \frac{8\pi h}{c^3}\left(\frac{kT}{h}\right)^4 \int dx \frac{x^3}{e^x-1} = \frac{8\pi^5(kT)^4}{15c^3h^3} = a_R T^4\,, \tag{3.9b}$$

[2]It is possible to show (see Section 3.2.4) that $\mu(x)$ deviates from a constant value only at very low frequencies and then it is possible to approximate it as a constant, which is verified everywhere except deep in the Rayleigh-Jeans tail, i.e. for $\nu \longrightarrow 0$ (see Eq. (3.6)).

where ζ_i indicates the Riemann ζ-function[3] and a_R and b_R are the radiation constants [5]. Notice that $N_\gamma^{\rm Pl} \propto T^3$ and $\rho_\gamma^{\rm Pl} \propto T^4$, which define the fundamental blackbody relations.

3.2.1 Temperature shift

In general, the photon distribution can be decomposed as

$$n(\tau, x) \simeq n_0(x) + \Delta n(\tau, x)\,, \tag{3.10}$$

assuming $h\nu/kT_{\rm e} \ll 1$, $kT_{\rm e}/m_{\rm e}c^2 \ll 1$, $\Delta\tau = \int n_{\rm e}\sigma_{\rm T} c dt \ll 1$ and that at $\tau = 0$ one gets $n_0 = n_{\rm BB} = 1/(e^x - 1)$. In this context, Δn can be treated as a distortion of the blackbody spectrum. This expression also contemplates the possibility of a deviation from the temperature T. In order to obtain a blackbody of temperature $T' \neq T$, the photon number density has to change by

$$\begin{aligned}\Delta n = n_{\rm BB}(T') - n_{\rm BB}(T) &= \frac{1}{e^{x'} - 1} - \frac{1}{e^x - 1} \\ &\simeq -x\frac{\partial n_{\rm BB}}{\partial x}\frac{\Delta T}{T} = G(x)\frac{\Delta T}{T}\,,\end{aligned} \tag{3.11}$$

with $x' = xT/T'$ and $\Delta T \ll 1$. Here, it has been defined the shape of a temperature shift as

$$G(x) = -x\frac{\partial n_{\rm BB}}{\partial x} = \frac{xe^x}{(e^x - 1)^2} \simeq \begin{cases} \frac{1}{x} & \text{for } x \ll 1 \\ xe^{-x} & \text{for } x \gg 1\,. \end{cases} \tag{3.12}$$

In this case, there are no distortions, but a departure with respect to a blackbody spectrum with temperature T, as long as $\Delta T/T$ remains sufficiently small. This is the reason why such deviations are considered as temperature shifts instead of distortions of the spectrum. The shape of the spectrum of a temperature shift is shown in Fig. 3.1.

Now, let us suppose to change the value of the temperature T, for instance, increasing it to a value T' by increasing the energy of the photons in some way. Defining $\mathcal{E} = \Delta\rho_\gamma/\rho_\gamma^{\rm Pl}(T)$, for $\mathcal{E} \ll 1$, it results

$$\mathcal{E} = \left(\frac{T'}{T}\right)^4 - 1 \qquad \Longrightarrow \qquad \frac{\Delta T}{T} = (1 + \mathcal{E})^{1/4} - 1 \simeq \frac{1}{4}\frac{\Delta\rho_\gamma}{\rho_\gamma^{\rm Pl}}\,. \tag{3.13}$$

Notice that, in this case, the spectrum cannot be a blackbody anymore, due to the fact that the photon number density is unchanged, and this leads to distortions in the spectrum. To maintain the blackbody shape, then to keep the dependence $N_\gamma^{\rm Pl} \propto T^3$ unchanged, it

[3] In general, the Riemann ζ-function is defined as $\zeta(k) = \frac{1}{\Gamma(k)}\int dx \frac{x^{k-1}}{e^x - 1}$, with $\Gamma(k) = \int dx\, x^{k-1}e^{-x}$.

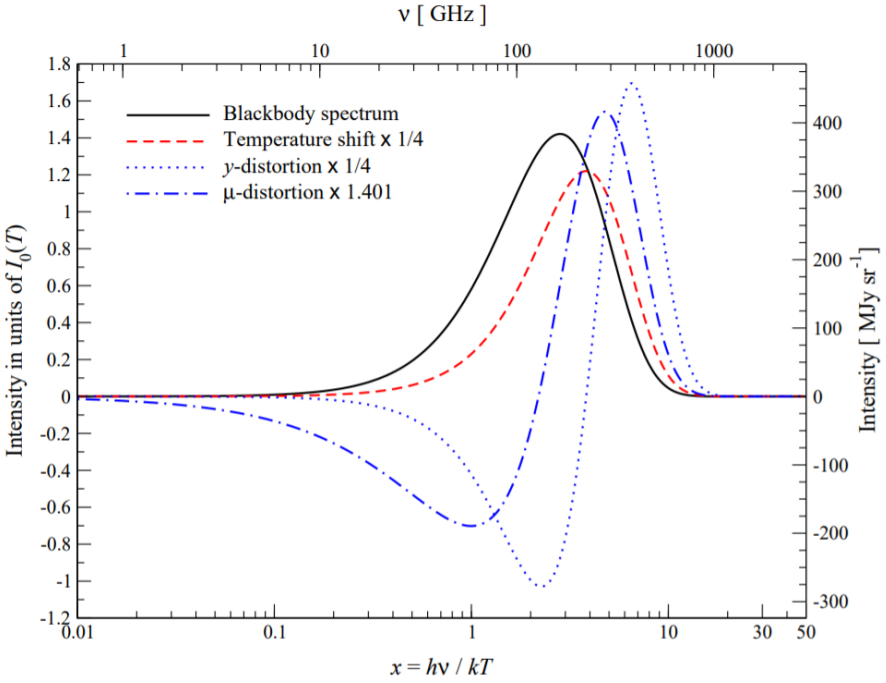

Figure 3.1: Comparison of a Compton y-distortion, $Y_{\rm SZ}(x)$, a μ-distortion, $M(x)$, and a temperature shift, $G(x)$, with respect to the blackbody spectrum. The left y-axis is normalized by $I_0(T) = (2h/c^2)/(kT/h)^3 \simeq 270$ MJy sr$^{-1}(T/2.726$ K). The upper x-axis and right y-axis give the corresponding frequency and spectral intensity for $T = 2.726$ K. Image credit [5].

is necessary to add an amount of photons equal to

$$\frac{\Delta N_\gamma}{N_\gamma^{\rm Pl}} = \left(\frac{T'}{T}\right)^3 - 1 \simeq 3\frac{\Delta T}{T} \qquad \Longrightarrow \qquad \frac{\Delta N_\gamma}{N_\gamma^{\rm Pl}} \simeq \frac{3}{4}\frac{\Delta \rho_\gamma}{\rho_\gamma^{\rm Pl}}\,. \tag{3.14}$$

However, this condition is not sufficient, since it does not specify the energy distributions of missing photons (see [5] for more details).

3.2.2 y-type distortions

Let us start our discussion focusing on the y-type distortions, which formed at late times, for redshift $z \lesssim 10^4$. At this redshift, Comptonization becomes inefficient: the shape of the distortions changes, marking a transition from the μ-type distortion to the y-type. Recall the Kompaneets equation,

$$\left.\frac{\partial n}{\partial \tau}\right|_{\rm CS} = \frac{\theta_{\rm e}}{x^2}\frac{\partial}{\partial x}x^4\left[\frac{\partial n}{\partial x} + \frac{T_z}{T_{\rm e}}n(1+n)\right]. \tag{3.15}$$

This has no general analytic solution, but it is possible to solve it in limiting cases.

Scatterings between photons and electrons characterized by inefficient exchange of energy cause a y-distortion. Let us assume that $h\nu/kT_{\rm e} \ll 1$, $kT_{\rm e}/m_{\rm e}c^2 \ll 1$, $\Delta\tau \ll 1$ and

that at $\tau = 0$ one starts with $n_0 = n_{\rm BB} = 1/(e^x - 1)$. In general, one can write the $\partial n(\tau, x)/\partial\tau = f(\tau, n)$ and, neglecting the dependence for a more compact notation, it results

$$\frac{\partial n}{\partial \tau} \simeq \frac{\Delta n}{\Delta \tau} = \frac{n - n_0}{\Delta \tau} \simeq f \quad \Longrightarrow \quad \Delta n \simeq \Delta\tau f \quad \Longrightarrow \quad n \simeq n_0 + \Delta\tau f\,, \tag{3.16}$$

with

$$f(\tau, n_0) = \frac{\theta_{\rm e}}{x^2}\frac{\partial}{\partial x} x^4 \left[\frac{\partial n_0}{\partial x} + \frac{T_z}{T_{\rm e}} n_0(1 + n_0)\right]. \tag{3.17}$$

In particular [4] , one obtains

$$\frac{\partial n_0}{\partial x} = -n_0^2 \frac{1 + n_0}{n_0} = -n_0(1 + n_0)\,, \tag{3.19}$$

and then,

$$\begin{aligned}\frac{\partial n_0}{\partial x} + \frac{T_z}{T_{\rm e}} n_0(1 + n_0) &= -n_0(1 + n_0) + \frac{T_z}{T_{\rm e}} n_0(1 + n_0) \\ &= n_0(1 + n_0)\left(\frac{T_z}{T_{\rm e}} - 1\right).\end{aligned} \tag{3.20}$$

Moreover, Eq. (3.17) becomes

$$f \simeq (\theta_{\rm z} - \theta_{\rm e})\frac{1}{x^2}\frac{\partial}{\partial x} x^4 n_0(1 + n_0)\,, \tag{3.21}$$

recalling the definition of the dimensionless electron temperature, $\theta_{\rm e} = kT_{\rm e}/m_{\rm e}c^2$, and that $T_z = T_{\rm e}(1 + z)$. Calculating the derivative [5] and using Eq. (3.19), one can write

$$\frac{\partial}{\partial x} n_0(1 + n_0) = -n_0(1 + n_0)(1 + 2n_0)\,. \tag{3.23}$$

Therefore,

$$\begin{aligned} f &= (\theta_{\rm z} - \theta_{\rm e})\big[4x n_0(1 + n_0) - x^2 n_0(1 + n_0)(1 + 2n_0)\big] \\ &= (\theta_{\rm z} - \theta_{\rm e}) x n_0^2 e^x \left[4 - x n_0\left(\frac{1}{n_0} + 2\right)\right] \\ &= (\theta_{\rm z} - \theta_{\rm e})\frac{x e^x}{(e^x - 1)^2}\left[4 - x\frac{e^x + 1}{e^x - 1}\right]. \end{aligned} \tag{3.24}$$

---

[4] In fact,

$$\frac{\partial n_0}{\partial x} = \frac{\partial}{\partial x}\frac{1}{e^x - 1} = -\frac{e^x}{(e^x - 1)^2} = -n_0^2 e^x, \qquad \text{where} \quad \frac{1 + n_0}{n_0} = e^x\,. \tag{3.18}$$

[5] The derivative results

$$\frac{1}{x^2}\frac{\partial}{\partial x} x^4 n_0(1 + n_0) = \frac{4x^3}{x^2} n_0(1 + n_0) + x^2 \frac{\partial}{\partial x} n_0(1 + n_0)\,. \tag{3.22}$$

Let us define the *Compton-y distortion* as

$$Y_{\rm SZ}(x) = \frac{x e^x}{(e^x-1)^2}\Big[x\coth\Big(\frac{x}{2}\Big)-4\Big]\,, \tag{3.25}$$

which is present in the limit of inefficient energy exchange scatterings. Finally,

$$f = (\theta_{\rm e}-\theta_{\rm z})Y_{\rm SZ}(x)\,, \tag{3.26}$$

and the spectrum of distortion takes the form

$$\Delta n \simeq \Delta\tau(\theta_{\rm e}-\theta_{\rm z})Y_{\rm SZ}(x)\,. \tag{3.27}$$

Recalling the definition Eq. (3.12), one can write

$$\frac{\partial}{\partial x}n_0 = -n_0(1+n_0) = -\frac{e^x}{(e^x-1)^2} = -\frac{G(x)}{x}\,, \tag{3.28}$$

and notice that

$$Y_{\rm SZ}(x) = G(x)\Big[x\coth\Big(\frac{x}{2}\Big)-4\Big]\,. \tag{3.29}$$

The main variable is the *Compton-y parameter* defined as (see e.g. [115])

$$y = \int_{\tau_0}^{\tau} d\tau\,\frac{T_{\rm e}-T_z}{m_{\rm e}c^2} = \int_{\tau_0}^{\tau} dt\,\sigma_{\rm T}n_{\rm e}c(\theta_{\rm e}-\theta_{\rm z}) \simeq \Delta\tau(\theta_{\rm e}-\theta_{\rm z})\,, \tag{3.30}$$

which depends on the net energy exchange, proportional to $(\theta_{\rm e}-\theta_z)$, and on the number of scatterings, related to τ. Notice that the solution of Eq. (3.27) is valid as long $|y| \ll 1$: this means that electron temperature does not change much due to scatterings. Moreover, in this limit, one can study two interesting cases:

$$\begin{aligned} &y>0: \text{all the energy flows from electrons to photons} \quad &\Longrightarrow \quad &\textsc{Comptonization}\\ &y<0: \text{energy flows from photons to electrons} \quad &\Longrightarrow \quad &\textsc{Compton Cooling}\,. \end{aligned}$$

The negative y-distortions are usually not considered, since most of the processes tend to heat the matter in the Universe, making the positive contribution relevant [5]. Since $T_\gamma \propto a^{-1}$ and $T_{\rm e} \propto a^{-2}$, at all times electrons try to be cooler and extract energy from the CMB. However, this effect is small since the heat capacity of photons is bigger than the heat capacity of electrons. For that reason, it is usually neglected [93, 116]. Dark matter interactions can enhance the cooling effect beyond the standard baryonic level, thereby providing the opportunity to shed light on the nature of dark matter [117].

The frequency dependence of the y-distortion for $T_0 = 2.725$ K is shown in Fig. 3.1. Notice the characteristic shape with a deficit of photons in the Rayleigh-Jeans part and

instead an increment of photons in the Wien tail of the CMB spectrum. The limiting behaviours of the Compton-y distortions are

$$Y_{\rm SZ}(x) = G(x)\left[x\frac{e^x+1}{e^x-1} - 4\right] \simeq \begin{cases} -\frac{2}{x} & \text{for } x \ll 1 \\ xe^{-x}(x-4) & \text{for } x \gg 1\,, \end{cases} \tag{3.31}$$

which corresponds to

$$\frac{\Delta T}{T} \simeq \begin{cases} -2y & \text{for } x \ll 1 \\ (x-4)y & \text{for } x \gg 1\,. \end{cases} \tag{3.32}$$

For a y-distortion, it holds

$$\Delta N_\gamma \propto \int dx\, x^2 Y_{\rm SZ}(x) = 0 \tag{3.33a}$$

$$\Delta\rho_\gamma = 4y\rho_\gamma^{\rm Pl} \propto \int dx\, x^3 Y_{\rm SZ}(x)\,. \tag{3.33b}$$

Proof. For instance, let us evaluate ΔN_γ:

$$\Delta N_\gamma \propto \int x^2 Y_{\rm SZ}(x)dx = \int x^2\left[-\frac{\frac{\partial}{\partial x}\left(x^3G(x)\right)}{x^2}\right]dx\,,$$

since it is possible to write

$$Y(x) = -\frac{\frac{\partial}{\partial x}\left(x^3G(x)\right)}{x^2}\,. \tag{3.34}$$

In fact

$$\frac{\frac{\partial}{\partial x}\left(x^3G(x)\right)}{x^2} = \frac{3x^2G(x) + x^3\partial_x G(x)}{x^2} = 3G(x) + x\partial_x G(x)\,,$$

and

$$\partial_x G(x) = \frac{(e^x+xe^x)(e^x-1)^2 - xe^x 2(e^x-1)e^x}{(e^x-1)^4} = \frac{e^x(1+x)}{(e^x-1)^2} - \frac{2xe^{2x}}{(e^x-1)^3}\,.$$

Therefore,

$$\begin{aligned}\frac{\frac{\partial}{\partial x}\left(x^3G(x)\right)}{x^2} &= -\left[3\frac{xe^x}{(e^x-1)^2} + \frac{xe^x(1+x)}{(e^x-1)^2} - \frac{2x^2e^{2x}}{(e^x-1)^3}\right] \\ &= -\frac{xe^x}{(e^x-1)^2}\left[4 - x\frac{e^x+1}{e^x-1}\right] \equiv Y(x)\,.\end{aligned}$$

Then,

$$\Delta N_\gamma \propto -\int \frac{\partial}{\partial x}[x^3G(x)]dx = -x^3G(x)\Big|_0^\infty = 0\,.$$

□

The condition $\Delta N_\gamma = 0$ reflects the fact that Compton scattering does not change the

number of photons. Instead, the relation (3.33b) expresses the fraction of energy of electrons exchanged with the initial blackbody spectrum, giving a first simple approximation for the distortion [115]. To prove Eq. (3.33b) one simply needs to re-trace the same steps outlined above.

3.2.3 μ-type distortions

The μ-type distortion is generated when energy exchange is extremely efficient. This signal is a clear witness of processes occurring deep into the pre-recombination era, i.e., for $10^4 \lesssim z \lesssim 10^6$. When many scatterings occur, the equilibrium with respect to Compton scattering is reached and so, neglecting emission and absorption processes, it results

$$0 \simeq \frac{\theta_{\rm e}}{x^2}\frac{\partial}{\partial x}x^4\left[\frac{\partial}{\partial x}n + \frac{T_\gamma}{T_{\rm e}}n(1+n)\right]. \tag{3.35}$$

If $T_{\rm e} \equiv T_\gamma$, a solution is $n_{\rm BB} = 1/(e^x - 1)$. In fact, recalling Eq. (3.19), one finds

$$\begin{aligned} 0 &\simeq \frac{\theta_{\rm e}}{x^2}\frac{\partial}{\partial x}x^4\left[\frac{\partial}{\partial x}n_{\rm BB} + n_{\rm BB}(n_{\rm BB}+1)\right] \\ &\simeq \frac{\theta_{\rm e}}{x^2}\frac{\partial}{\partial x}x^4[-n_{\rm BB}(1+n_{\rm BB}) + n_{\rm BB}(1+n_{\rm BB})] = 0\,. \end{aligned} \tag{3.36}$$

For a more general solution it is necessary to solve the equation

$$\frac{\partial}{\partial x}n = -\frac{T_\gamma}{T_e}n(n+1)\,. \tag{3.37}$$

The factor $T_\gamma/T_{\rm e}$ can be reabsorbed by the redefined frequency $x \longrightarrow x_{\rm e} = h\nu/kT_{\rm e}$ so that the equation becomes

$$\frac{\partial}{\partial x_{\rm e}}n = -n(n+1)\,. \tag{3.38}$$

Integrating:

$$\ln(1+n) - \ln(n) = x_{\rm e} + c\,. \tag{3.39}$$

A function like $n_{\rm BE} = 1/(e^{x_{\rm e}+c} - 1)$ satisfies the previous equation (simply substitute the solution $n_{\rm BE}$ and verify that it satisfies the Eq. (3.39)). Introducing the integration constant μ_0, the solution becomes

$$n_{\rm BE} = \frac{1}{e^{x_{\rm e}+\mu_0} - 1}\,. \tag{3.40}$$

This represents a Bose-Einstein distribution with a constant chemical potential given by μ_0[6]. In principle, the chemical potential could be both positive and negative:

[6]Notice the opposite sign with respect to the thermodynamic convention.

$\mu_0 = 0$: BB with temperature T_e $\implies$ FULL EQUILIBRIUM

$\mu_0 > 0$: fewer photons than a BB at T_e $\implies$ ENERGY RELEASE/PHOTON EMISSION

$\mu_0 < 0$: more photons than a BB at T_e $\implies$ ENERGY EXTRACTION/PHOTON ABSORPTION .

However, the solution with $\mu < 0$ is not physical, since $x_\mathrm{e} + \mu_0$ could vanish for some positive frequency; however, the photons would form a Bose-Einstein condensate at $x_\mathrm{e} = 0$, with $\mu_0 = 0$ elsewhere. In a real plasma, actually, Bremsstrahlung and double Compton scattering emission will prevent even this from happening (see [5] and Refs. therein).

Now, let us define the distortion. For $\mu_0 \ll 1$, one can write

$$\begin{aligned} n_\mathrm{BE} = \frac{1}{e^{x_\mathrm{e}+\mu_0}-1} &\simeq \frac{1}{e^{x_\mathrm{e}}-1} - \frac{e^{x_\mathrm{e}} x_\mathrm{e}}{(e^{x_\mathrm{e}}-1)^2}\frac{\mu_0}{x_\mathrm{e}} + \mathcal{O}(\mu_0^2) \\ &\simeq \frac{1}{e^{x_\mathrm{e}}-1} - \frac{G(x_\mathrm{e})}{x_\mathrm{e}}\mu_0 + \mathcal{O}(\mu_0^2)\,. \end{aligned} \tag{3.41}$$

From this result, recalling the general decomposition Eq. (3.10), it is possible to define the distortion from a blackbody spectrum as

$$\Delta n(x) = -\frac{G(x)}{x}\mu_0 = -\frac{e^x}{(e^x-1)^2}\mu_0\,, \tag{3.42}$$

where the reference temperature is the electron temperature T_e and the spectrum of μ-distortion is represented by the ratio $G(x)/x$. To be rigorous, this solution should be written in terms of x_e instead of x. However, the difference between x_e and x is equivalent to a temperature shift distortion [6]. Let us integrate Δn in order to obtain the total number density,

$$\int dx\, x^2 \Delta n = -\mu_0 \int dx\, x^2 \frac{e^x}{(e^x-1)^2}\,. \tag{3.43}$$

and define $G_k = \int x^k G(x) dx = (k+1)!\zeta(k+1)$, where $\zeta(k)$ is the Riemann ζ-function. In particular, one recognizes

$$G_1 = \int dx\, x^2 \frac{e^x}{(e^x-1)^2} = 2\zeta(2) = \frac{\pi^2}{3}\,. \tag{3.44}$$

Thus, from (3.43), it results

$$\int dx\, x^2 \Delta n = -\mu_0 \frac{\pi^2}{3} \simeq -3.2899\mu_0\,. \tag{3.45}$$

Eq. (3.42) suggests a possible definition of the shape of the μ-distortion, that is

$$M(x) = -\frac{G(x)}{x} + G(x)\alpha_\mu = G(x)\left(\alpha_\mu - \frac{1}{x}\right), \tag{3.46}$$

where an additional term $G(x)\alpha_\mu$ is introduced to satisfy the condition $\int x^2 M(x)dx = 0$: the value of α_μ can be calculated explicitly as

$$\begin{aligned}\int dx\, x^2 M(x) = 0 \quad &\Longrightarrow \quad \int dx\, x^2 G(x)\alpha_\mu - \int dx\, x^2 \frac{G(x)}{x} = 0 \\ &\Longrightarrow \quad G_2\alpha_\mu - G_1 = 0 \\ &\Longrightarrow \quad 6\zeta(3)\alpha_\mu - 2\zeta(2) = 0 \\ &\Longrightarrow \quad \alpha_\mu = \frac{\zeta(2)}{3\zeta(3)} \simeq \frac{1.6449}{3\cdot 1.2021} \simeq 0.4561\,. \end{aligned} \tag{3.47}$$

Therefore,

$$M(x) = G(x)\left[0.4561 - \frac{1}{x}\right], \tag{3.48}$$

and one can write

$$\Delta n = \mu M(x)\,. \tag{3.49}$$

Finally, the spectrum of the μ-distortion is given by [5]

$$M^*(x) \approx 1.401 G(x)\left[0.4561 - \frac{1}{x}\right] \simeq \begin{cases} -\frac{1.401}{x^2} & \text{for } x \ll 1 \\ 0.6390 x e^{-x} & \text{for } x \gg 1\,. \end{cases} \tag{3.50}$$

This corresponds to

$$\frac{\Delta T}{T} \simeq \begin{cases} -\frac{\mu_0}{x} & \text{for } x \ll 1 \\ 0.4561\mu_0 & \text{for } x \gg 1\,. \end{cases} \tag{3.51}$$

The frequency dependence of $M(x)$ is shown in the Fig. 3.1. Notice that, comparing with the y-distortion, the μ-type is shifted towards lower frequencies. This feature is important since, at least in principle, it makes the two types distinguishable from each other and, therefore, a μ-distortion, if detected, would be a clear sign of a signal generated in the pre-recombination epoch.

This is a simplified description of primordial distortions since transition between μ- and y-type distortions is gradual. The distortion signature from different energy-release scenarios is generally not just given by a superposition of pure μ- and y-distortion. The resulting signal contains valuable time-dependent information (see Fig. 3.2) and it is called *residual distortion* or r-type distortion (see e.g. [5] for more details).

In this Thesis, we will focus on the μ-type distortion (even though our calculations can be applied also to y-type distortions) and how they can be used to probe primordial non-Gaussianity (see Section 3.4). However, it should be noticed that, although analytical estimates will be developed, a numerical study of the system is needed, if one looks for precise predictions.

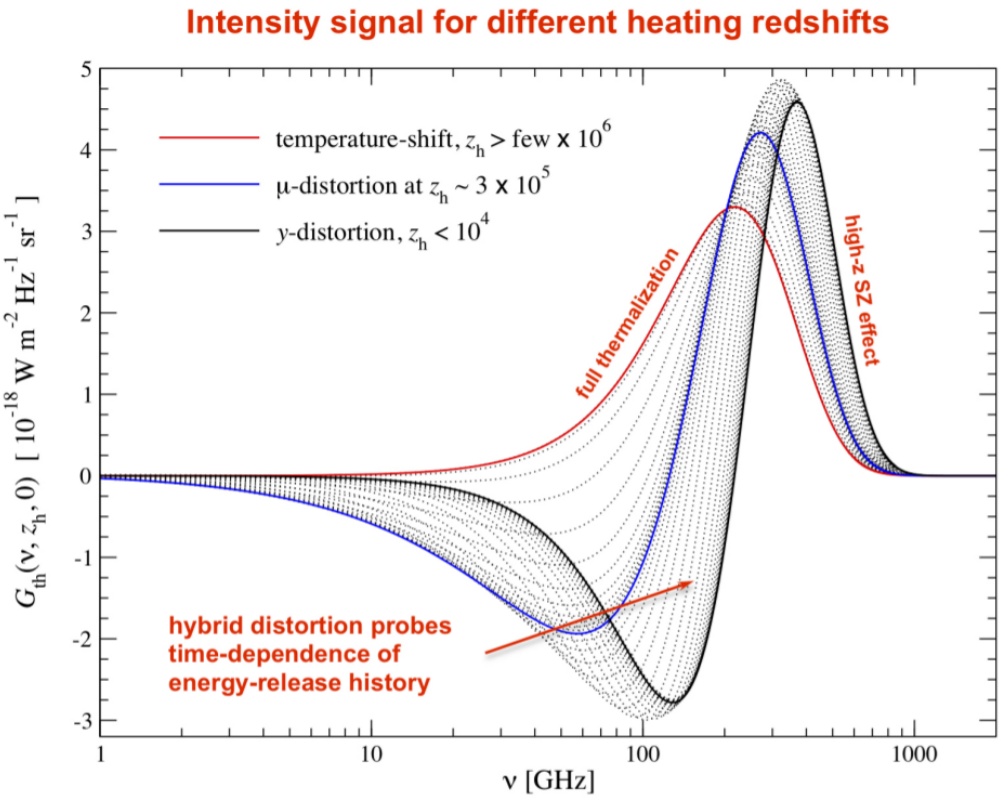

Figure 3.2: Change in the CMB spectrum due to energy release at different heating redshifts z_h. At $z \gtrsim$ few $\times\, 10^6$, a temperature shift is created. μ and y type of distortions formed, respectively, around $z \simeq 3 \times 10^5$ and at $z \lesssim 10^4$. Intermediate distortions contain information about the time-dependence of the energy-release process [5].

3.2.4 Distortion visibility functions

In general, the total distortion of the photon spectrum is given by

$$\Delta n \simeq y Y_{\rm SZ} + \mu_0 M \,. \tag{3.52}$$

In order to calculate each contribution to the energy density, it is necessary to evaluate how the photon distribution changes throughout the thermal history of the Universe. This information is encoded in the collision operator of the Boltzmann equation [118]. Following [6], let us start integrate the Boltzmann equation, which gives

$$\begin{aligned}
\dot{Q} &\equiv \int d^3p\, E C[n] = \int d^3p\, E \frac{dn}{dt} = \int dp\, 4\pi p^3 \frac{dn}{dt} \\
&= \int dp\, 4\pi p^3 \left[\left(\frac{\partial n}{\partial t}\right)_p - Hp \left(\frac{\partial n}{\partial p}\right)_t \right] = \frac{\partial \rho}{\partial t} - 4\pi H \int dp\, p^4 \left(\frac{\partial n}{\partial p}\right)_t \\
&= \frac{\partial \rho}{\partial t} - 4\pi H [p^4 n]\Big|_0^\infty + 4 \cdot 4\pi H \int dp\, p^3 n \\
&= \frac{\partial \rho}{\partial t} + 4H\rho \,,
\end{aligned} \tag{3.53}$$

where the contribution $4\pi H p^4 n$ goes to zero since the photon distribution vanishes sufficiently rapidly either for $x \longrightarrow 0$ and $x \longrightarrow \infty$. Then,

$$\frac{\partial \rho_\gamma}{\partial t} + 4H\rho_\gamma = \dot{Q} \qquad \Longleftrightarrow \qquad \frac{1}{a^4}\frac{\partial(\rho_\gamma a^4)}{\partial t} = \dot{Q}\,. \tag{3.54}$$

This represents a differential equation whose solution can be written as

$$\rho_\gamma(t) = \rho_{\rm z}(t) + \Delta\rho(t)\,. \tag{3.55}$$

The homogeneous solution $\rho_{\rm z}(t)$ can be found setting the right-hand side of the previous equation equal to zero and so it corresponds to the background solution, without any heating. Therefore, it evolves as $\rho_{\rm z}(t) \propto a^{-4}$. On the contrary, the particular solution $\Delta\rho(t)$ is given by

$$\Delta\rho(t) = \frac{1}{a^4}\int_0^t a^4 \dot{Q} d\tilde{t} = \rho_{\rm z}(t)\int_0^t \frac{\dot{Q}}{\rho_{\rm z}(\tilde{t})} d\tilde{t}\,. \tag{3.56}$$

Hence, the total change in energy density turns out to be

$$\left.\frac{\Delta\rho}{\rho_\gamma}\right|_{\rm tot} = \frac{\Delta\rho(t_0)}{\rho_{\rm z}(t_0)} = \int_0^t \frac{\dot{Q}}{\rho_{\rm z}(\tilde{t})} d\tilde{t} = \int_z^\infty \frac{\dot{Q}}{(1+z)H\rho_{\rm z}} dz\,, \tag{3.57}$$

where it has been used the relation $dz = -(1+z)Hdt$. In conclusion,

$$\frac{\Delta\rho(t)}{\rho_{\rm z}(t)} = \int_z^\infty \frac{\dot{Q}}{(1+z)H\rho_{\rm z}} dz = \int_z^\infty \frac{dQ/dz}{\rho_{\rm z}} dz\,. \tag{3.58}$$

From Eq. (3.54), using $\rho(z) \propto a^{-4}$ and $\rho_\gamma(t) = \rho_{\rm z}(t) + \Delta\rho(t)$, we can show that

$$\begin{aligned}\frac{\dot{Q}}{\rho_{\rm z}} &= \frac{1}{a^4}\frac{\partial(\rho_\gamma a^4)}{\partial t}\frac{1}{\rho_{\rm z}} = \frac{1}{\rho_{z,0}}\frac{\partial(\rho_\gamma a^4)}{\partial t} = \frac{\partial}{\partial t}\left(\frac{\rho_\gamma}{\rho_{\rm z}}\right) \\ &= \frac{\partial}{\partial t}\left(1 + \frac{\Delta\rho}{\rho_{\rm z}}\right) = \frac{\partial}{\partial t}\left(\frac{\Delta\rho}{\rho_{\rm z}}\right).\end{aligned} \tag{3.59}$$

During the thermal evolution of the Universe, any injection of energy is redistributed in a different way according to the processes causing the number count change and to the efficiency of the Compton scattering [6]. In order to determine how much of this energy give rise to each of the distortions, for a generic distortion of type a it is possible to define the branching ratio of deposited energy into the distortion itself as

$$\left.\frac{\Delta\rho_\gamma}{\rho_\gamma}\right|_a \equiv \int \frac{dQ/dz}{\rho_\gamma}\mathcal{J}_a(z) dz\,, \tag{3.60}$$

with $\mathcal{J}_a(z)$ indicating the fractional energy release into a given distortion a as a function of redshift z. This is a useful split, since one can recognize a model-dependent heating function, dQ/dz, and a model independent branching ratios, $\mathcal{J}_a(z)$. To evaluate the shape

of the branching ratios, there are different approaches which lead to different levels of accuracy (for more details, see e.g. [6]). On the whole, the y- and μ-distortions can be written as [5]

$$y \simeq \frac{1}{4}\frac{\Delta\rho_\gamma}{\rho_\gamma}\bigg|_y = \frac{1}{4}\int_0^\infty \frac{dQ/dz'}{\rho_\gamma}\mathcal{J}_y(z')dz' \tag{3.61a}$$

$$\mu \simeq 1.401\frac{\Delta\rho_\gamma}{\rho_\gamma}\bigg|_\mu = 1.401\int_0^\infty \frac{dQ/dz'}{\rho_\gamma}\mathcal{J}_\mu(z')dz' \,. \tag{3.61b}$$

In particular, notice that in the previous analysis there has not been included the photon production by double Compton scattering and Bremsstrahlung. This will be of particular relevance for the evolution of μ-distortions, since not all energy release or photon production eventually is visible as a distortion. This means that the distortion visibility function is smaller than unity because thermalization reduces the effective amount of energy release that survives as a distortion [5]. Including both Bremsstrahlung and double Compton scattering processes in the μ-distortion era (for a more detailed discussion, see [119]), one can write the approximate solution of the Kompaneet's equation as

$$\mu(z, x_\mathrm{e}) \simeq \mu_0(z)e^{-x_\mathrm{c}(z)/x_\mathrm{e}} \,, \tag{3.62}$$

where the critical frequency x_c is usually $x_\mathrm{c}(z) \simeq 10^{-3}$ during the thermalization period [105, 120]. Notice that at $x_\mathrm{e} \gg x_\mathrm{c}$, the chemical potential becomes constant, $\mu(z, x_\mathrm{e}) \simeq \mu_0(z)$, while at low frequencies it vanishes exponentially, leading to a blackbody at the temperature of the electrons. Thereafter, it is possible to approximate μ as constant, which is valid everywhere except deep into the Rayleigh-Jeans tail.

3.3 Dissipation of primordial acoustic modes

As already mentioned, there exist several physical mechanisms that lead to spectral distortion, covering both standard and non-standard processes. Having a particular physical mechanism for energy release in mind, one can specify the energy injection rate associated to this process. Among all these processes, we focus on the dissipation of primordial acoustic modes (see e.g. [79, 121, 122]). The physics behind this mechanism is simple and based on the fact that the mixing of blackbodies with different temperatures does not produce a purely blackbody spectrum [123]. The distortions is sensitive to the amplitude and the shape of the power spectrum at very small scales, corresponding to $1\ \mathrm{Mpc}^{-1} \lesssim k \lesssim 2\times10^4\ \mathrm{Mpc}^{-1}$. In particular, perturbation modes with $1\ \mathrm{Mpc}^{-1} \lesssim k \lesssim 50\ \mathrm{Mpc}^{-1}$ lead to y-distortions, while modes with $50\ \mathrm{Mpc}^{-1} \lesssim k \lesssim 2\times10^4\ \mathrm{Mpc}^{-1}$ lead to μ-distortions. These scales are inaccessible with any other means; this is the reason why CMB spectral distortions provide a promising way for constraining inflation.

During the radiation-dominated era, photons from different phases of the sound waves, characterized by different temperatures, diffuse through the plasma of baryons and electrons and mix together. This causes the dissipation of the sound waves and gives rise to spectral distortions in the CMB [123]. Let us consider the sum of two blackbodies, with temperature $T_1 = T + \delta T$ and $T_2 = T - \delta T$, where $\delta T \ll T$. Therefore, the average temperature is T. By mixing these two blackbodies, keeping terms of the second order, the resulting average energy density is [124]

$$\begin{aligned}\rho_{av} &= a_R\left(\frac{T_1^4 + T_2^4}{2}\right) = a_R T^4\left[\frac{\left(1+\frac{\delta T}{T}\right)^4 + \left(1-\frac{\delta T}{T}\right)^4}{2}\right] \\ &\simeq a_R T^4\left[1 + 6\left(\frac{\delta T}{T}\right)^2\right] > a_R T^4\,,\end{aligned} \tag{3.63}$$

where a_R is the radiation constant and $a_R T^4$ is the energy density of a blackbody of temperature T. In the same way, it is possible to derive the average photon number density,

$$\begin{aligned}N_{av} &= b_R\left(\frac{T_1^3 + T_2^3}{2}\right) = b_R T^3\left[\frac{\left(1+\frac{\delta T}{T}\right)^3 + \left(1-\frac{\delta T}{T}\right)^3}{2}\right] \\ &\simeq b_R T^3\left[1 + 3\left(\frac{\delta T}{T}\right)^2\right] > b_R T^3\,,\end{aligned} \tag{3.64}$$

with $b_R T^3$ giving the number density of photons of a blackbody at temperature T. Therefore, one can notice that the resulting new spectrum is characterized by an energy and a number density which are larger than the ones of the blackbody at the average temperature T. The effective temperature and energy density of a blackbody characterized by N_{av} and ρ_{av} are given by

$$T_{\rm BB} = \left(\frac{N_{av}}{b_R}\right)^{\frac{1}{3}} \simeq T\left[1 + 3\left(\frac{\delta T}{T}\right)^2\right]^{\frac{1}{3}} \simeq T\left[1 + \left(\frac{\delta T}{T}\right)^2\right] \tag{3.65a}$$

$$\rho_{\rm BB} = a_R T_{\rm BB}^4 \simeq a_R T^4\left[1 + \left(\frac{\delta T}{T}\right)^2\right]^4 \simeq a_R T^4\left[1 + 4\left(\frac{\delta T}{T}\right)^2\right] < \rho_{av}\,. \tag{3.65b}$$

The excess energy density turns out to be

$$\begin{aligned}\Delta\rho_{y|\mu} &= \rho_{av} - \rho_{BB} \\ &= a_R T^4\left[1 + 6\left(\frac{\delta T}{T}\right)^2 - 1 - 4\left(\frac{\delta T}{T}\right)^2\right] = a_R T^4\left[2\left(\frac{\delta T}{T}\right)^2\right],\end{aligned} \tag{3.66}$$

which leads to a y-type spectral distortion with [124]

$$y \simeq \frac{1}{4}\frac{\Delta\rho}{\rho} \simeq \frac{1}{4}\frac{2\left(\frac{\delta T}{T}\right)^2}{1+4\left(\frac{\delta T}{T}\right)^2} \simeq \frac{1}{2}\left(\frac{\delta T}{T}\right)^2 . \tag{3.67}$$

Moreover, since at $z \gtrsim 5\times 10^4$ this distortion is quickly converted into a μ-type, the spectrum relaxes to Bose-Einstein distribution with chemical potential

$$\mu \simeq 1.4\frac{\Delta\rho}{\rho} \simeq 2.8\left(\frac{\delta T}{T}\right)^2 . \tag{3.68}$$

A crucial quantity in the determination of spectral distortions is the *effective heating rate*, defined as the fractional energy release Q relative to the photon energy density $\rho_\gamma(z)$. The explicit expression for the effective heating rate from scalar perturbations is given by

$$\begin{aligned}\frac{d(Q/\rho_\gamma)}{dt} \simeq 4\dot{\tau}\int \frac{dkk^2}{2\pi^2}P_\zeta(k)\Bigg[&\frac{(3\Theta_1 - v)^2}{3} \\ &+ \frac{9}{2}\Theta_2^2 - \frac{1}{2}\Theta_2\left[\Theta_0^{\rm P} + \Theta_2^{\rm P}\right] + \sum_{\ell\geq 3}(2\ell+1)|\Theta_\ell|^2\Bigg] ,\end{aligned} \tag{3.69}$$

where $\dot{\tau} = \sigma_{\rm T} n_{\rm e} c$ is the rate of Thomson scattering, Θ_ℓ and $\Theta_\ell^{\rm P}$ denote, respectively, the photon temperature and polarization transfer functions and v the baryon velocity transfer function [125]. Here, one has to take into account that only 1/3 of the dissipated energy sources spectral distortions. For more details and a more accurate description of the expression of the effective heating rate, see [123–125]. Just say that the first term in the previous expression mixes the blackbodies in the dipole resulting in transfer of heat along the temperature gradient, then corresponding to the effect of thermal conductivity. The second mixes the blackbodies in the quadrupole and can be identified as the effect of shear viscosity. The third term takes into account the polarization dependence of the Compton scattering and it is a correction to the shear viscosity [126]. These three terms constitute the main contribution to the dissipation of sound waves.

We conclude by stressing once again that CMB spectral distortions could add a new dimension to CMB science, probing the the thermal history at different stages of the Universe, providing complementary and independent information about, e.g., various models of inflation, decaying particles and other exotic sources of distortions, in synergy with CMB anisotropy studies. In particular, the damping signal is also sensitive to primordial non-Gaussianity in the squeezed limit, leading to spatially varying spectral signal which correlates with CMB temperature anisotropies as large angular scales [91, 92]. This provides a unique way to study the scale dependence of the $f_{\rm NL}$ parameter.

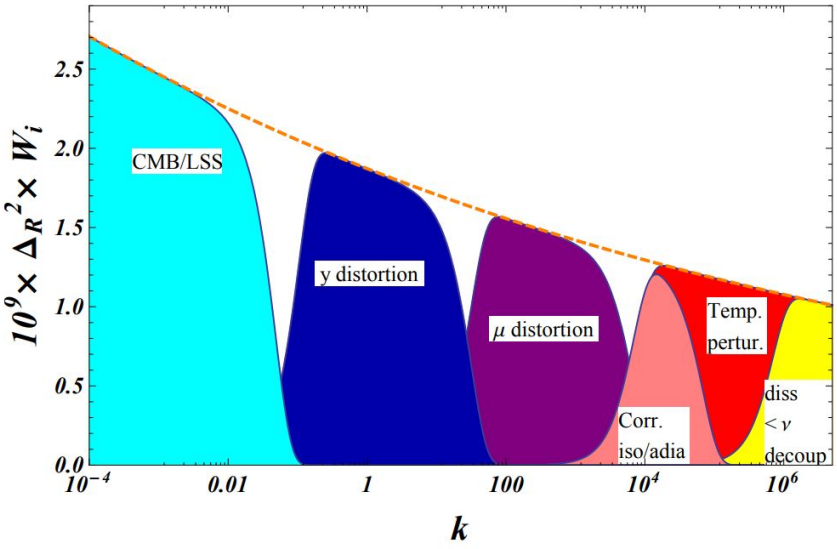

Figure 3.3: Different k-space windows responsible for different observable. In particular, CMB anisotropies are visible for $k \lesssim 0.1$ Mpc^{-1}, with the cut-off at small-scale derived by the Silk damping. Compton y-type distortions are formed by the damping of modes with 1 Mpc$^{-1} \lesssim k \lesssim 50$ Mpc^{-1}, while μ-distortions derived by modes with 50 Mpc$^{-1} \lesssim k \lesssim 10^4$ Mpc^{-1}. Here, R is an alternative variable to indicate the primordial curvature perturbation (Fig. taken from [13]).

3.3.1 Insight on μ-distortion

As known, it is very difficult to accurately probe the initial conditions of the Universe, due to a complicated and often non-linear evolution of the adiabatic modes until today. However, measurements of the μ-type distortion of the CMB spectrum could provide a unique opportunity to probe these scales over the unexplored range 50 Mpc$^{-1} \lesssim k \lesssim 10^4$ Mpc^{-1} (see Fig. 3.3). For our purposes, we will focus on the energy injection coming from the dissipation of acoustic waves of the adiabatic modes, that is a Silk damping (see Section 2.2), as these re-enter the horizon and start oscillating. For the moment, neglecting all other sources or assuming that they lead to smaller and then negligible distortions, the μ-distortion caused by Silk damping is the only relevant signal.

The redshifts of interest are $z_{\mu,f} = 5 \times 10^4 \lesssim z \lesssim 10^6 = z_{\mu,i}$. Recalling the expression of the diffusion damping scale $k_{\rm D}(z)$, Eq. (2.3), one can write [91]

$$\begin{aligned} k_{\rm D} &\equiv \left[\int_z^\infty dz \frac{1+z}{6(1+R)n_{\rm e}\sigma_{\rm T}H}\left[\frac{R^2}{(1+R)}+\frac{16}{15}\right]\right]^{-1/2} \\ &\simeq \left[\int_z^\infty dz \frac{1+z}{6n_{\rm e}\sigma_{\rm T}H}\left(\frac{16}{15}\right)\right]^{-1/2} \\ &\simeq \left[\int_z^\infty dz \frac{8(1+z)}{45n_{\rm e}\sigma_{\rm T}H}\right]^{-1/2} \\ &\simeq (1+z)^{3/2} 4.1 \times 10^{-6}\ \text{Mpc}^{-1}\,, \end{aligned} \tag{3.70}$$

since $R = 3\rho_{\rm B}/4\rho_\gamma \ll 1$. In this case, it results $k_{\rm D}(z_{\mu,i}) \simeq 12000$ Mpc^{-1} and $k_{\rm D}(z_{\mu,f}) \simeq 46$ Mpc^{-1} [12].

Moreover, in order to evaluate the energy injection due to damping of acoustic waves, let us consider the energy density in acoustic waves in the photon-baryon plasma (neglecting the baryon energy density), given by [91]

$$Q = \frac{\rho_\gamma \langle \delta_\gamma(x)^2 \rangle_{\rm P} c_s^2}{1 + c_s^2}, \tag{3.71}$$

where ρ_γ is the energy density (indicated in this way since at this time the Universe is dominated by radiation), $\delta_\gamma = \delta\rho_\gamma/\bar{\rho}_\gamma$ is the dimensionless amplitude of perturbations averaged of a period P and $c_s \simeq 1/3$ is the sound speed. Then,

$$\frac{\delta E}{E} \simeq -\int_{z_{\mu,i}}^{z_{\mu,f}} \frac{d}{dz}\frac{Q}{\rho_\gamma} \simeq \frac{1}{4}\langle \delta_\gamma(x)^2 \rangle_{\rm P}\Big|_{z_{\mu,i}}^{z_{\mu,f}}. \tag{3.72}$$

This heat generated by diffusion damping is converted into a μ-distortion given by

$$\mu \simeq \frac{1.4}{4}\left[\langle \delta_\gamma^2(z) \rangle_{\rm P}\right]_{z_{\rm f}}^{z_{\rm i}}, \tag{3.73}$$

where $\langle \delta_\gamma^2(z) \rangle_{\rm P}$ represents the density fluctuations affecting μ, averaged over an oscillation period,

$$\langle \delta_\gamma^2(\mathbf{x}) \rangle_{\rm P} \simeq 1.45 \int \frac{d^3k_1 d^3k_2}{(2\pi)^6} \zeta(k_1)\zeta(k_2)\langle \Delta_\gamma(k_1)\Delta_\gamma(k_2) \rangle_{\rm P} e^{i(\mathbf{k}_1+\mathbf{k}_2)\cdot\mathbf{x}}. \tag{3.74}$$

The numerical coefficient has been added to consider the contribution of neutrinos [127]. Δ_γ represents the photon transfer function: a good approximation for that is to write it as an oscillating term times a decreasing exponential term which reproduces the Silk damping (see e.g. [128]) and so

$$\Delta_\gamma(k) \simeq 3\cos(kr)e^{-k^2/k_{\rm D}^2(z)}, \tag{3.75}$$

with the damping wavenumber $k_{\rm D}$ defined as in Eq. (3.70) [19] and

$$kr = \int_0^t \frac{k dt'}{a\sqrt{3(1+R)}} \simeq \frac{2kt}{a\sqrt{3}}, \tag{3.76}$$

with r indicating the physical distance so that kr is dimensionless. An important final comment is that, as one can notice in Eq. (3.74), μ is not linear but it is intrinsically of second order in the primordial curvature perturbation ζ. Hence, it results

$$\begin{aligned}\mu(\mathbf{x}) &\simeq \frac{1.4}{4}\cdot 1.45\int\frac{d^3k_1d^3k_2}{(2\pi)^6}\zeta(k_1)\zeta(k_2)\langle\Delta_\gamma(k_1)\Delta_\gamma(k_2)\rangle_{\rm P}e^{i(\mathbf{k}_1+\mathbf{k}_2)\cdot\mathbf{x}}\Big|_{z_{\rm f}}^{z_{\rm i}}\\ &\simeq \frac{2}{4}\cdot 9\int\frac{d^3k_1d^3k_2}{(2\pi)^6}\zeta(k_1)\zeta(k_2)\langle\cos(k_1r)\cdot\cos(k_2r)\rangle_{\rm P}e^{i(\mathbf{k}_1+\mathbf{k}_2)\cdot\mathbf{x}}\left[e^{-(k_1^2+k_2^2)/k_{\rm D}^2}\right]_{z_{\rm f}}^{z_{\rm i}}\\ &\simeq \frac{9}{4}\int\frac{d^3k_1d^3k_2}{(2\pi)^6}\zeta(k_1)\zeta(k_2)W\left(\frac{k_3}{k_{\rm s}}\right)\left[e^{-(k_1^2+k_2^2)/k_{\rm D}^2}\right]_{z_{\rm f}}^{z_{\rm i}}\\ &\simeq \int\frac{d^3k_1d^3k_2}{(2\pi)^6}\zeta(k_1)\zeta(k_2)f(k_1,k_2,k_3)e^{-i\mathbf{k}_3\cdot\mathbf{x}}\,,\end{aligned}\tag{3.77}$$

with

$$f(k_1,k_2,k_3)\equiv\frac{9}{4}W\left(\frac{k_3}{k_{\rm s}}\right)\left[e^{-(k_1^2+k_2^2)/k_{\rm D}^2}\right]_{z_{\rm f}}^{z_{\rm i}},\tag{3.78}$$

and where $W(k_3/k_{\rm s})$ is the Fourier transform of the top-hat filter in real space

$$W(x)=\frac{3j_1(x)}{x}=\frac{3}{x}\left[\frac{\sin(x)}{x^2}-\frac{\cos(x)}{x}\right]=3x^{-3}[\sin(x)-x\cos(x)]\,,\tag{3.79}$$

which smears the dissipated energy over a volume of radius $k_{\rm s}^{-1}\gtrsim k_{{\rm D},f}^{-1}$ [19, 91]. Notice that it has been imposed $\mathbf{k}_1+\mathbf{k}_2+\mathbf{k}_3=0$.

Now, it could be also interesting to evaluate the ensemble average of the μ-distortion. Recalling how we defined the power spectrum of density perturbations in Eq. (1.63) and Eq. (1.64), we can write the power spectrum of ζ as

$$\langle\zeta(\mathbf{k}_1)\zeta(\mathbf{k}_2)\rangle=(2\pi)^{(3)}\delta^{(3)}(\mathbf{k}_1+\mathbf{k}_2)P_\zeta(k_1)\tag{3.80a}$$

$$P_\zeta(k_1)=\frac{2\pi^2\Delta_\zeta^2(k_1)}{k_1^3}\,.\tag{3.80b}$$

Due to the Dirac delta, in Eq. (3.77) it occurs that $k_3\longrightarrow 0$ and so $W(k_3/k_{\rm s})\simeq 1$ and $e^{-i\mathbf{k}_3\cdot\mathbf{x}}\simeq 1$. Taking the expectation value of Eq. (3.77),

$$\begin{aligned}\langle\mu(x)\rangle &\simeq \frac{9}{4}\int\frac{d^3k}{4\pi}\frac{\Delta_\zeta^2(k)}{k^3}\left[e^{-2k^2/k_{\rm D}^2}\right]_{z_{\rm f}}^{z_{\rm i}}\\ &\simeq 2.3\int d\log k\,\Delta_\zeta^2(k)\left[e^{-2k^2/k_{\rm D}^2}\right]_{z_{\rm f}}^{z_{\rm i}}.\end{aligned}\tag{3.81}$$

It represents the log-integral of the primordial power spectrum from $z_{\mu,i}$ to $z_{\mu,f}$. In particular, using $n_s\simeq 0.96$ (according to the best fit of the *Planck* data [36]) and then $\Delta_\zeta^2(k)\simeq\Delta_\zeta^2(k_0)\simeq 2.4\times10^{-9}$, it results $\langle\mu\rangle\simeq 1.9\times10^{-8}$ [13].

3.4 CMB spectral distortions as a probe of primordial non-Gaussianity

As we mentioned in Section 1.5.2, among the various primordial non-Gaussianity shapes, one of the most relevant is the so called local-model bispectrum, which can be described as a spatial modulation of the small-scale, i.e., large wavenumber, power spectrum by long-wavelength density fluctuations. For instance, local-model non-Gaussianity can be constrained observing the CMB (see e.g. [69, 129, 130]) and the large-scale structure (e.g. [131]). While this model predicts a scale-independent spatial modulation, many variants could show some scale-dependence [13]; up to date, we can only set upper limits. In particular, it has been shown that μT and yT correlations can probe the scale-dependence of non-Gaussianity. In fact, since y and μ type probe different wavenumbers (see Fig. 3.3), the relative strength of the yT and μT correlations can be used to probe scale dependence of primordial non-Gaussianity at wavenumbers 1 $\mathrm{Mpc}^{-1} \lesssim k \lesssim 10^4$ Mpc^{-1}, far smaller than those accessible with CMB temperature fluctuations, galaxy surveys or 21cm observations [132].

In the following, we will focus on the derivation of the μT cross-correlation. In the squeezed limit, if the long wavelength curvature perturbation, which also gives rise to large-angle temperature fluctuations, modulates the amplitude of the small-scale distortions, then a μT correlation is induced [13, 133]. In order to relate with observations, both the $\mu(\hat{\mathbf{x}})$ and $T(\hat{\mathbf{x}})$, which are direction dependent, are decomposed in spherical harmonics on the surface of a sphere, i.e., the last scattering surface. The coefficients for the temperature multipoles expansion have already been calculated in Section 2.3. In a similar way, one can decompose μ into spherical harmonics,

$$\mu(\hat{\mathbf{x}}) = \sum_{\ell=0}^{\infty} \sum_{m=-\ell}^{\ell} a^{\mu}_{\ell m}(\mathbf{x}, \eta) Y_{\ell m}(\hat{\mathbf{x}})\,. \tag{3.82}$$

Therefore, recalling Eq. (3.77), the projection of $\mu(\mathbf{x})$ on the last scattering surface leads to

$$\begin{aligned}
a^{\mu}_{\ell m} &= \int d\hat{\mathbf{n}}\, \mu(\hat{\mathbf{n}}) Y^*_{\ell m}(\hat{\mathbf{n}}) \\
&= \int d\hat{\mathbf{n}} \int \frac{d^3k_1 d^3k_2}{(2\pi)^6} \zeta(\mathbf{k}_1)\zeta(\mathbf{k}_2) f(k_1, k_2, k_3) e^{-i\mathbf{k}_3\cdot\mathbf{x}}\, Y^*_{\ell m}(\hat{\mathbf{n}}) \\
&= \int d\hat{\mathbf{n}} \int \frac{d^3k_1 d^3k_2}{(2\pi)^6} \zeta(\mathbf{k}_1)\zeta(\mathbf{k}_2) f(k_1, k_2, k_3) \\
&\quad \times \sum_{\ell'} i^{\ell'} 4\pi j_{\ell'}(k_3 r_{\mathrm{LS}}) \sum_{m'=\ell'}^{\ell'} (-1)^{\ell'} Y^*_{\ell' m'}(\hat{\mathbf{k}}_3) Y_{\ell' m'}(\hat{\mathbf{n}}) Y^*_{\ell m}(\hat{\mathbf{n}})
\end{aligned}$$

$$
\begin{aligned}
&= 4\pi \int \frac{d^3k_1 d^3k_2}{(2\pi)^6} \zeta(\mathbf{k}_1)\zeta(\mathbf{k}_2) f(k_1,k_2,k_3) \\
&\quad \times \sum_{\ell'} (-i)^{\ell'} j_{\ell'}(k_3 r_{\rm LS}) \sum_{m'=\ell'}^{\ell'} Y^*_{\ell' m'}(\hat{\mathbf{k}}_3)\delta_{\ell\ell'}\delta_{mm'} \\
&= 4\pi(-i)^{\ell} \int \frac{d^3k_1 d^3k_2}{(2\pi)^6} \zeta(\mathbf{k}_1)\zeta(\mathbf{k}_2) f(k_1,k_2,k_3) j_{\ell}(k_3 r_{\rm LS}) Y^*_{\ell m}(\hat{\mathbf{k}}_3)\,. \qquad (3.83)
\end{aligned}
$$

The cross-correlation between CMB temperature anisotropy and μ-distortions leads to

$$
\begin{aligned}
\langle a^{\mu}_{\ell_1 m_1} a^{T}_{\ell_2 m_2}\rangle &= 4\pi(-i)^{\ell_1}\frac{12}{5}\pi i^{\ell_2} \int \frac{d^3k_1 d^3k_2}{(2\pi)^6} f(k_1,k_2,k_3) j_{\ell_1}(k_3 r_{\rm LS}) Y^*_{\ell_1 m_1}(\hat{\mathbf{k}}_3) \\
&\quad \times \int \frac{d^3k}{(2\pi)^3} \mathcal{T}_{\ell_2}(k) Y^*_{\ell_2 m_2}(\hat{\rm k}) \langle \zeta(\mathbf{k}_1)\zeta(\mathbf{k}_2)\zeta(\mathbf{k})\rangle\,. \qquad (3.84)
\end{aligned}
$$

This result is not surprising. In fact, as already noted, $\mu \propto \zeta^2$ and then, since $T \propto \zeta$, we expected that $\mu T \propto \zeta^3$, at lowest order.

In order to obtain constraints on the non-Gaussian parameter $f_{\rm NL}$, let us remember Eq. (1.75). However, restricting to the squeezed limit configuration, this expression simplifies into Eq. (1.77). Moreover, let us also remember that

$$
f(k_1,k_2,k_3) \equiv \frac{9}{4} W\left(\frac{k_3}{k_{\rm s}}\right)\left[e^{-(k_1^2+k_2^2)/k_{\rm D}^2}\right]_{z_{\rm f}}^{z_{\rm i}}. \qquad (3.85)
$$

In order to estimate a lower bound on the μ-distortion, let us take $k_{\rm s}$ to be $k_{\rm D}(z_{\rm f})$ and then the transfer function $f(k_1,k_2,k_3)$ filters the squeezed-limit signals, satisfying $k_1, k_2 > k_{\rm D}(z_{\rm f}) > k_3$ [12]. Thus, the transfer function simplifies to

$$
f(k_1) = \frac{9}{4}\left[e^{-2k_1^2/k_{\rm D}^2}\right]_{z_{\rm f}}^{z_{\rm i}}. \qquad (3.86)
$$

Therefore,

$$
\begin{aligned}
\langle a^{\mu}_{\ell_1 m_1} a^{T}_{\ell_2 m_2}\rangle &\simeq -\frac{48}{5}\pi^2(-i)^{\ell_1} i^{\ell_2} \int \frac{d^3k_1 d^3k_2}{(2\pi)^6} f(k_1) j_{\ell_1}(k_3 r_{\rm LS}) Y^*_{\ell_1 m_1}(\hat{\mathbf{k}}_3) \\
&\quad \times \int \frac{d^3k}{(2\pi)^3} \mathcal{T}_{\ell_2}(k) Y^*_{\ell_2 m_2}(\hat{\mathbf{k}}) (2\pi)^3 \delta^3(\mathbf{k}_1+\mathbf{k}_2+\mathbf{k}) \frac{12}{5} f_{\rm NL} P(k_1) P(k) \\
&= -\frac{48}{5}\frac{12}{5}\pi^2 i^{\ell_2-\ell_1} \int \frac{d^3k_1 d^3k_3}{(2\pi)^6} f(k_1) j_{\ell_1}(k_3 r_{\rm LS}) Y^*_{\ell_1 m_1}(\hat{\mathbf{k}}_3) \\
&\quad \times \mathcal{T}_{\ell_2}(k_3) Y^*_{\ell_2 m_2}(\hat{\mathbf{k}}_3) f_{\rm NL} P(k_1) P(k_3) \\
&= -\frac{36}{25} i^{\ell_2-\ell_1} \int \frac{d^3k_1}{2\pi^2} \int \frac{dk_3 k_3^2 d\hat{\mathbf{k}}_3}{2\pi^2} Y^*_{\ell_1 m_1}(\hat{\mathbf{k}}_3) Y^*_{\ell_2 m_2}(\hat{\mathbf{k}}_3) \mathcal{T}_{\ell_2}(k_3) j_{\ell_1}(k_3 r_{\rm LS}) \\
&\quad \times f(k_1) f_{\rm NL} P(k_1) P(k_3)\,. \qquad (3.87)
\end{aligned}
$$

Normalized spherical harmonic functions satisfy

$$Y^*_{\ell m}(\hat{\mathbf{n}}) = (-1)^m Y_{\ell -m}(\hat{\mathbf{n}})\,. \tag{3.88}$$

Then,

$$\begin{aligned}\int d\hat{\mathbf{k}}_3\, Y^*_{\ell_1 m_1}(\hat{\mathbf{k}}_3) Y^*_{\ell_2 m_2}(\hat{\mathbf{k}}_3) &= \int d\hat{\mathbf{k}}_3\, (-1)^{m_1} Y_{\ell_1 -m_1}(\hat{\mathbf{k}}_3) Y^*_{\ell_2 m_2}(\hat{\mathbf{k}}_3) \\ &= (-1)^{m_1}\delta_{\ell_1\ell_2}\delta_{m_1 -m_2}\,,\end{aligned} \tag{3.89}$$

and therefore, taking also the SW approximation, $\mathcal{T}_{\ell_2}(k_3) \longrightarrow -j_{\ell_2}(k_3 r_{\rm LS})/3$, Eq. (3.87) becomes

$$\begin{aligned}\langle a^{\mu}_{\ell_1 m_1} a^{T}_{\ell_2 m_2}\rangle &\simeq -\frac{36}{25}(-1)^{m_1}\int \frac{dk_1 k_1^2}{2\pi^2} 4\pi \int \frac{dk_3 k_3^2}{2\pi^2}\mathcal{T}_{\ell_1}(k_3) j_{\ell_1}(k_3 r_{\rm LS}) \\ &\quad \times f(k_1) f_{\rm NL}\frac{2\pi^2}{k_1^3}\Delta^2_{\zeta}(k_1)\frac{2\pi^2}{k_3^3}\Delta^2_{\zeta}(k_3)\delta_{\ell_1\ell_2}\delta_{m_1 -m_2} \\ &= -\frac{48}{25}\pi(-1)^{m_1}\int\frac{dk_1}{k_1}\int\frac{dk_3}{k_3} j^2_{\ell_1}(k_3 r_{\rm LS}) f(k_1) f_{\rm NL}\Delta^2_{\zeta}(k_1)\Delta^2_{\zeta}(k_3)\delta_{\ell_1\ell_2}\delta_{m_1 -m_2} \\ &= 12(-1)^{m_1}\left[\frac{4\pi}{25}\int\frac{dk_3}{k_3} j^2_{\ell_1}(k_3 r_{\rm LS})\Delta^2_{\zeta}(k_3)\right]\int\frac{dk_1}{k_1} f(k_1) f_{\rm NL}\Delta^2_{\zeta}(k_1)\delta_{\ell_1\ell_2}\delta_{m_1 -m_2} \\ &= 12(-1)^{m_1} C^{TT,{\rm SW}}_{\ell_1}\int\frac{dk_1}{k_1} f(k_1) f_{\rm NL}\Delta^2_{\zeta}(k_1)\delta_{\ell_1\ell_2}\delta_{m_1 -m_2}\,.\end{aligned} \tag{3.90}$$

Recalling Eq. (3.86) and Eq. (3.81), Eq. (3.90) becomes

$$\begin{aligned}C^{\mu T}_{\ell} &\simeq 12(-1)^{m_1} C^{TT,{\rm SW}}_{\ell}\int d\log k_1 \frac{9}{4}\left[e^{-2k_1^2/k_{\rm D}^2}\right]^{z_{\rm i}}_{z_{\rm f}} f_{\rm NL}\Delta^2_{\zeta}(k_1) \\ &\simeq 12(-1)^{m_1} C^{TT,{\rm SW}}_{\ell} f_{\rm NL}\langle\mu(x)\rangle\,.\end{aligned} \tag{3.91}$$

As one can notice, $C^{\mu T}_{\ell} \propto f_{\rm NL}$ in the squeezed limit. This result has been pointed out in several papers (e.g. [12, 91, 92, 134]) and it is now well established.

Another approach to derive the previous result is offered by the configuration-space description of the local-model of non-Gaussianity. In this case, the power spectrum $\Delta^2_{\zeta}(k_{\rm s}, \mathbf{x})$, with $k_{\rm s}$ indicating small-scale modes, will be different from one causal patch at position $\mathbf{x}$ to another. The fluctuation will be correlated with the long wavelength curvature fluctuation. Following [13], the local-model curvature perturbation at position $\mathbf{x}$ can be written as

$$\zeta(\mathbf{x}) = \zeta_{\rm g}(\mathbf{x}) + \frac{3}{5} f_{\rm NL}\zeta^2_{\rm g}(\mathbf{x})\,, \tag{3.92}$$

where $\zeta_{\rm g}(\mathbf{x})$ indicates a Gaussian random variable. Then, it is possible to split

$$\zeta(\mathbf{x}) = \zeta_{\rm L}(\mathbf{x}) + \zeta_{\rm s}(\mathbf{x})\,, \tag{3.93}$$

where $\zeta_{\rm L}(\mathbf{x})$ is the contribution coming from long wavelength Fourier modes of the $\zeta(\mathbf{x})$ perturbation, while $\zeta_{\rm s}(\mathbf{x})$ the one from short wavelength Fourier modes. Similarly,

$$\zeta_{\rm g}(\mathbf{x}) = \zeta_{\rm gL}(\mathbf{x}) + \zeta_{\rm gs}(\mathbf{x}). \tag{3.94}$$

From Eq. (3.92), one can write

$$\zeta_{\rm L} + \zeta_{\rm s} = \zeta_{\rm gL} + \zeta_{\rm gs} + \frac{3}{5} f_{\rm NL}\left[\zeta_{\rm gL}^2 + 2\zeta_{\rm gL}\zeta_{\rm gs} + \zeta_{\rm gs}^2\right]. \tag{3.95}$$

Notice that, for some fixed long wavelength curvature fluctuation $\zeta_{\rm L}$, the small-scale curvature fluctuation is, to linear order in $f_{\rm NL}$,

$$\zeta_{\rm s} = \zeta_{\rm gs}\left[1 + \frac{6}{5} f_{\rm NL}\zeta_{\rm L}\right]. \tag{3.96}$$

Therefore, the fraction change in small-scale power within a region with fixed long wavelength curvature perturbation turns out to be

$$\frac{\delta\langle\zeta^2\rangle}{\langle\zeta^2\rangle} \simeq \frac{12}{5} f_{\rm NL}\zeta_{\rm L}\,. \tag{3.97}$$

Given this result, one can deduce that, with local-model non-Gaussianity, the fractional μ-distortion in a given region is modulated by the long-wavelength curvature perturbation in that region at the surface of last scattering [13]. The same can be said for large-angle temperature fluctuations, mainly determined by the curvature perturbations at the surface of last scattering and with $\Delta T/T \simeq \zeta/5$. Thus, the cross-correlation between the fractional μ-distortion $\Delta\mu/\mu \simeq \delta\langle\zeta^2\rangle/\langle\zeta^2\rangle$ and the temperature anisotropies $\Delta T/T$ results [13, 91]

$$C_\ell^{\mu T} \simeq 12 f_{\rm NL} C_\ell^{TT}\,. \tag{3.98}$$

Notice that this corresponds to the already obtained result, Eq. (3.91), with the difference that there the $C_\ell^{\mu T}$ was for the μ-distortion, here for the fractional μ-distortion. This result has been pointed out in several papers in the literature [12, 91, 92, 134] and extended also to trispectra (four-point correlation functions) [66].

Chapter 4

Tensor fossils from Inflation

Cosmological observations are in agreement with the single-field slow-roll inflation as the source of the density perturbations in the CMB and the origins of structures in the Universe [36, 69, 135]. We are here referring to the simplest standard models of inflation, namely those where the accelerated expansion in the early Universe is driven by a single slowly-rolling scalar. However, there could be other types of fields, i.e., additional scalar, vector and tensor modes which could play a role during inflation in a distinguishable way, see, e.g. [9]. For that reason, it would be important to search for their observational imprints. At the very least we know that tensor [1] modes should be unavoidably generated during inflation and therefore, they are very interesting. Indeed recently there has been an increasing effort in searching for the imprints of the gravitational waves (GWs) in the CMB [136–138], nevertheless there was no detection of primordial tensor modes.

As already known, random curvature fluctuations in the Universe are almost Gaussian and they can be described by the power-spectrum which is statistically homogeneous and isotropic. A a nearly scale-invariant power spectrum of almost Gaussian primordial curvature perturbation is a very generic prediction of single-field inflation with a slow-roll attractor solution [51, 52, 69, 139, 140]. However, while the phenomenology is universal and very predictive, it could be that the physics of inflation is richer than the characterization of the single-field slow-roll model. In particular, one might think that a single scalar field is not the only physical degree of freedom relevant around the energy scale of inflation. For example, in many inflationary models, extra particle fields are introduced in order to explain some problems of the elementary particle physics, such as UV completion, naturalness or supersymmetry [141–143]. Therefore, new fields might play a role in extensions of single-field inflation paradigm (e.g. [144–149]). The majority of alternative scenarios (for instance, see [148–152]) predict complex statistics different from the nearly Gaussian one for single-field slow-roll inflation. This constitutes a powerful tool to

[1] In literature, the tensor is also known as *graviton*, which indicates the particle associated to the tensor fluctuations.

investigate inflationary dynamics through inhomogeneities in the late-time Universe [47, 69].

In particular, different inflationary models can correlate small-scale density (curvature) perturbations with long-wavelength GWs through the tensor-scalar-scalar bispectrum. This correlation affects the mass-distribution in the Universe, leading to off-diagonal two-point correlation function between different Fourier modes of the density fluctuations in the form of the quadrupole anisotropy. Interestingly, this effect survives even after the tensor modes decay when they re-enter the horizon, known as the fossil effect. Models of single field slow-roll inflation generically predict a very small quadrupole anisotropy in the tensor-scalar-scalar bispectrum, while in models of multiple fields inflation this effect can be observable. Therefore, this quadrupole anisotropy can be thought as a way to discern different inflationary models.

Supposing to have density perturbations, of small wavelength, and a tensor mode, which is the long wavelength mode, then one can consider the tensor-scalar-scalar three-point function in the squeezed limit. It results that this bispectrum reduces to a power spectrum with a quadrupole anisotropy. Subsequently, one should consider the non-linear evolution of this bispectrum during the radiation and matter dominated eras and also the projection effects, in order to deal with the observed mass distribution [2] [11, 153, 154]. These different contributions must be taken into account in the evaluation of the observed power spectrum of the mass distribution in the Universe. However, only the primordial distortion depends on the specific inflationary model and one can consider only the primordial bispectrum, neglecting the non-linear and projection effects [11]. It has been claimed that for single-field slow-roll inflation models (and, more in general, for all models which satisfy the Maldacena's consistency condition [51]), all these effects are of the same order and they cancel each other out, making the quadrupole amplitude not observable. Thus, it could be very interesting to go beyond these models and see how the violation of the consistency relation appears in the observed power spectrum (for instance, see [155–158]) [3].

In the following, the extra field will be named as *fossil* field, in the sense that there are no direct cosmological trace of it at late-time, unlike CMB anisotropies and large-scale structure. Nevertheless, although there is no direct cosmological or astrophysical evidence for any new field in the low redshift Universe, this does not imply they do not leave any indirect signature. In fact, these fossil fields may interact significantly with the primordial curvature perturbations during inflation and may alter their statistical properties. In particular, one fossil mode might cross-correlate with curvature perturbations in a primordial

[2] One can find the position of the galaxies by using their apparent position and redshift in the sky. However, the apparent position will be affected by the presence of the tensor mode and it will not be the same as the original position of the object.

[3] However, notice that such a claim has been recently criticized, in. e.g. [159]. However, for the purposes of this Thesis, what it will matter is the general expression for the tensor-scalar-scalar bispectrum.

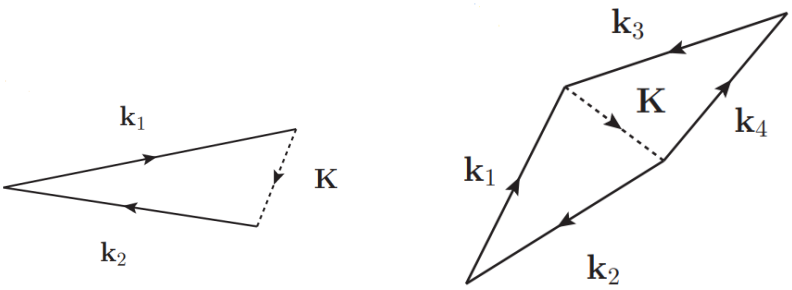

(a) Bispectrum involving two Fourier scalar modes of the curvature perturbation, for a given realization of the fossil field.

(b) Trispectrum for the curvature perturbation induced by an internal mode of the fossil field.

Figure 4.1: Representation of the primordial correlations of scalar perturbations by the extra tensor field. Solid lines represent the curvature perturbation, dashed ones represent the fossil field. Image credit [10].

fossil-scalar-scalar bispectrum, as shown in Fig. 4.1a, leading to a modulation of the curvature two-point correlation. This causes an apparent breaking of statistical isotropy in the curvature perturbation.

4.1 Consistency relations

In Section 1.5.2, we considered the most general configuration for the three momenta of the perturbation modes. In particular, Ref. [51] sets the main results about both scalars and tensors bispectrum functions of the primordial perturbations. In the following, we will focus on the squeezed limit, that we remember is the case in which one of the three momenta is much smaller than the other two, for instance, $k_3 \ll k_1 \simeq k_2$. In this configuration, k_3 crosses the horizon much earlier than the other two modes and, when the two modes k_1, k_2 cross the horizon, k_3 is already constant. Its only effect is to make the k_1, k_2 modes cross the horizon at a slightly different time [51, 156]. Before going on, let us briefly outline the consistency relations for scalars and tensors.

For the three-point scalar correlation function, in the squeezed limit, one gets [51]

$$\langle\zeta(\mathbf{k}_1)\zeta(\mathbf{k}_2)\zeta(\mathbf{k}_3)\rangle \simeq -(n_s-1)\langle\zeta(\mathbf{k}_3)\zeta(-\mathbf{k}_3)\rangle\langle\zeta(\mathbf{k}_1)\zeta(\mathbf{k}_2)\rangle\,, \tag{4.1}$$

where n_s is the scalar spectral index and the (n_s-1) measures the deviation from a scale invariant power spectrum. Eq. (4.1) is the so-called consistency relation for the scalar perturbations, which holds in a more general case of single-field slow-roll model [68]. For a complete review of the validity of these consistency relations, see e.g. [55, 59, 160, 161]. Here, we briefly report the main steps of the proof of the leading order scalar consistency relation.

In the squeezed limit, the long-wavelength mode $\zeta(\mathbf{k}_3)$ leaves the horizon much earlier than the other two and so it acts as a constant background for them. The bispectrum can be calculated in two steps. First one has to compute the two-point function $\langle\zeta(\mathbf{k}_1)\zeta(\mathbf{k}_2)\rangle$ in the presence of a background $\zeta_{\rm B}(\mathbf{k})$, i.e., $\langle\zeta(\mathbf{k}_1)\zeta(\mathbf{k}_2)\rangle_{\zeta_{\rm B}(\mathbf{k})}$. Then, this two-point function has to be averaged over all possible realizations of the background,

$$\langle\zeta(\mathbf{k}_1)\zeta(\mathbf{k}_2)\zeta(\mathbf{k}_3)\rangle \simeq \langle\zeta(\mathbf{k}_3)\langle\zeta(\mathbf{k}_1)\zeta(\mathbf{k}_2)\rangle_{\zeta_{\rm B}(\mathbf{k})}\rangle\,. \tag{4.2}$$

Therefore, the function $\langle\zeta(\mathbf{k}_1)\zeta(\mathbf{k}_2)\rangle_{\zeta_{\rm B}(\mathbf{k})}$ needs to be conveniently computed. In real space, if the background is assumed to be homogeneous (i.e., $\zeta_{\rm B}(\mathbf{k}) \equiv \zeta_{\rm B}$), it can be reabsorbed by rescaling the coordinates, $\tilde{x}^i = e^{\zeta_{\rm B}} x^i$; after such rescaling, the two-point function in the new coordinates is the same as in the absence of $\zeta_{\rm B}$. In the limit of $\zeta_{\rm B}$ constant,

$$\langle\zeta(\mathbf{x}_1)\zeta(\mathbf{x}_2)\rangle_{\zeta_{\rm B}} = \langle\zeta(\mathbf{x}_1)\zeta(\mathbf{x}_2)\rangle\,. \tag{4.3}$$

When $\zeta_{\rm B}$ varies slowly, it is convenient to evaluate this correlation function in the middle point $\mathbf{x}_c = (\mathbf{x}_1 + \mathbf{x}_2)/2$, assumption which is meaningful if the correlation scale is smaller than the typical variation scale of the long mode. Hence, at linear order in $\zeta_{\rm B}$, the two-point function can be written as [160]

$$\langle\zeta(\mathbf{x}_1)\zeta(\mathbf{x}_2)\rangle_{\zeta_{\rm B}} \simeq \langle\zeta(\mathbf{x}_1)\zeta(\mathbf{x}_2)\rangle + \zeta_{\rm B}(\mathbf{x}_c)\frac{d}{d\zeta_{\rm B}}\langle\zeta(\mathbf{x}_1)\zeta(\mathbf{x}_2)\rangle\,. \tag{4.4}$$

Here, $\langle\zeta(\mathbf{x}_1)\zeta(\mathbf{x}_2)\rangle$ is the two-point function computed in the vacuum state, equal to

$$\langle\zeta(\mathbf{x}_1)\zeta(\mathbf{x}_2)\rangle = \int \frac{d^3k_{\rm s}}{(2\pi)^3} e^{i\mathbf{k}_{\rm s}\cdot(\mathbf{x}_2-\mathbf{x}_1)} P_\zeta(k_{\rm s})\,, \tag{4.5}$$

where $\mathbf{x}_{\rm s} = (\mathbf{x}_1 - \mathbf{x}_2)/2$. Following [59, 160], Fourier-transforming, one finally obtains

$$\langle\zeta(\mathbf{k}_1)\zeta(\mathbf{k}_2)\zeta(\mathbf{k}_3)\rangle \simeq (2\pi)^3\delta^{(3)}(\mathbf{k}_1+\mathbf{k}_2+\mathbf{k}_3)(n_s-1)P_\zeta(k_{\rm L})P_\zeta(k_{\rm s})\,, \tag{4.6}$$

where $\mathbf{k}_{\rm L} = \mathbf{k}_1 + \mathbf{k}_2$ and $\mathbf{k}_{\rm s} = (\mathbf{k}_1 - \mathbf{k}_2)/2$.

We said in Section 1.5.2 that the theoretical prediction about the non-Gaussianity in single-field slow-roll models of inflation is very small, much smaller of the present observable constraints. This implies an objective difficulty at present in testing the validity or the violation of the consistency relation Eq. (4.1) for these models with adequate precision. However, it should be noted that a violation of the consistency relation would rule out all the standard single-field models of inflation. For this reason, a great deal of research has been done in searching new models which violate these conditions.

In Ref. [51] the consistency relation involving also the tensor degrees of freedom in the squeezed limit have been similarly obtained. However, we will focus on the three-point

correlation function which involves two scalar modes and one tensor mode. In the squeezed limit $k_3 \ll k_1 \simeq k_2$, the consistency relation takes the form [51]

$$\langle\zeta(\mathbf{k}_1)\zeta(\mathbf{k}_2)h^p(\mathbf{k}_3)\rangle \simeq -(2\pi)^3\langle h^p(\mathbf{k}_3)h^p(-\mathbf{k}_3)\rangle\epsilon^p_{ij}(\mathbf{k}_3)k_1^i k_2^j\frac{\partial}{\partial k_1^2}\langle\zeta(\mathbf{k}_1)\zeta(\mathbf{k}_2)\rangle\,, \tag{4.7}$$

where $\epsilon^p_{ij}(\mathbf{k}_3)$ is the the polarization tensor. The effect of such a tensor mode on the scalar perturbation would be to modulate the power spectrum of the scalar perturbation when they cross the horizon. Ref. [68] points out that this effect can be reabsorbed by a simple coordinate redefinition. However, as already mentioned, this is a sensitive topic that needs to be treated carefully. Another expression for the tensor-scalar-scalar consistency relation in the squeezed limit is given by (see e.g. [11, 156] and Refs. therein)

$$\langle\zeta(\mathbf{k}_1)\zeta(\mathbf{k}_2)h^p(\mathbf{K})\rangle \overset{K\ll k_1\simeq k_2}{\longrightarrow} (2\pi)^3\delta^{(3)}(\mathbf{k}_1+\mathbf{k}_2+\mathbf{K})\frac{1}{2}\frac{d\ln P_\zeta}{d\ln k}\epsilon^p_{ij}(\mathbf{K})\hat{k}_{1i}\hat{k}_{2j}P_h(K)P_\zeta(k)\,, \tag{4.8}$$

where $\mathbf{K} = \mathbf{k}_3$ indicates the long-wavelength tensor mode and $\mathbf{k} = (\mathbf{k}_1 + \mathbf{k}_2)/2$. This expression of the bispectrum will be resumed later for our calculations.

To conclude, let us stress again that an observation of the violation of the consistency relation would exclude single-field models of inflation. In the following we will study a possible indirect way to observe the gravitational wave background, i.e., tensor fossils, which allows us a more precise reconstruction of what happened in the early Universe.

4.2 Primordial Gravitational Waves

Before getting to the heart of our discussion, let us briefly see how to parameterize GWs. In the basic inflationary scenario the fields involved in the dynamics of the Universe are the inflaton and the metric tensor, which describes the gravitational degrees of freedom. It is possible to consider in such a scenario the fluctuations of these fields and study their dynamics (see e.g. [162]). To get the dynamical equations for the perturbations, it is necessary to perturb tensor objects, the metric and the stress-energy tensor. The most useful way to do it consists in decomposing perturbations in parts which have well-defined transformation properties with respect to the underlying three-dimensional space [162]. The spatially flat, homogeneous and isotropic background space-time possesses a great deal of symmetry. These symmetries allow a decomposition of the metric and the stress-energy perturbations into independent scalar, vector and tensor components. We will focus on the perturbations of the metric tensor.

The different components of the perturbed spatially flat FRW metric can be decomposed as [52, 163]

$$g_{00} = -a^2(\eta)\left[1 + 2\sum_{r=1}^{\infty}\frac{1}{r!}\psi^{(r)}\right] \tag{4.9a}$$

$$g_{0i} = a^2(\eta)\sum_{r=1}^{\infty}\frac{1}{r!}\omega_i^{(r)} \tag{4.9b}$$

$$g_{ij} = a^2(\eta)\left\{\left[1 - 2\sum_{r=1}^{\infty}\frac{1}{r!}\phi^{(r)}\right]\delta_{ij} + \sum_{r=1}^{\infty}\frac{1}{r!}h_{ij}^{(r)}\right\}, \tag{4.9c}$$

where $d\eta = dt/a(t)$ is the conformal time, r indicates the order of the perturbation and $\psi^{(r)}$, $\omega^{(r)}$, $\phi^{(r)}$ and $h_{ij}^{(r)}$ are the r^{th}-order perturbations of the metric. We focus on linear first order perturbations, $r = 1$, thus we can drop the index.

It is common to decompose these perturbations into the so-called scalar, vector and tensor part, according to their transformation properties under spatial rotations. The scalar (or longitudinal) part includes the functions ψ and ϕ, related to the scalar potential. Exploiting the Helmholtz theorem, the vector (or divergence-free) parts can be decomposed as

$$\omega_i = \partial_i\omega^{\parallel} + \omega_i^{\perp}\,, \tag{4.10}$$

where the first term represents the scalar contribution and the second one the vector part, meaning $\partial^i\omega_i^{\perp} = 0$. Similarly, the traceless perturbation, which encodes tensor perturbations, can be written as

$$h_{ij} = D_{ij}h^{\parallel} + \partial_i h_j^{\perp} + \partial_j h_i^{\perp} + h_{ij}^{T}\,, \tag{4.11}$$

where $h^{\parallel}$ is a suitable scalar function, $h_i^{\perp}$ represents a vector field and h_{ij}^{T} is the tensor part, which is transverse and traceless ($\partial^i h_{ij}^{T} = 0$, $h^{Ti}{}_{i} = 0$). D_{ij} is a trace-free operator defined as

$$D_{ij} = \partial_i\partial_j - \frac{1}{3}\delta_{ij}\nabla^2\,. \tag{4.12}$$

Therefore, the FLRW metric becomes

$$ds^2 = -(1+2\psi)dt^2 + 2a(t)w_i dx^i dt + a^2(t)[(1-2\phi)\delta_{ij} + h_{ij}]dx^i dx^j\,. \tag{4.13}$$

Here Latin indices are related to the three-dimensional flat space, then $i, j, k, ... = 1, 2, 3$. Moreover, for simplicity of notation, the time dependence of variable is suppressed. For the decomposition of the perturbations of the stress-energy tensor, see for instance [162].

The inflaton and metric perturbations have to be studied at the same time. Then, one has to manipulate perturbations of objects which live on a manifold, such as the stress-energy tensor, and at the same time consider the perturbation of the manifold itself, described by the metric tensor. This leads to the so-called *gauge problem* [164]. Let us

consider a generic tensor field T; a generic perturbation ΔT of the tensor field is usually defined as the difference between the value that T assumes in the physical perturbed space-time and the value T_0 which it has in the given background space-time. Thus, these two tensors are defined on two different varieties, the physical and the background space-times [162]. For the comparison of tensors to be meaningful, they have to be considered at the same point. Therefore, it is necessary a prescription for identifying points of these varieties, that is a one-to-one correspondence between the background and the physical space-time, known as *gauge choice*. A change in the correspondence between physical and background points, keeping the background coordinates fixed, is known as a *gauge transformation*. Generally, the standard procedure consists in finding the relation between quantities defined in several gauges and then constructing variables, which describe the physical quantities, that do not change under gauge transformations. These objects are said *gauge-invariant*. Tensor perturbations h_{ij} are referred to as gauge-invariant objects at linear order [162].

The recent detection of GWs has opened a new era in cosmology. There has been an increasing interest in primordial gravitational waves background and in constraining its properties. Now, let us briefly review their main features (see e.g. [8, 165–167]). The evolution of GWs is described by the linearized Einstein equation,

$$\ddot{h}_{ij} + 3H\dot{h}_{ij} - \frac{\nabla^2}{a^2}h_{ij} = 16\pi G\Pi_{ij}^{TT}\,, \tag{4.14}$$

where the (double) dot represents the (second) derivative with respect to the cosmic time t and G is the Newton's gravitational constant. The right-hand side of the equation encodes the source of the GWs; Π_{ij}^{TT} represents the transverse-traceless part of the anisotropic stress Π_{ij}. The latter is defined in terms of the spatial components of the stress-energy tensor T_{ij}, of the metric tensor g_{ij} and of the background homogeneous pressure p [165],

$$a^2\Pi_{ij} = T_{ij} - pg_{ij}\,. \tag{4.15}$$

Characterizing the physical properties of the stochastic gravitational waves background is a key to identify and distinguish the sources of GWs. h_{ij} can be conveniently decomposed into Fourier modes as following [168],

$$h_{ij}(t,\mathbf{x}) = \int \frac{d^3k}{(2\pi)^3}e^{i\mathbf{k}\cdot\mathbf{x}}\sum_{\lambda=\pm 2}h^{\lambda}(t,\mathbf{k})e_{ij}^{\lambda}(\mathbf{k})\,, \tag{4.16}$$

where $\lambda = \{+,\times\}$ and $e_{ij}^{\lambda}(\mathbf{k})$ are the spin-2 polarization tensors satisfying the normalization conditions

$$e_{ij}^{\lambda}e^{\lambda',ij} = 2\delta_{\lambda\lambda'}\,. \tag{4.17}$$

The gravitational wave background is originated from the quantum fluctuations during inflation. For modes far outside the horizon ($k \ll aH$), the source term and the third term of the left-hand side of Eq. (4.14) can be neglected, implying $h \propto const.$ When these modes reenter the horizon ($k > aH$), they start to evolve according to Eq. (4.14) and the solution of the equation, in terms of Fourier modes, can be written as

$$h^{\lambda}(t, \mathbf{k}) = h^{\lambda}_{\rm prim}(t, \mathbf{k}) \mathcal{T}_{\rm GW}(k, t)\,, \tag{4.18}$$

where $h^{\lambda}_{\rm prim}$ represents the amplitude of the primordial tensor perturbations and $\mathcal{T}_{\rm GW}$ is the GW transfer function. For single-field slow-roll inflation, at linear order, the source term is vanishing. The evolution of the modes inside the horizon is $\mathcal{T}_{\rm GW} \propto e^{\pm ik\eta}/a$, where η is the conformal time (recall the definition $d\eta = dt/a$).

The energy density of the relic GWs is given by

$$\rho_{\rm GW}(t) = \frac{1}{32\pi G} \langle h'_{ij}(t, \mathbf{x}) h'_{ij}(t, \mathbf{x}) \rangle\,, \tag{4.19}$$

where the prime denotes conformal time derivative. The spectrum of GWs is described in terms of the fractional energy density per unit frequency [167],

$$\begin{aligned} \Omega_{\rm GW}(k, \eta) &= \frac{1}{\rho_c(\eta)} \frac{\partial \rho_{\rm GW}(k, \eta)}{\partial \ln k} \\ &= \frac{P_h(k)}{12 a^2(\eta) H^2(\eta)} \left[\mathcal{T}'_{\rm GW}(k, \eta)\right]^2, \end{aligned} \tag{4.20}$$

where $P_h(k)$ is the tensor power spectrum and $\rho_c = 3H^2/8\pi G$ is the critical energy density of the Universe (for more details, see e.g. [169–172]). Given that now we have two different polarization states for the tensor perturbations, it is possible to define the tensor power spectrum as

$$P_h(k) = \frac{k^3}{2\pi^2} \sum_{\lambda = \pm 2} \left| h^{\lambda}_{\rm prim}(t, \mathbf{k}) \right|^2, \tag{4.21}$$

so that on super-horizon scales the following power spectrum holds [162]

$$P_h(k) = \frac{8}{M^2_{\rm Pl}} \left(\frac{H}{2\pi}\right)^2 \left(\frac{k}{aH}\right)^{2\epsilon}, \tag{4.22}$$

where ϵ is the slow-roll parameter and $M_{\rm Pl} = \sqrt{(\hbar c)/4\pi G} \simeq 2.4 \times 10^{18}$ GeV is the reduced Planck mass [165].

In analogy with the scalar perturbations, Eq. (1.67), it is useful to parameterize the tensor power spectrum as

$$P_h(k) = A_h \left(\frac{k}{k_0}\right)^{n_{\rm T}}, \tag{4.23}$$

where A_h is the tensor amplitude at some pivot scale k_0 and $n_{\rm T}$ is the spectral index for

the tensor perturbation, given by

$$n_{\rm T} = \frac{d\ln P_h}{d\ln k} = -2\epsilon\,. \tag{4.24}$$

In single-field model of inflation, $n_{\rm T} = -2\epsilon < 0$. In this case, the power spectrum is said to be *red*, while for $n_{\rm T} > 0$ is *blue*. Having defined this, it is also possible to introduce the *tensor-to-scalar ratio*,

$$r \equiv \frac{A_\zeta}{A_h}\,, \tag{4.25}$$

which yields the amplitude of the GWs with respect to that of the scalar perturbation at some fixed pivot scale k_0. This allows us to define an interesting consistency relation between quantities which involve tensor perturbations. At horizon crossing,

$$A_\zeta = \left(\frac{H^2}{2\pi\dot\varphi}\right)^2 \tag{4.26a}$$

$$A_h = \frac{8}{M_{\rm Pl}^2}\left(\frac{H}{2\pi}\right)^2, \tag{4.26b}$$

and, since it is possible to show that $\dot H = -4\pi G\dot\varphi^2$, one gets

$$r = 16\epsilon\,, \tag{4.27}$$

or, analogously, at the lowest order in slow-roll parameters, one finds the following consistency relation [173]

$$r = -8n_{\rm T}\,. \tag{4.28}$$

This equality can be checked only with a measurement of the tensor power spectrum, that is not only of its amplitude, but also of its spectral index. Thus, if this relation holds true, it will be very hard to measure any scale dependence of the tensors, since a large spectral index would invalidate the consistency relation [162]. Assuming the consistency relation, an actual upper bound on the tensor-to-scalar ratio is $r_{0.002} < 0.0056$ (95% CL) [36], where the subscript indicates the pivot scale in Mpc^{-1} units.

To conclude this Section, let us say that primordial GWs represent a very interesting tool to constrain different aspects of the early Universe. For instance, they can be used to test and constrain single-field slow-roll inflation. If the single-field slow-roll paradigm holds, GWs would provide an estimate of the fundamental scales involved. In particular, since during inflation $H^2 \simeq V(\varphi)/(3M_{\rm Pl})^2$, one finds that the amplitude of GWs scales as

$$A_h = \frac{2}{3\pi^2}\frac{V(\varphi)}{M_{\rm Pl}^4}\,. \tag{4.29}$$

From this, it is possible to define the energy scale of inflation,

$$E_{\rm inf} = V^{1/4}. \tag{4.30}$$

Thus, the amplitude of the primordial GWs is directly proportional to the energy scale at which inflation took place. This is a fundamental point: observing GWs, in the context of single field slow-roll models, would entail constraints on the inflationary period. Moreover, thanks to the consistency relation, it is possible to give an estimation of this scale energy [36]

$$E_{\rm inf} = V^{1/4} \simeq 1.6 \times 10^{16}\ {\rm GeV}\Big(\frac{r}{0.10}\Big)^{1/4} \qquad (95\%\ {\rm CL})\,. \tag{4.31}$$

Notice that constraining r is equivalent to provide the energy scale of inflation. A measurement of the primordial GWs would be crucial for the description of the primordial Universe.

4.3 Inflationary fossils from primordial Universe

A possible indirect probe of primordial GWs would be through the effect of them on the curvature perturbation power spectrum. The main effect of a long-wavelength GW on the curvature perturbation power spectrum is that the long-wavelength tensor mode can be seen as a change of coordinates with respect to the standard cosmic frame, in which homogeneity and isotropy hold (e.g., see [174]). As we will see, the net effect of the tensor mode will be a local departure from statistical isotropy. If during inflation the inflaton couples to a new degree of freedom, the fossil field, which could be a scalar, a vector o a tensor field, this interaction induces a fossil-scalar-scalar bispectrum. This inflationary fossil does not interact or interacts very weakly at late times and the only observable effects is its imprint in the primordial curvature perturbations. In particular, tensor fossils refer to long-wavelength relic GWs from inflation and they are the fields on which we will focus in the following study.

Let us consider the interaction between the curvature perturbation ζ and a tensor fossil field h. This could generate a bispectrum $\langle\zeta\zeta h\rangle$ at horizon crossing. Following [9–11], let us consider two Fourier modes of primordial scalar perturbations, whose wave vectors are indicated with lower-case $\mathbf{k}$'s, and a plane wave of generic fossil field h, having wave vector $\mathbf{K}$ and polarization p. The most general form for the fossil-scalar-scalar bispectrum is given by [9, 10]

$$\langle\zeta(\mathbf{k}_1)\zeta(\mathbf{k}_2)h_p(\mathbf{K})\rangle = (2\pi)^3\delta^{(3)}(\mathbf{k}_1+\mathbf{k}_2+\mathbf{K})f^p(k_1,k_2,K)[h^p(\mathbf{K})]^*\epsilon^p_{ij}(\mathbf{K})\hat{k}^i_1\hat{k}^j_2\,. \tag{4.32}$$

Here, f^p is a generic bispectrum shape function, connected to the bispectrum as

$$B^p(\mathbf{k}_1, \mathbf{k}_2, \mathbf{K}) = P_h^p(K) f^p(k_1, k_2, K) \epsilon_{ij}^p(\mathbf{K}) k_1^i k_2^j \,, \tag{4.33}$$

where P_h^p is the isotropic power spectrum for the fossil field. Eq. (4.32) implies a modulation of the observable two-point correlation function, due to the presence of the fossil field. Thus, as for the notation, an equivalent mathematical expression for the bispectrum is $\langle \zeta(\mathbf{k}_1)\zeta(\mathbf{k}_2)\rangle_{h_p(\mathbf{K})}$. The notation $\langle \dots \rangle_h$ denotes correlations computed for a given tensor perturbation realization.

In general, the fossil field could be a scalar field, a vector field or a spin-2 tensor field; $\epsilon_{ij}^p(\mathbf{K})$ indicates the symmetric 3×3 polarization tensor, where the index p labels the six orthogonal polarization states, $p = +, -, 0, z, x, y$. This tensor satisfies the orthonormality condition $\epsilon_{ij}^p \epsilon^{p',ij} = 2\delta_{pp'}$. Each state describes a different polarization of the perturbation, producing a local departure from homogeneity and statistical isotropy. They can be [9]:

TWO SCALAR MODES	$\epsilon_{ij}^0 \propto \delta_{ij}$
	$\epsilon_{ij}^z \propto K_i K_j - \frac{1}{3} K^2 \delta_{ij}$
TWO TRANSVERSE-VECTOR MODES[4]	$\epsilon_{ij}^{x.y} \propto K^{(i} w^{j)}$ with $K^i w^i = 0$
TWO TRANSVERSE TRACELESS MODES	$\epsilon_+,\ \epsilon_\times$

where w_i is a perpendicular, unit vector $w_i K^i = 0$ [175]. Notice that the transverse traceless modes correspond to the tensor mode, which has its polarization completely perpendicular to the direction of propagation, i.e., $K^i \epsilon_{ij}^p(\mathbf{K}) = 0$. Moreover, the $\epsilon_{ij}^p \hat{k}_1^i \hat{k}_2^j$ term in Eq. (4.32) is due to the fact that the bispectrum might be linearly proportional to the fossil polarization tensor ϵ_{ij}^p, since the superposition of two different polarization states is also a possible polarization state. This tensorial structure determines the polarization dependence of the bispectrum.

Meaning of polarization In order to understand the meaning of these six polarization states, let us consider the case in which the long-mode $\mathbf{K}$ is along the $\hat{\mathbf{z}}$ direction [9]. The only non-vanishing components are $\epsilon_{xx}^+ = -\epsilon_{yy}^+ = 1$ for the $+$ polarization and $\epsilon_{xy}^\times = \epsilon_{yx}^\times = 1$ for the $\times$ polarization. Fig. 4.2 shows the distortions to the scalar two-point correlation function induced by the fossil field which points in the $\hat{\mathbf{z}}$-direction. In particular, the first two polarizations correspond to the two tensor modes $(+, \times)$, i.e., GWs, and represents quadrupolar distortions in the plane transverse to the $\hat{\mathbf{z}}$ direction. Then, the other two

[3]Here the notation $K^{(i}w^{j)}$ stands for

$$K_{(\mu}\omega_{\nu)} = \frac{1}{2}[K_\mu \omega_\nu + K_\nu \omega_\mu] \,,$$

and similar for upper indices.

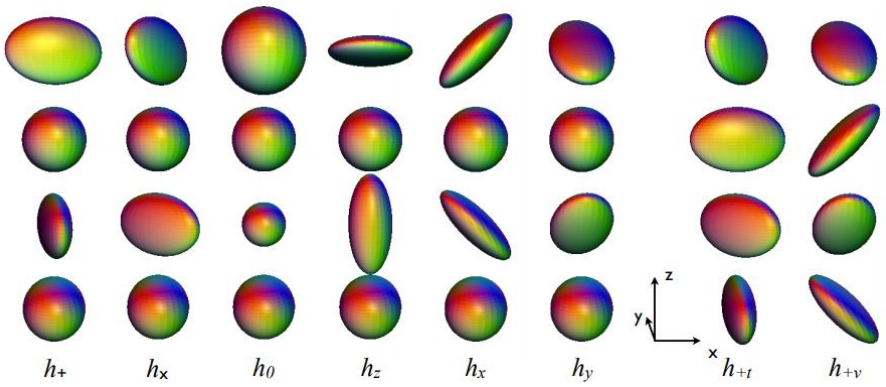

Figure 4.2: Polarizations induced to a statistically isotropic two-point correlation function (Fig. edit from [9]). On the left, the six orthogonal polarization states, $p = +, \times, 0, z, x, y$, are reported. On the right, there are the circular polarizations of the tensor mode h_{+t} and the vector mode h_{+v}.

modes correspond to the scalar modes which describe a distortion invariant under rotations around the $\hat{\mathbf{z}}$ direction. The scalar mode takes the form $\epsilon^0_{ij} = \sqrt{2/3}\delta_{ij}$ and represent an isotropic modulation. The longitudinal-vector distortion has $\epsilon^z_{ij} \propto \mathrm{diag}(-1, -1, 2)/\sqrt{3}$, indicating a deformation (stretching and compression) along $\hat{\mathbf{z}}$. The (x, y) modes correspond to the vector modes. The only non-vanishing components are $\epsilon^z_{xz} = \epsilon^x_{zx} = 1$ and $\epsilon^y_{yz} = \epsilon^y_{zy} = 1$. They represent deformation, respectively, along $\pm xz$ and $\pm yz$ directions [9].

4.4 Inflationary fossils in CMB

In this Section, the effects of a fossil field on CMB temperature anisotropies will be quantified. Following [10], it is possible to determine estimators for that contribution in terms of bipolar spherical harmonics (BiPoSHs). In order to do that, one can take the advantage of the so-called TAM (total-angular-momentum) formalism to decompose the fields [176, 177], performing an expansion using spherical waves. In the following, after a brief explanation of such formalism, the derivation of estimators for the tensor fossils in the CMB will be summarized.

TAM formalism

It is possible to calculate some estimators for the contribution of the fossil field to the observed CMB temperature anisotropies by using the TAM formalism [176, 178]. One can perform an expansion using spherical waves, useful to exploit the spherical symmetry of the background. These wave functions are eigenfunctions of the total angular momentum J and its third component, M.

Since all cosmological observations are performed on a spherical sky, it could be useful

to decompose the perturbations using spherical functions. Let us consider a scalar field solution of the Helmholtz equation $(\nabla^2 + k^2)\varphi(\mathbf{x}) = 0$, written in terms of plane waves

$$\varphi(\mathbf{x}) = \int \frac{d^3k}{(2\pi)^3}\varphi_{\mathbf{k}} e^{i\mathbf{k}\cdot\mathbf{x}}\,. \tag{4.34}$$

Recall the plane-wave expansion

$$e^{i\mathbf{k}\cdot\mathbf{x}} = \sum_{\ell} 4\pi i^{\ell} j_{\ell}(kr) \sum_{m} Y^{*}_{\ell m}(\hat{\mathbf{k}}) Y_{\ell m}(\hat{\mathbf{n}})\,, \tag{4.35}$$

with $\mathbf{x} = r\hat{\mathbf{n}}$. The TAM basis is defined as

$$\Psi^{k}_{\ell m}(\mathbf{x}) \equiv j_{\ell}(kr) Y_{\ell m}(\hat{\mathbf{n}})\,. \tag{4.36}$$

For the spherical Bessel functions the orthogonality relation is ($\ell > -1$)

$$\int_0^{\infty} dk k^2 j_{\ell}(kr) j_{\ell}(kr') = \frac{\pi}{2r^2}\delta(r - r')\,, \tag{4.37}$$

and the completeness relation for the spherical harmonics is ($0 \leq \vartheta \leq \pi$, $0 \leq \varphi \leq 2\pi$)

$$\sum_{\ell=0}^{\infty}\sum_{m=-\ell}^{\ell} Y^{*}_{\ell m}(\vartheta,\varphi) Y_{\ell m}(\vartheta',\varphi') = \delta(\varphi - \varphi')\delta(\cos\vartheta - \cos\vartheta')\,. \tag{4.38}$$

Therefore, (4.34) becomes

$$\varphi(\mathbf{x}) = \sum_{\ell m}\int \frac{dk k^2}{(2\pi)^3}\varphi_{\ell m}(k) 4\pi i^{\ell}\Psi^{k}_{\ell m}(\mathbf{x})\,, \tag{4.39}$$

with the definition

$$\varphi_{\ell m}(k) = \int d^3x \Big[4\pi i^{\ell}\Psi^{k}_{\ell m}(\mathbf{x})\Big]^{*}\varphi(\mathbf{x})\,. \tag{4.40}$$

Thanks to these angular-momentum dependent coefficient, one can decompose the scalar perturbation ζ. This formalism allows to simplify the calculations, especially in the case of vector and tensor which have to be projected onto two-dimensional sphere. Because of dealing with scalar, vector and tensor fossil degrees of freedom, they can be all incorporated into a symmetric traceless tensor field $h_{ab}(\mathbf{x})$. Then, the longitudinal mode $h^{L}_{JM}(\mathbf{K})$ represents a scalar fossil field, the two divergence-free vectorial modes $h^{VE}_{JM}(\mathbf{K})$ and $h^{VB}_{JM}(\mathbf{K})$ a transverse vector fossil and the two divergence-free tensorial modes $h^{TE}_{JM}(\mathbf{K})$ and $h^{TB}_{JM}(\mathbf{K})$ a transverse-tensorial fossil. Thus, Eq. (4.32) can be rewritten in terms of the TAM modes

as

$$\langle\zeta_{\ell_1 m_1}(k_1)\zeta_{\ell_2 m_2}(k_2)\rangle_{h^\alpha_{JM}(\mathbf{K})} = [h^\alpha_{JM}(K)]^* f^\alpha(k_1,k_2,K)(4\pi)^3(-i)^{\ell_1+\ell_2+J}\frac{1}{K_1 k_2} \times \int d^3x \Big(\nabla^a \Psi^{k_1}_{(\ell_1 m_1)}(\mathbf{x})\Big)\Big(\nabla^b \Psi^{k_2}_{(\ell_2 m_2)}(\mathbf{x})\Big)\Psi^{\alpha,K}_{(JM)ab}(\mathbf{x})\,. \tag{4.41}$$

Here, α indicates a generic mode of the fossil field, i.e., $\alpha = L, VE, VB, TE, TB$. One can notice that a statistically homogeneous and isotropic interaction between scalar and fossil fields would require $f_h^{VE}(k_1,k_2,K) = f_h^{VB}(k_1,k_2,K) = f_h^{V}(k_1,k_2,K)$ and $f_h^{TE}(k_1,k_2,K) = f_h^{TB}(k_1,k_2,K) = f_h^{T}(k_1,k_2,K)$.

CMB Bipolar Spherical Harmonics

Focusing on cross-correlation of CMB temperature, the covariance matrix for multipole moments is diagonal,

$$\langle a^T_{\ell_1 m_1} a^{T*}_{\ell_2 m_2}\rangle = C^{TT}_{\ell_1}\delta_{\ell_1\ell_2}\delta_{m_1 m_2}\,. \tag{4.42}$$

However, long-wavelength tensor fossil would modulate the scalar perturbation. In general, for a given realization of the fossil field which correlates with the initial perturbation, statistical isotropy is explicitly broken. The most general form of the covariant matrix is [10, 179].

$$\begin{aligned}\langle a^T_{\ell_1 m_1} a^{T*}_{\ell_2 m_2}\rangle_h &= \langle a^T_{\ell_1 m_1} a^{T*}_{\ell_2 m_2}\rangle + \Delta h \\ &= C^{TT}_{\ell_1}\delta_{\ell_1\ell_2}\delta_{m_1 m_2} + \sum_{JM}(-1)^{m_2}\langle \ell_1 m_1 \ell_2, -m_2|JM\rangle A^{JM}_{\ell_1\ell_2}\,,\end{aligned} \tag{4.43}$$

where Δh encodes the contribution of the fossil field which breaks isotropy and it has been written through a bipolar spherical harmonics (BiPoSH) expansion. Here, $\langle \ell_1 m_1 \ell_2, -m_2|JM\rangle$ denotes the Clebsh-Gordan coefficients, instead $A^{JM}_{\ell_1\ell_2}$, signal of a violation of statistical isotropy, represents the BiPoSH coefficients, given by

$$A^{JM}_{\ell_1\ell_2} = (-1)^{\ell_1+\ell_2+M}\sqrt{2J+1}\sum_{m_1 m_2}(-1)^{m_2}\begin{pmatrix}\ell_1 & \ell_2 & J\\ m_1 & -m_2 & -M\end{pmatrix}\langle a^T_{\ell_1 m_1} a^{T*}_{\ell_2 m_2}\rangle_h\,. \tag{4.44}$$

The matrix stands for the standard Wigner 3-j symbol (general compact notation $\mathcal{W}^{\ell_1\ell_2\ell_3}_{m_1 m_2 m_3}$), which imposes that BiPoSH components exist only for $|\ell_1 - \ell_2| \leq J \leq \ell_1 + \ell_2$. Since the fossil field is parameterized as asymmetric tensor field, it only reduces the analysis to $J \geq 2$.

The interpretation for the BiPoSH coefficients as a signature for departure from statistical isotropy becomes simple when $J \ll \ell_1, \ell_2$ [175]. They describe power of fluctuation on small angular scales which are spatially modulated by large angular-scale fluctuations. Considering circular hot/cold spots of a typical angular scale, fossil modulation distorts

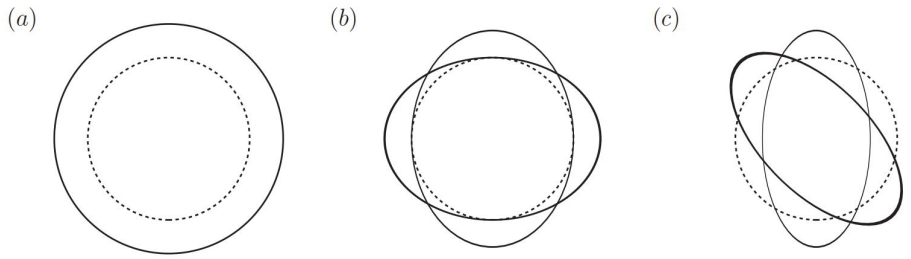

Figure 4.3: Local distorion of hot/cold spots due to the modulation of tensor harmonics [175].

their sizes and shapes. These distortions are proportional to the value of the TAM wave function $\Psi^{\alpha,k}_{(JM)ab}(\mathbf{x})$ on the surface of last scattering, which can be expanded into tensor spherical harmonics $Y^{\alpha}_{(JM)}(\hat{\mathbf{n}})$ [10]. On the two dimensional last scattering surface from a projected perspective, three types of local distortions may arise, as shown in Fig. 4.3. (a) The longitudinal harmonic $Y^{L}_{(JM)ab}(\hat{\mathbf{n}})$ induces a purely radial distortion; isothermal contours expand or shrink in an isotropic way. (b) The vectorial components $Y^{VE,VB}_{(JM)ab}(\hat{\mathbf{n}})$ induce elongation of the isothermal contour along a preferred direction $\hat{\mathbf{n}}$. (c) The transverse tensorial components $Y^{TE,TB}_{(JM)ab}(\hat{\mathbf{n}})$ induce shear of the isothermal contour aligned with a preferred set of perpendicular major axis: the center of hot and cold spots is unchanged, but the spots are elongated along one of the principle directions and squashed along the other. It should be noted that, for a given TAM mode, the previous three types of distortion are usually simultaneously present. Due to a reduced amount of information that can be extracted from a two-dimensional projected survey, scalar, vector and tensor fossil fields cannot be geometrically distinguished, unlike the case of a three-dimensional redshift survey of large-scale structure. For more details, see [10, 175].

Since scalar perturbation sources CMB anisotropies, it is possible to relate the TAM coefficients $\zeta_{\ell m}$ with the CMB temperature multipoles

$$a^{T}_{\ell m} = (-i)^{\ell} \int \frac{dk k^2}{2\pi^2} g^{T}_{\ell}(k) \zeta_{\ell m}(k)\,, \tag{4.45}$$

where $g^{T}_{\ell}(k)$ is the scalar radiation transfer function for the temperature [10]. Thus, considering Eqs. (4.41), (4.44) and (4.45), the modulation of the BiPoSH of the temperature due to a fossil wave in the TAM formalism is given by

$$\begin{aligned} A^{JM}_{\ell_1\ell_2}|_{h^{\alpha}_{JM}(K)} = & -(-i)^{J}(-1)^{\ell_1+\ell_2+P(\alpha)} h^{\alpha}_{JM}(K) \frac{16}{\pi} \\ & \times \left[\frac{(2\ell_1+1)(2\ell_2+1)}{4\pi}\right]^{1/2} \int dk_1 k_1^2\, g^{T}_{\ell_1}(k_1) \int dk_2 k_2^2\, g^{T}_{\ell_2}(k_2) \\ & \times f^{\alpha}_{h}(k_1,k_2,K) \mathcal{I}^{\alpha}_{\ell_1\ell_2 J}(k_1,k_2,K)\,, \end{aligned} \tag{4.46}$$

with the integral function given by [178]

$$\mathcal{I}^{\alpha}_{\ell_1\ell_2 J}(k_1,k_2,K) = \left[\frac{4\pi}{(2\ell_1+1)(2\ell_2+1)(2J+1)}\right]^{1/2} \times \left[\int d^3x\, \Psi^{L,k_1,a}_{(\ell_1 m_1)}(\mathbf{x})\Psi^{L,k_2,a}_{(\ell_2 m_2)}(\mathbf{x})\Psi^{\alpha,K}_{(JM)ab}(\mathbf{x})\right]/\mathcal{W}^{J\ell_2\ell_1}_{Mm_2m_1}\,. \tag{4.47}$$

In the Eq. (4.46), the polarization $P(\alpha)$ assumes different values, depending on the nature of the fossil field: it is 0 for the scalar mode and the E vector and tensor mode, 1 for the B vector and tensor mode [10, 176].

The effects of vector and tensor fossils can be distinguished from those of scalar fossils through the evaluation of parity of the BiPoSHs they induce. In fact, due to parity conservation, L, VE and TE modes induce even-parity BiPoSHs, i.e., $J+\ell_1+\ell_2$ equals to an even integer, while VB and TB induce odd-parity BiPoSHs, i.e., $J+\ell_1+\ell_2$ equals to an odd integer [180, 181]. Nevertheless, vectors and tensors cannot be geometrically distinguished from each other, due to the two-dimensional nature of the CMB sky. This can be seen as a loss of information, since, observing the CMB, one is looking at a two-dimensional image, which is the projection of the three-dimensional correlation function of the scalar perturbations [10]. Such a loss could be regained with three-dimensional surveys [9].

Now, let us evaluate the power spectrum for the fossil field, given by

$$\langle h^{\alpha}_{JM}(\mathbf{k}) h^{\alpha'}_{J'M'}(\mathbf{k}')\rangle = P^{\alpha}_h(K)\frac{(2\pi)^3}{K^2}\delta^{(3)}(\mathbf{k}-\mathbf{k}')\delta_{JJ'}\delta_{MM'}\delta_{\alpha\alpha'}\,. \tag{4.48}$$

In order to provide estimators for the fossil fields, one needs an estimator which takes into account the coefficients $A^{JM}_{\ell_1\ell_2}$ (see 4.44). Averaging over all possible realizations of the fossil field, it is possible to evaluate the imprint of the fossil by defining the bipolar auto-/cross-power spectra [10]

$$C^{J}_{\ell_1\ell_2,\ell_3\ell_4} = \frac{1}{2J+1}\left\langle \sum_{M=-J}^{J} A^{JM}_{\ell_1\ell_2}[A^{JM}_{\ell_1\ell_2}]^* \right\rangle. \tag{4.49}$$

Assuming a phenomenological parametrization for the fossil field, the latter can be described by two parameters, that are the normalization $\mathcal{P}^Z_h$ of the power spectrum,

$$P^Z_h = \mathcal{P}^Z_h \tilde{P}^Z_h(K)\,, \tag{4.50}$$

and the normalization of the fossil-scalar-scalar bispectrum $\mathcal{B}^Z_h$,

$$f^Z_h(k_1,k_2,K) = \mathcal{B}^Z_h \tilde{f}^Z_h(K)(k_1,k_2,K)\,. \tag{4.51}$$

Here, the tilde indicates the fiducial shape of the power spectrum and bispectrum, while Z can be $Z = L, VE, VB, TE, TB$. Using these parametrization, Eq. (4.44) can be written in the form

$$A^{JM}_{\ell_1\ell_2}|_{h^\alpha_{JM}(K)} = \mathcal{B}^Z_h F^{J,\alpha}_{\ell_1\ell_2}(K) h^\alpha_{JM}(K)\,, \tag{4.52}$$

with $\alpha \in Z$ and the coefficient function being

$$\begin{aligned} F^{J,\alpha}_{\ell_1\ell_2}(K) = &-(-i)^J(-1)^{\ell_1+\ell_2+P(\alpha)} h^\alpha_{JM}(K)\frac{16}{\pi} \\ &\times \left[\frac{(2\ell_1+1)(2\ell_2+1)}{4\pi}\right]^{1/2} \int dk_1 k_1^2\, g^T_{\ell_1}(k_1) \int dk_2 k_2^2\, g^T_{\ell_2}(k_2) \\ &\times \tilde{f}^Z_h(k_1,k_2,K)\mathcal{I}^\alpha_{\ell_1\ell_2 J}(k_1,k_2,K)\,. \end{aligned} \tag{4.53}$$

Defining the reduced amplitude $\mathcal{A}^Z_h \equiv P^Z_h(\mathcal{B}^Z_h)^2$, the bipolar power spectra then read

$$\begin{aligned} C^J_{\ell_1\ell_2,\ell_3\ell_4} &= \frac{\mathcal{A}^Z_h}{(2\pi)^3}\sum_{\alpha\in Z}\int dK\, K^2 \tilde{P}^Z_h(K) F^{J,\alpha}_{\ell_1\ell_2}(K)\Big[F^{J,\alpha}_{\ell_3\ell_4}(K)\Big]^* \\ &\equiv \mathcal{A}^Z_h \mathcal{F}^{J,Z}_{\ell_1\ell_2\ell_3\ell_4}\,. \end{aligned} \tag{4.54}$$

An estimator for the BiPoSH coefficients can be given by

$$\widehat{A^{JM}_{\ell_1\ell_2}} \sum_{m_1 m_2}(-1)^{m_2}\langle \ell_1 m_1 \ell_2, m_2|JM\rangle a^T_{\ell_1 m_1} a^{T*}_{\ell_2 m_2}\,, \tag{4.55}$$

while the estimators for the bipolar power spectra can be written as

$$\begin{aligned} \widehat{C^J_{\ell_1\ell_2,\ell_3\ell_4}} = &\frac{1}{2J+1}\sum_{M=-J}^{J} \widehat{A^{JM}_{\ell_1\ell_2}}[\widehat{A^{JM}_{\ell_1\ell_2}}]^* \\ &\times -C^{TT}_{\ell_1} C^{TT}_{\ell_2}\Big(\delta_{\ell_1\ell_3}\delta_{\ell_2\ell_4} + \delta_{\ell_1\ell_4}\delta_{\ell_2\ell_3}(-)^{\ell_1+\ell_2+J}\Big)\,. \end{aligned} \tag{4.56}$$

Therefore, an estimator for the reduced amplitude for each possible combination of J and ℓ_i, with $i = 1, ..., 4$, is

$$\widehat{\mathcal{A}^{J,Z}_{h,\ell_1\ell_2,\ell_3\ell_4}} = \frac{\widehat{C^J_{\ell_1\ell_2,\ell_3\ell_4}}}{\mathcal{F}^{J,Z}_{\ell_1\ell_2,\ell_3\ell_4}}\,. \tag{4.57}$$

These estimators are useful to construct an estimator for the total reduced amplitude $\widehat{A^Z_h}$. Treating the estimators in Eq. (4.57) as statistically independent, one can write the inverse-variance-weighted estimator,

$$\widehat{\mathcal{A}^Z_h} = \left[\sum_J \sum_{(\ell_1\ell_2\ell_3\ell_4)} \widehat{\mathcal{A}^{J,Z}_{h,\ell_1\ell_2,\ell_3\ell_4}}\left\langle\left[\widehat{\mathcal{A}^{J,Z}_{h,\ell_1\ell_2,\ell_3\ell_4}}\right]^2\right\rangle_0^{-1}\right]\cdot\left[\sum_L \sum_{(\ell_1\ell_2\ell_3\ell_4)}\left\langle\left[\widehat{\mathcal{A}^{J,Z}_{h,\ell_1\ell_2,\ell_3\ell_4}}\right]^2\right\rangle_0^{-1}\right]^{-1}. \tag{4.58}$$

The sum over $(\ell_1\ell_2\ell_3\ell_4)$ is performed over all the independent combinations of the multipoles [10]. The denominator is equal to the inverse variance of the reduced amplitude estimator, which is found to be

$$(\sigma^Z_{\mathcal{A}})^{-2} \equiv \left\langle [\widehat{\mathcal{A}^Z_h}] \right\rangle_0^{-1} = \frac{1}{8}\sum_J \sum_{\ell_1\ell_2\ell_3\ell_4} \frac{2J+1}{C^{TT}_{\ell_1}C^{TT}_{\ell_2}C^{TT}_{\ell_3}C^{TT}_{\ell_4}} \mathcal{F}^{J,Z}_{\ell_1\ell_2,\ell_3\ell_4} \left[\mathcal{F}^{J,Z}_{\ell_1\ell_2,\ell_3\ell_4}\right]^* . \tag{4.59}$$

Concluding, a high signal-to-noise $\mathcal{S} = \mathcal{A}^Z_h/\sigma^Z_{\mathcal{A}}$ indicates a detectable BiPoSH signature in the CMB from inflation fossils. Our analysis ends here; for numerical results about the detectability of these fossils, see Refs. [10, 175].

4.5 Inflationary fossils in large-scale structure

The effects of tensor perturbations from inflation on cosmic structure formation manifest themselves as distortions of the primordial scalar power spectrum. In the post-inflationary era, when all perturbation modes of interest are beyond the Hubble scale, the tensor-scalar-scalar bispectrum in the squeezed limit $K \ll k_1 \simeq k_2 \simeq k = |(\mathbf{k}_2 - \mathbf{k}_1)|/2$ is simply related to the scalar spectral slope, at least for the majority of inflationary models which obey the following consistency relation [11, 51, 68, 156], that is Eq. (4.8),

$$\langle \zeta(\mathbf{k}_1)\zeta(\mathbf{k}_2)h_p(\mathbf{K})\rangle \overset{K\to 0}{\longrightarrow} (2\pi)^3\delta^{(3)}(\mathbf{k}_1+\mathbf{k}_2+\mathbf{K})\frac{1}{2}\frac{d\ln P_\zeta}{d\ln k}\epsilon^p_{ij}(\mathbf{K})\hat{k}_{1i}\hat{k}_{2j}P_h(K)P_\zeta(k)\,. \tag{4.60}$$

Here, $\epsilon^p_{ij}(\mathbf{K})$ is the polarization tensor for a plane wave with wave vector $\mathbf{K}$ and polarization state $p = +, \times$. For a given realization of the long-wavelength tensor mode, the fossil equation becomes [11]

$$\begin{aligned}\langle \zeta(\mathbf{k}_1)\zeta(\mathbf{k}_2)\rangle_{h_p(\mathbf{K})} &= (2\pi)^3\delta^{(3)}(\mathbf{k}_1+\mathbf{k}_2)P_\zeta(k) \\ &+ \int \frac{d^3K}{(2\pi)^3}\sum_p (2\pi)^3\delta^{(3)}(\mathbf{k}_1+\mathbf{k}_2+\mathbf{K})\frac{1}{2}\frac{d\ln P_\zeta}{d\ln k}P_\zeta(k) \\ &\times h^*_p(\mathbf{K})\epsilon^s_{ij}(\mathbf{K})\hat{k}_{1i}\hat{k}_{2j} + \mathcal{O}\left(\left(\frac{K}{k}\right)^2\right).\end{aligned} \tag{4.61}$$

Note that the model-dependent correction is of the order $\mathcal{O}((K/k)^2)$ and thus negligible. In order to understand the role of the long-wavelength tensor mode, let us write the expression for the primordial two-point correlation function for the scalar perturbations, by considering the inverse Fourier-transform of Eq. (4.61). Let us evaluate this correlation function between two points $\mathbf{x}_1$ and $\mathbf{x}_2$, separated by $\mathbf{x} = \mathbf{x}_2 - \mathbf{x}_1$. The value of the background long perturbation mode has been evaluated in the middle point $\mathbf{x}_c = (\mathbf{x}_1 +$

$\mathbf{x}_2)/2$, assumption which is meaningful if the correlation scale is smaller than the typical variation scale of the long mode. In Fourier space, this corresponds to the condition $K|\mathbf{x}| \ll 1 \longleftrightarrow K \ll k$. Therefore,

$$\begin{aligned}\langle\zeta(\mathbf{x}_1)\zeta(\mathbf{x}_2)\rangle_{h_p(\mathbf{K})} &= \int \frac{d^3k_1}{(2\pi)^3} e^{i\mathbf{k}_1\cdot\mathbf{x}_1} \int \frac{d^3k_2}{(2\pi)^3} e^{i\mathbf{k}_2\cdot\mathbf{x}_2} \langle\zeta(\mathbf{k}_1)\zeta(\mathbf{k}_2)\rangle_{h_p(\mathbf{K})} \\ &= \int \frac{d^3k_1}{(2\pi)^3}\frac{d^3k_2}{(2\pi)^3} e^{i(\mathbf{k}_1\cdot\mathbf{x}_1+\mathbf{k}_2\cdot\mathbf{x}_2)} (2\pi)^3\delta^{(3)}(\mathbf{k}_1+\mathbf{k}_2) P_\zeta(k) \\ &\quad + \int \frac{d^3k_1}{(2\pi)^3}\frac{d^3k_2}{(2\pi)^3} e^{i(\mathbf{k}_1\cdot\mathbf{x}_1+\mathbf{k}_2\cdot\mathbf{x}_2)} \int \frac{d^3K}{(2\pi)^3} \sum_p (2\pi)^3\delta^{(3)}(\mathbf{k}_1+\mathbf{k}_2+\mathbf{K}) \\ &\quad \times \frac{1}{2}\frac{d\ln P_\zeta}{d\ln k} P_\zeta(k) h_p^*(\mathbf{K}) \epsilon_{ij}^p(\mathbf{K}) \hat{k}_{1i}\hat{k}_{2j} \,. \end{aligned} \tag{4.62}$$

As derived in [11], the final results is

$$\langle\zeta(\mathbf{x}_1)\zeta(\mathbf{x}_2)\rangle_h = \int \frac{d^3k}{(2\pi)^3} e^{i\mathbf{k}\cdot\mathbf{x}} P_\zeta(k) \left[1 - \frac{1}{2}\frac{d\ln P_\zeta}{d\ln k} h_{ij}^p(\mathbf{x}_c)\hat{k}_i\hat{k}_j\right]. \tag{4.63}$$

This shows as this correlation leads to an anisotropic primordial scalar power spectrum given by

$$\tilde{P}_\zeta(\mathbf{k},\mathbf{x}_c) = P_\zeta(k)\left[1 - \frac{1}{2}\frac{d\ln P_\zeta}{d\ln k} h_{ij}^p(\mathbf{x}_c)\hat{k}_i\hat{k}_j\right]. \tag{4.64}$$

Notice that this result is valid for a local volume smaller that $1/K$ around $\mathbf{x}_c$. This equation suggests that superhorizon tensor modes with arbitrary long wavelengths contribute and induce a quadrupole in the scalar power spectrum. However, if $K \longrightarrow 0$, there are no observable effects, since this mode acts as an anisotropic background metric. When the modes are outside the horizon, the power spectrum is of the form of Eq. (4.63). Then, when inflation ends, density modes re-enter the horizon and evolve influenced by the long-wavelength tensor mode. As a result, by considering a constant tensor field (corresponding to a tensor mode of infinite wavelength), the correlation function does not differ from the one derived without it [11, 156].

4.5.1 Clustering fossils

The correlation of primordial scalar perturbations with primordial tensor perturbations can have observational consequences in the mass distribution. In particular, it has been shown that a tensor fossil field would causes a quadrupolar anisotropy in the mass distribution of the large-scale-structure [9, 11, 156]. Focusing on the observable consequences of the tensor-scalar-scalar bispectrum in the squeezed limit, the contribution arising from the non-violating consistency relation bispectrum gives rise to an infrared-divergent term in the local power quadrupole moment and to a late-time effect [11, 153]. These two contributions cancel each other out, leaving a small, but non vanishing, local power quadrupole,

observable at least in principle [11, 154]. This spurred the investigations of models where a stronger signature could be arise, corresponding to inflationary models where the usual consistency relations can be violated. In this case the tensor field gives rise to a local matter (or curvature) power spectrum that takes the form [156, 182]

$$P_\zeta(\mathbf{k})|_{h_p(\mathbf{K})} = P(k)\Big[1 + \mathcal{Q}^p_{ij}(\mathbf{K})\hat{k}_i\hat{k}_j\Big]\,, \tag{4.65}$$

where $\mathcal{Q}^p_{ij}$ defines the power quadrupole, given by

$$\mathcal{Q}^p_{ij}(\mathbf{K}) = \frac{B_{\not{\mathcal{CR}}}(k,k,K)}{P_h(K)P_\zeta(k)}h^p_{ij}(\mathbf{K})\,. \tag{4.66}$$

Here, $B_{\not{\mathcal{CR}}}(k,k,K)$ encodes the consistency-relation-violating part of the tensor-scalar-scalar bispectrum.The observed power quadrupole is then obtained by summing over both gravitational wave polarizations $p = \{+,\times\}$. The variance associated to the power quadrupole is

$$\overline{\mathcal{Q}^2} = \frac{8}{15}\langle\mathcal{Q}_{ij}\mathcal{Q}^{ij}\rangle = \frac{16}{15\pi}\int_{K^{\rm min}}^{k^{\rm min}} dK K^2\left[\frac{B_{\not{\mathcal{CR}}}(k,k,K)}{P_h(K)P_\zeta(k)}\right]^2 P_h(K)\,, \tag{4.67}$$

where the upper limit of integration, $k^{\rm min}$, corresponds to the smallest wavenumber probed by observations, while the lower limit, $K^{\rm min}$ is the longest wavelength gravitational wave mode produced during inflation.

In order to measure the effect of these tensor fossils in clustering of galaxies, it is possible to provide some estimators [9, 156]. A correlation such as that in Eq. (4.32) provides an estimator for the fossil field of the form [5]

$$\widehat{h_p(\mathbf{K})} = \zeta(\mathbf{k}_1)\zeta(\mathbf{k}_2)\Big[f_p(\mathbf{k}_1,\mathbf{k}_2)\epsilon^p_{ij}k^i_1k^j_2\Big]^{-1} = \frac{\zeta(\mathbf{k}_1)\zeta(\mathbf{k}_2)P_h(K)}{B_p(\mathbf{k}_1,\mathbf{k}_2,\mathbf{K})}\,, \tag{4.68}$$

where Eq. (4.33) has been used. Following [9] to evaluate the variance of this estimator, let us consider that for a general field one can write

$$\langle|\delta(\mathbf{k})|^2\rangle = VP^{\rm tot}(k)\,, \tag{4.69}$$

where V is the volume of the survey and $P(k)$ the measured matter power spectrum, which includes the signal $P(k)$ and the noise $P^{\rm n}(k)$,

$$P^{\rm tot}(k) = P(k) + P^{\rm n}(k)\,. \tag{4.70}$$

[5] Note that the sign of $\mathbf{K}$ has been re-defined, i.e., $\mathbf{K} = \mathbf{k}_1 + \mathbf{k}_2$.

Hence, the variance of the estimator in Eq. (4.68) can be written as

$$\mathrm{var}\Big(\widehat{h_p(\mathbf{K})}\Big) = 2VP^{\rm tot}(k_1)P^{\rm tot}(k_2)\Big[f_p(\mathbf{k}_1,\mathbf{k}_2)\epsilon^p_{ij}k_1^i k_2^j\Big]^{-2}. \tag{4.71}$$

For a good measure it is necessary to find the estimator which minimizes the variance; this is obtained by summing over all the possible mode pairs $(\mathbf{k}_1,\mathbf{k}_2)$ weighted by the variance,

$$\widehat{h_p(\mathbf{K})}_{\rm min} = P^{\rm n}_p(K)\sum_{\mathbf{k}}\frac{f^*_p(\mathbf{k},\mathbf{K}-\mathbf{k})\epsilon^p_{ij}k^i(K-k)^j}{2VP^{\rm tot}(k)P^{\rm tot}(|\mathbf{K}-\mathbf{k}|)}\zeta(\mathbf{k})\zeta(\mathbf{K}-\mathbf{k})\,, \tag{4.72}$$

where the noise power spectrum is the variance with which the tensor estimator $\widehat{h_p(\mathbf{K})}$ is measured, given by

$$P^{\rm n}_p(K) = \left[\sum_{\mathbf{k}}\frac{\Big|f_p(\mathbf{k},\mathbf{K}-\mathbf{k})\epsilon^p_{ij}k^i(K-k)^j\Big|^2}{2VP^{\rm tot}(k)P^{\rm tot}(|\mathbf{K}-\mathbf{k}|)}\right]^{-1}. \tag{4.73}$$

The power spectrum can be written in terms of an amplitude A_h and fiducial power spectrum P^f_h, which gives only the scale-dependence of the power spectrum. So, $P_h(K) = A_h P^f_h(K)$.

Now, let us proceed writing the optimal estimator for these amplitudes. Using Eq. (4.69) and the previous definition, the unbiased estimator is given by

$$\widehat{A^{\mathbf{K},p}_h} = \Big[P^f_h(K)\Big]^{-1}\left[V^{-1}\Big|\widehat{h_p(\mathbf{K})}\Big|^2 - P^{\rm n}_p(K)\right], \tag{4.74}$$

whose variance is

$$\mathrm{var}\left(\widehat{A^{\mathbf{K},p}_h}\right) = 2\Big[P^f_h(K)\Big]^{-2}\big[P^{\rm n}_p(K)\big]^2. \tag{4.75}$$

Again, the minimum-variance estimator for the amplitude is

$$\widehat{A^{\mathbf{K},p}_h}_{\rm min} = \sigma^2_h\sum_{\mathbf{K},p}\frac{\Big[P^f_h(K)\Big]^2}{2\big[P^{\rm n}_p(K)\big]^2}\left[V^{-1}\Big|\widehat{h_p(\mathbf{K})}\Big|^2 - P^{\rm n}_p(K)\right], \tag{4.76}$$

with

$$\sigma_h^{-2} = \sum_{\mathbf{K},p}\frac{\Big[P^f_h(K)\Big]^2}{2\big[P^{\rm n}_p(K)\big]^2}\,, \tag{4.77}$$

where it has been summed over the possible values for the tensor polarizations, i.e., $p = \{+,\times\}$.

One can evaluate the smallest amplitude which can be detected with a given survey. By considering the prediction for the bispectrum in [51] and then passing from discrete to continue limit $\sum_{\mathbf{k}} \longrightarrow V\int d^3k/(2\pi)^3$, it results that the integrand in Eq. (4.73) is

dominated by the squeezed limit ($K \ll k_1 \simeq k_2$), where $f_p(\mathbf{k}_1, \mathbf{k}_2) \simeq -(3/2)P(k_1)/k_1^2$. [9]. Then, the following approximation holds

$$\frac{P(k)}{P^{\rm tot}(k)} \simeq \begin{cases} 1 & \text{for } k < k_{\rm max} \\ 0 & \text{for } k > k_{\rm max}\,, \end{cases} \tag{4.78}$$

where $k_{\rm max}$ represents the largest wavenumber for which the power spectrum can be measured with high signal-to-noise. This leads to a noise power spectrum for a tensor fossil

$$P_h^{\rm n}(K) = \frac{20\pi^2}{k_{\rm max}^3}\,. \tag{4.79}$$

Therefore, Eq. (4.77) becomes

$$\begin{aligned} \sigma_h^{-2} &\simeq 2V \int \frac{d^3k}{(2\pi)^3} \frac{1}{k^6} \frac{k_{\rm max}^6}{800\pi^4} \\ &= 2\frac{(2\pi)^3}{k_{\rm min}^3} \frac{1}{(2\pi)^3} \frac{k_{\rm max}^6}{800\pi^4} 4\pi \int_{k_{\rm min}}^{k_{\rm max}} \frac{dk k^2}{k^6} \\ &= \frac{1}{100\pi^3} \frac{k_{\rm max}^6}{k_{\rm min}^3} \int_{k_{\rm min}}^{k_{\rm max}} \frac{dk}{k^4} \\ &\simeq \frac{1}{300\pi^3} \left(\frac{k_{\rm max}}{k_{\rm min}}\right)^6 . \end{aligned} \tag{4.80}$$

The factor 2 in the first step is due to the sum over the two polarizations of the GW, while in the last step it has been used the fact that $k_{\rm max} \gg k_{\rm min}$. Here, k_{min} indicates the smallest wavenumber detectable in the survey. The detectable tensor amplitudes at $\gtrsim 3\sigma_h$ turns out to be

$$3\sigma_h = 30\pi\sqrt{3\pi} \left(\frac{k_{\rm max}}{k_{\rm min}}\right)^{-3} . \tag{4.81}$$

This result shows that the smallest detectable GW power spectrum amplitude is inversely proportional to the Fourier modes present in the survey. It is possible to see that a possible detection a tensor fossil power spectra requires dynamic range beyond the actual reach of galaxy surveys [9].

Chapter 5

Imprint of tensor fossils on μ-distortion

Cross-correlations between μ-distortion and CMB temperature anisotropies are relevant to estimate primordial scalar bispectra in the squeezed limit in a range of scales inaccessible to CMB temperature fluctuations (see e.g. [12, 13, 66, 91, 92, 133, 183]). As already mentioned, single-field slow-roll models of inflation predict a negligible level of non-Gaussianity [51, 52, 139]. Therefore, a measurement of a non-Gaussian signal would be critical to rule out the simplest scenario of the inflationary epoch. Actually, the tightest constraints on primordial non-Gaussianity are provided by *Planck* through the measurements of the bispectrum of the CMB temperature and polarization anisotropies [69]. However, it might also be interesting to investigate and constrain non-Gaussianity sourced by primordial GWs. Also in this case, one could look at primordial non-Gaussianity peaking in the squeezed limit so as to test the cross-correlation between short and long scales. Other examples are given by the cross-correlation between the anisotropies in the CMB temperature and in the stochastic GW background (see e.g. [169, 184]) or imprints on galaxies (see e.g. [9, 185]). The feature shared by all these approaches is that they aim to provide an estimate of the non-Gaussianity over a range of scale not accessible by CMB fluctuations alone.

In the following, we report the original part of this Thesis. First, we will see how the expectation value of the μ-distortion can be affected by the modulation due to a long-wavelength tensor mode in the squeezed limit. Afterwards, we will review and extend existing studies about the cross-correlation between μ-type spectral distortion and CMB temperature anisotropies in the squeezed limit configuration. We will derive the μT cross-correlation in the case in which μ-distortions are generated by dissipation of tensor perturbations, evaluating the effect of a long-wavelength scalar mode on the primordial tensor power spectrum. Then, we will derive the same correlation but in the case of a modulation of the scalar power spectrum due to a long-wavelength tensor mode. In this respect these results are completely new, since for the first time the cross-correlation be-

tween μ-distortions and CMB anisotropies has been extended as a new observable to probe primordial bispectra involving tensor modes. Notice that, while writing this Thesis, Ref. [186] appeared, dealing with the same issues about the μT cross-correlations (but not dealing with the results about the anisotropies in the average of μ induced by tensor fossils). We will refer to [186] in order to make comparisons with our results about cross-correlations.

5.1 Averaged μ-distortion

We are now ready to study the effect of a long tensor mode on the CMB spectral distortions. In particular, for the derivation of our results we will focus on μ-distortion: however the main results can be easily extended also to y-distortions. In this Section we will see how tensor fossils could leave a signature in the distribution of the μ-distortion.

First, recall that, in the squeezed limit $k_3 \ll k_1 \simeq k_2$, the consistency relation dictates that the tensor-scalar-scalar bispectrum takes the form [156]

$$B_{\rm CR}(k_1,k_2,k_3) = -\frac{1}{2}P_\gamma(K)P_\zeta(k)\frac{\partial \ln P_\zeta(k)}{\partial \ln k}\,, \tag{5.1}$$

where $\mathbf{K} = \mathbf{k}_3$ defines the long-wavelength mode and $\mathbf{k} \simeq \mathbf{k}_1 \simeq \mathbf{k}_2$ short-wavelength modes. This bispectrum implies that, in the presence of a tensor perturbation $h_p(\mathbf{K})$, the correlation between two scalar perturbations $\zeta(\mathbf{k}_1)$ and $\zeta(\mathbf{k}_2)$ is given by [9, 156]

$$\begin{aligned}\langle\zeta(\mathbf{k}_1)\zeta(\mathbf{k}_2)\rangle_{h_p(\mathbf{K})} &= (2\pi)^3\delta^{(3)}(\mathbf{k}_1+\mathbf{k}_2)P_\zeta(k_1)\\ &\quad-(2\pi)^3\delta^{(3)}(\mathbf{k}_1+\mathbf{k}_2+\mathbf{K})\frac{1}{2}\frac{d\ln P_\zeta(k_1)}{d\ln k_1}P_\zeta(k_1)h^p_{ij}(\mathbf{K})\hat{k}_{1i}\hat{k}_{2j}\,,\end{aligned} \tag{5.2}$$

where $p=\{+,\times\}$ and the total contribution is obtained by summing over both GW polarizations. Recall the expression for the projection of the μ-distortion on the last scattering surface, i.e., Eq. (3.83). In order to evaluate the effect of the long-wavelength tensor mode, one substitutes Eq. (5.2) in the mean value of the μ-distortion. The computation of the ensemble averages of y-distortion anisotropies in cosmological perturbation theory has already been calculated and is present in the literature (see, e.g. [187]). Now, taking the ensemble average of Eq. (3.83), one gets

$$\begin{aligned}\langle a^\mu_{\ell m}\rangle &\simeq 4\pi(-i)^\ell\int\frac{d^3k_1d^3k_2}{(2\pi)^6}f(k_1,k_2,k_3)j_\ell(k_3r_{\rm LS})Y^*_{\ell m}(\hat{\mathbf{k}}_3)\langle\zeta(\mathbf{k}_1)\zeta(\mathbf{k}_2)\rangle|_{h_p(\mathbf{K})}\\ &= 4\pi(-i)^\ell\int\frac{d^3k_1d^3k_2}{(2\pi)^6}f(k_1,k_2,k_3)j_\ell(k_3r_{LS})Y^*_{\ell m}(\hat{\mathbf{k}}_3)\Bigg[(2\pi)^3\delta^{(3)}(\mathbf{k}_1+\mathbf{k}_2)P_\zeta(k_1)\\ &\quad-(2\pi)^3\delta^{(3)}(\mathbf{k}_1+\mathbf{k}_2+\mathbf{K})\frac{1}{2}\frac{d\ln P_\zeta(k_1)}{d\ln k_1}P_\zeta(k_1)h_{ij}(\mathbf{K})\hat{k}_{1i}\hat{k}_{2j}\Bigg]\,.\end{aligned} \tag{5.3}$$

From this expression, one can notice that the tensor field gives rise to two contributions in the anisotropies of the distortion, the first proportional to the scalar power spectrum, as defined by (1.63), while the second proportional to the local power quadrupole. Let us analyze them separately.

Regarding the first contribution, recalling that $\mathbf{k}_1 + \mathbf{k}_2 + \mathbf{k}_3 = 0$, one can write

$$\begin{aligned}\langle a^{\mu}_{\ell m}\rangle &= 4\pi(-i)^{\ell}\int \frac{d^3k_1 d^3k_2}{(2\pi)^6} f(k_1,k_2,k_3) j_{\ell}(k_3 r_{\rm LS}) Y^*_{\ell m}(\hat{\mathbf{k}}_3)(2\pi)^3\delta^{(3)}(\mathbf{k}_1+\mathbf{k}_2)P_{\zeta}(k_1)\\ &= 4\pi(-i)^{\ell}\frac{1}{\sqrt{4\pi}}\delta_{\ell 0}\int \frac{d^3k_1}{(2\pi)^3} f(k_1,-k_1,0)P_{\zeta}(k_1)\,. \end{aligned} \tag{5.4}$$

In the second equality it has been used the fact that $\int dx\, j_{\ell}(x)\delta(x)f(x) = 0$ if $\ell \neq 0$ and that $Y_{00}(\mathbf{k}) \equiv 1/\sqrt{4\pi}$ is well-defined even for $k \to 0$. Moreover, also remember that

$$f(k_1,k_2,k_3) \equiv \frac{9}{4} W\left(\frac{k_3}{k_s}\right)\left[e^{-(k_1^2+k_2^2)/k_D^2}\right]_{z_f}^{z_i}, \tag{5.5}$$

and then, since $\mathbf{k}_2 = -\mathbf{k}_1$ and so $k_3 = 0$, it simplifies to

$$f(k_1) \simeq \frac{9}{4}\left[e^{-2k_1^2/k_D^2}\right]_{z_f}^{z_i}. \tag{5.6}$$

Hence, Eq. (5.4) becomes

$$\begin{aligned}\langle a^{\mu}_{\ell m}\rangle &= 4\pi(-i)^{\ell}\frac{1}{\sqrt{4\pi}}\frac{9}{4}\delta_{\ell 0}\int \frac{d^3k_1}{(2\pi)^3}P_{\zeta}(k_1)\left[e^{-2k_1^2/k_D^2}\right]_{z_f}^{z_i}\\ &= \frac{9}{4}(4\pi)^{3/2}(-i)^{\ell}\delta_{\ell 0}\int \frac{dk_1 k_1^2}{(2\pi)^3}\frac{2\pi^2\Delta^2_{\zeta}(k_1)}{k_1^3}\left[e^{-2k_1^2/k_D^2}\right]_{z_f}^{z_i}\\ &= \frac{9}{2}\sqrt{\pi}(-i)^{\ell}\delta_{\ell 0}\int d\log k_1 \Delta^2_{\zeta}(k_1)\left[e^{-2k_1^2/k_D^2}\right]_{z_f}^{z_i}. \end{aligned} \tag{5.7}$$

Recalling the expression for the average μ-distortion, i.e., Eq. (3.81),

$$\langle\mu(x)\rangle \simeq \frac{9}{4}\int d\log k \Delta^2_{\zeta}(k)\left[e^{-2k^2/k_D^2}\right]_{z_f}^{z_i}, \tag{5.8}$$

it results

$$\langle a^{\mu}_{\ell m}\rangle \simeq 2\sqrt{\pi}(-i)^{\ell}\delta_{\ell 0}\langle\mu(x)\rangle\,. \tag{5.9}$$

This corresponds to the monopole term.

Now, let us evaluate the second contribution deriving from Eq. (5.3),

$$\begin{aligned}\langle a^{\mu}_{\ell m}\rangle &= 4\pi(-i)^{\ell}\int \frac{d^3k_1 d^3k_2}{(2\pi)^6} f(k_1,k_2,k_3) j_{\ell}(k_3 r_{\rm LS}) Y^*_{\ell m}(\hat{\mathbf{k}}_3)\\ &\quad\times\left[-(2\pi)^3\delta^{(3)}(\mathbf{k}_1+\mathbf{k}_2+\mathbf{K})\frac{1}{2}\frac{d\ln P_{\zeta}(k_1)}{d\ln k_1}P_{\zeta}(k_1)h_{ij}(\mathbf{K})\hat{k}_{1i}\hat{k}_{2j}\right]. \end{aligned} \tag{5.10}$$

Due to the Dirac delta, it occurs that $\mathbf{k}_2 = -(\mathbf{k}_1 + \mathbf{K}) \Longrightarrow \mathbf{k}_3 = -(\mathbf{k}_1 + \mathbf{k}_2) = \mathbf{K}$. So

$$\langle a^{\mu}_{\ell m} \rangle \simeq 2\pi(-i)^{\ell} \int \frac{d^3k_1}{(2\pi)^3} f(k_1, |\mathbf{k}_1 + \mathbf{K}|, K) j_{\ell}(K r_{\rm LS}) Y^*_{\ell m}(\hat{\mathbf{K}}) \times \frac{d\ln P_{\zeta}(k_1)}{d\ln k_1} P_{\zeta}(k_1) h_{ij}(\mathbf{K}) \hat{k}_{1i} \widehat{(k_1 + K)}_j \,. \tag{5.11}$$

We thus have found, in Eq. (5.11), that long-wavelength tensor modes (tensor fossils) generate a specific anisotropic imprint in the μ-distortions. Since we derived the primordial bispectrum in the squeezed limit when the consistency relation is satisfied, we could expect that the resulting power quadrupole should be very small, based on what is reported in the literature (see e.g. [156]). However, it should be noticed that, although this analytical estimate, a numerical study is needed, for more precise predictions.

5.2 μ-distortions from dissipation of tensor perturbations

In the following, we want to correlate the μ-distortions with the temperature anisotropies of the CMB in the case in which the distortions are originated by the dissipation of tensor perturbations. After a brief explanation on the generation of μ-distortion from tensor perturbations, we will analyze the case in which small scale tensor power spectrum is modulated by a long wavelength scalar mode, which also gives rise to anisotropies in temperature.

Existing studies of spectral distortions focus essentially on primordial scalar metric perturbations, as already studied in Chapter 3. However, similarly, also vector and tensor perturbations should source CMB spectral distortions. Refs. [188, 189] provide general expressions for the effective heating rate caused by these types of perturbations, including previously neglected contributions from CMB polarization and higher multipoles. In particular, in Ref. [188] they show that for nearly scale invariant tensor power spectra, the overall distortion is some five orders of magnitudes smaller than from the damping of adiabatic scalar modes, finding a simple analytic expressions describing the effective heating rate from tensors using a quasi-tight coupling approximation. Moreover, in contrast to adiabatic modes, tensors cause heating without additional photon diffusion and therefore over a wider range of scales, as also pointed out by [189]. Furthermore, authors of [188] found that, at small scales, also the effect of neutrino damping on the tensor amplitude needs to be included and that small-scale modes beyond $k \simeq 2 \times 10^4$ Mpc^{-1} (which represents the diffusion scale around the thermalization redshift $z \simeq 2 \times 10^6$) cannot be neglected, leading to a larger distortion. While this is sufficient for scalars, the damping of tensors is efficient to much smaller scales. The damping of tensor is efficient to much smaller scales due to the fact that GWs directly source a qaudrupole anisotropy, not requiring intermediate photon

diffusion and making the damping process nearly scale invariant [188]. Another reason is that the total energy extracted from tensors due to damping in the photon fluid represents only a tiny correction to their power, meaning that tensors continue to source temperature fluctuations at basically all scales and dissipation is effective even in the quasi-free streaming regime at scales smaller than the photon mean free path. Thus, spectral distortions can probe tensor perturbations to much smaller scales than for scalar perturbations.

Primordial tensor perturbations entering the horizon slightly before the μ-era, when dissipating, generate μ-distortions of the CMB that are observable today [8]. Let us write the dependence of the distortion on scale, introducing k-space window function which determines the contributions to the μ-distortion from different modes. In analogy with the study in Chapter 3 and referring to [188], the contribution to the μ-distortion from tensor modes can be written as

$$\langle \mu_h \rangle \simeq \int_0^\infty \frac{dk k^2}{2\pi^2} P_h(k) W_h(k)\,, \tag{5.12}$$

where the window function is

$$W_h(k) \simeq 1.4 \int_{z_{\mu,y}}^\infty \frac{4H^2}{45\dot{\tau}} \mathcal{T}_h(k\eta)\mathcal{T}_\Theta(k/\tau') e^{-\Gamma_h^* \eta} e^{-(z/z_{dc})^{5/2}} dz\,. \tag{5.13}$$

Here, $\dot{\tau}$ is the time derivative of the Thomson optical depth, $z_{\mu,y} \simeq 5\times 10^4$ is the transition redshift between μ and y distortions, $z_{dc} \simeq 2\times 10^6$ is the redshift at which thermalization processes are very efficient and $\mathcal{T}_h$ is the tensor transfer function, given by

$$\mathcal{T}_h \simeq 2\left\{ \sum_{n \text{ even}} a_n [n j_n(x) - x j_{n+1}(x)] \right\}^2, \tag{5.14}$$

where $j_n(x)$ denote spherical Bessel functions [8, 188]. The term $\mathcal{T}_\Theta e^{-\Gamma_h^*\eta}$ in Eq. (5.13) contains the physics of how the GW transfer function $\mathcal{T}_h$ couples to the photon fluid [8]. In particular [188],

$$\mathcal{T}_\Theta(k/\tau') = \mathcal{T}_\Theta(\xi) = \frac{1 + \frac{341}{36}\xi^2 + \frac{625}{324}\xi^4}{1 + \frac{142}{9}\xi^2 + \frac{1649}{81}\xi^4 + \frac{2500}{729}\xi^6} \tag{5.15a}$$

$$e^{-\Gamma_h^*\eta} \simeq 1\,. \tag{5.15b}$$

Referring to Ref. [188], comparing the k-window functions for scalar adiabatic and tensor modes over a vast range of scales, it results that the main contribution to the value of μ-distortion arises from tensor perturbations modes with wavenumbers 0.1 $\text{Mpc}^{-1} \lesssim k \lesssim$ few $\times 10^5$ Mpc^{-1}, for nearly scale invariant power spectrum. Instead, for adiabatic perturbations, most of the contributions to μ arise from scales few $\text{Mpc}^{-1} \lesssim k \lesssim$ few$\times 10^4$ Mpc^{-1}. This is due to the fact that the damping by photon diffusion plays an important role for

adiabatic modes, while tensor perturbations dissipate only through free-streaming effects. As a consequence, dissipation of the perturbations sourced by tensors extends over a larger range of scales.

The μ-parameter is related to the tensor perturbations through

$$\mu(\mathbf{x}) \simeq \int \frac{d^3k_1 d^3k_2}{(2\pi)^6} h_{ij}(\mathbf{k}_1) h^{ij}(\mathbf{k}_2) e^{-i\mathbf{k}_3\cdot\mathbf{x}} W_h(k_1, k_2)\,, \tag{5.16}$$

with $\mathbf{k}_1 + \mathbf{k}_2 + \mathbf{k}_3 = 0$ and

$$h_{ij} = \sum_p h^p \epsilon^p_{ij} = h^+ e^+_{ij} + h^\times e^\times_{ij}\,, \tag{5.17}$$

where tensor satisfies the orthonormality condition $\epsilon^p_{ij}\epsilon^{p',ij} = 2\delta_{pp'}$. In the squeezed limit, which is the relevant configuration when considering cross correlations with CMB primary anisotropies, it is possible to approximate $W_h(k_1, k_2) \simeq W_h(k_1)\,\delta^{(3)}(\mathbf{k}_1 - \mathbf{k}_2)$ [1].

Now, let us decompose the μ-distortion into spherical harmonics to write the projection on the last scattering surface. One can expand the exponential term in Eq. (5.16) in plane waves using the following identities

$$e^{i\mathbf{k}\cdot\mathbf{x}} = \sum_\ell (2\ell+1) i^\ell P_\ell(\hat{\mathbf{k}}\cdot\hat{\mathbf{x}}) j_\ell(kx) \tag{5.18a}$$

$$P_\ell(\hat{\mathbf{k}}\cdot\hat{\mathbf{x}}) = \frac{4\pi}{2\ell+1} \sum_{m=-\ell}^{\ell} Y_{\ell m}(\hat{\mathbf{x}}) Y^*_{\ell m}(\hat{\mathbf{k}})\,, \tag{5.18b}$$

and then, recalling that $\mathbf{x} = r_{\rm LS}\hat{\mathbf{n}}$, it is possible to write

$$\begin{aligned}
a^\mu_{\ell m} &= \int d\hat{\mathbf{n}}\, Y^*_{\ell m}(\hat{\mathbf{n}}) \int \frac{d^3k_1 d^3k_2}{(2\pi)^6} h_{ij}(\mathbf{k}_1) h^{ij}(\mathbf{k}_2) e^{-i\mathbf{k}_3\cdot\mathbf{x}} W_h(k_1, k_2) \\
&= \int d\hat{\mathbf{n}} \int \frac{d^3k_1 d^3k_2}{(2\pi)^6} h_{ij}(\mathbf{k}_1) h^{ij}(\mathbf{k}_2) W_h(k_1, k_2) \\
&\quad \times \sum_{\ell'} (-i)^{\ell'} 4\pi j_{\ell'}(k_3 r_{\rm LS}) \sum_{m'=-\ell'}^{\ell'} Y^*_{\ell' m'}(\hat{\mathbf{k}}_3) Y^*_{\ell' m'}(\hat{\mathbf{n}}) Y^*_{\ell m}(\hat{\mathbf{n}}) \\
&= 4\pi \int \frac{d^3k_1 d^3k_2}{(2\pi)^6} h_{ij}(\mathbf{k}_1) h^{ij}(\mathbf{k}_2) W_h(k_1, k_2) \\
&\quad \times \sum_{\ell'} (-i)^{\ell'} j_{\ell'}(k_3 r_{\rm LS}) \sum_{m'=-\ell'}^{\ell'} Y^*_{\ell' m'}(\hat{\mathbf{k}}_3) \delta_{\ell\ell'} \delta_{mm'} \\
&= 4\pi (-i)^\ell \int \frac{d^3k_1 d^3k_2}{(2\pi)^6} h_{ij}(\mathbf{k}_1) h^{ij}(\mathbf{k}_2) W_h(k_1, k_2) j_\ell(k_3 r_{\rm LS}) Y^*_{\ell m}(\hat{\mathbf{k}}_3)\,.
\end{aligned} \tag{5.19}$$

[1] The explicit expression of $W_h(\mathbf{k}_1, \mathbf{k}_2)$ needs to be calculated, but this exceeds the scope of this Thesis.

As already seen, for the temperature anisotropies one has

$$a^T_{\ell m} = \frac{4\pi}{5}(-i)^\ell \int \frac{d^3K}{(2\pi)^3} j_\ell(Kr_{\rm LS})\zeta(\mathbf{K})Y^*_{\ell m}(\hat{\mathbf{K}})\,. \tag{5.20}$$

Then, recalling Eq. (5.17), the μT angular correlation turns out to be

$$\begin{aligned}\langle a^\mu_{\ell m} a^{T*}_{\ell' m'}\rangle = \frac{16\pi^2}{5}(-i)^\ell i^{\ell'} \int \frac{d^3k_1 d^3k_2}{(2\pi)^6} W_h(k_1,k_2) j_\ell(k_3 r_{\rm LS}) Y^*_{\ell m}(\hat{\mathbf{k}}_3) \\ \times \int \frac{d^3K}{(2\pi)^3} j^*_{\ell'}(Kr_{\rm LS}) Y_{\ell' m'}(\hat{\mathbf{K}}) \sum_{pp'} \epsilon^p_{ij}(\mathbf{k}_1)\epsilon^{p',ij}(\mathbf{k}_2)\langle h^p(\mathbf{k}_1)h^p(\mathbf{k}_2)\zeta(\mathbf{K})\rangle\,.\end{aligned} \tag{5.21}$$

The correlation is proportional to the scalar-tensor-tensor bispectrum. In the absence of specific modulations induced by couplings with long wavelength modes, the tensor power spectrum and the scalar-tensor-tensor bispectrum are generically given by

$$\langle h^p(\mathbf{k}_1)h^p(\mathbf{k}_2)\rangle = (2\pi)^3\delta^{(3)}(\mathbf{k}_1+\mathbf{k}_2)P_h(k_1) \tag{5.22}$$

$$\langle h^p(\mathbf{k}_1)h^p(\mathbf{k}_2)\zeta(\mathbf{K})\rangle = (2\pi)^3\delta^{(3)}(\mathbf{k}_1+\mathbf{k}_2+\mathbf{K})B_{hh\zeta}(k_1,k_2,K)\,. \tag{5.23}$$

However, we are interested in the effect of long wavelength scalar perturbation modes, which is the same that gives rise to CMB temperature anisotropies, on the μ-distortion. Therefore, the tensor power spectrum results modulated by the scalar field [153, 190–193]. In analogy with [156, 169, 182], the long-wavelength scalar mode $\zeta(\mathbf{K})$ (with $\mathbf{K} \ll \mathbf{k}$) modulates the tensor power spectrum according to (also in analogy to Eq. (4.65) and Eq. (4.66)

$$P^{\rm mod}_h(\mathbf{k}) = P_h(k)\Big[1 + F^{\zeta h}_{\rm NL}\zeta(\mathbf{K})\Big]\,, \tag{5.24}$$

where

$$F^{\zeta h}_{\rm NL} \simeq \frac{B_{hh\zeta}(k,k,K)}{P_h(k)P_\zeta(K)}\,. \tag{5.25}$$

Hence, from tensor modes there will have both an isotropic and an anisotropic contribution from the power spectrum in Eq. (5.24). In the squeezed limit, the mode $\zeta(\mathbf{K})$ leaves the Hubble radius much earlier than the other two modes and it acts as a constant background for them. Its effect on small scale perturbations is just a rescaling of their background [194]. The bispectrum can be computed in two steps: first one computes the two-point function $\langle h^p(\mathbf{k}_1)h^p(\mathbf{k}_2)\rangle_{\zeta(\mathbf{K}')}$ in the presence of a background $\zeta(\mathbf{K}')$ and then averages this two-point function over the realizations of the background, that is [160]

$$\langle h^p(\mathbf{k}_1)h(\mathbf{k}_2)\zeta(\mathbf{K})\rangle \simeq \langle \zeta(\mathbf{K})\langle h^p(\mathbf{k}_1)h^p(\mathbf{k}_2)\rangle_{\zeta(\mathbf{K}')}\rangle\,. \tag{5.26}$$

It is possible to parameterize this three-point cross correlation function in the squeezed limit as [195]

$$\langle h^p(\mathbf{k}_1)h^p(\mathbf{k}_2)\zeta(\mathbf{K})\rangle \simeq (2\pi)^3\delta^{(3)}(\mathbf{k}_1+\mathbf{k}_2+\mathbf{K})F_{\rm NL}^{\zeta h}P_h(k_1)P_\zeta(K), \tag{5.27}$$

Here, the parameter $F_{\rm NL}^{\zeta h}$ measures the three-point cross correlations between ζ and h and it is a generalization of the usual local non-Gaussianity parameter $f_{\rm NL}^{\rm loc}$. Notice that $F_{\rm NL}^{\zeta\zeta} = f_{\rm NL}^{\rm loc}$. In principle $F_{\rm NL}$ could also depend in the relevant scales (i.e. wavenumbers). Thus, in the squeezed limit, the anisotropic contribution leads to

$$\begin{aligned}
\langle a^{\mu}_{\ell m}a^{T*}_{\ell' m'}\rangle &\simeq \frac{16\pi^2}{5}(-i)^\ell i^{\ell'}\int\frac{d^3k_1d^3k_2}{(2\pi)^6}W_h(k_1,k_2)j_\ell(k_3r_{\rm LS})Y^*_{\ell m}(\hat{\mathbf{k}}_3)\\
&\quad\times\int\frac{d^3K}{(2\pi)^3}j_{\ell'}(Kr_{\rm LS})Y_{\ell' m'}(\hat{\mathbf{K}})\sum_{pp'}\epsilon^p_{ij}(\mathbf{k}_1)\epsilon^{p',ij}(\mathbf{k}_2)\\
&\quad\times F_{\rm NL}^{\zeta\gamma}(2\pi)^3\delta^{(3)}(\mathbf{k}_1+\mathbf{k}_2+\mathbf{K})P_h(k_1)P_\zeta(K)\\
&= \frac{16\pi^2}{5}i^{\ell'-\ell}F_{NL}^{\zeta\gamma}\int\frac{d^3k_1}{(2\pi)^3}W_h(k_1)j_\ell(Kr_{\rm LS})j_{\ell'}(Kr_{\rm LS})\\
&\quad\times\int\frac{d^3K}{(2\pi)^3}Y^*_{\ell m}(\hat{\mathbf{K}})Y_{\ell' m'}(\hat{\mathbf{K}})P_h(k_1)P_\zeta(K)\times(4)\\
&= \frac{64\pi^2}{5}i^{\ell'-\ell}F_{\rm NL}^{\zeta\gamma}\int\frac{dk_1k_1^2}{2\pi^2}W_h(k_1)P_h(k_1)\\
&\quad\times\int\frac{dKK^2}{(2\pi)^3}j_\ell(Kr_{\rm LS})j_{\ell'}(Kr_{\rm LS})P_\zeta(K)\delta_{\ell\ell'}\delta_{mm'}\\
&= 5F_{\rm NL}^{\zeta\gamma}\left[\int\frac{dk_1k_1^2}{2\pi^2}W_h(k_1)P_h(k_1)\right]\\
&\quad\times\left[\frac{4\pi}{25}\int\frac{dK}{K}j^2_\ell(Kr_{\rm LS})\Delta^2_\zeta(K)\right]\delta_{\ell\ell'}\delta_{mm'}\\
&= 5C_\ell^{TT,\rm SW}\langle\mu_h\rangle\delta_{\ell\ell'}\delta_{mm'}\,.
\end{aligned}\tag{5.28}$$

where we summed over the polarizations and, due to the Dirac δ, it results: $\mathbf{k}_2 = -(\mathbf{k}_1+\mathbf{K}) \Longrightarrow \mathbf{k}_3 = -(\mathbf{k}_1+\mathbf{k}_2) = \mathbf{K}$. Here, one has to remember Eq. (2.18) and Eq. (5.12). Therefore, Eq. (5.28) is the result for the cross-correlation between the μ-distortion and temperature fluctuation $\Delta T/T$.

5.3 μT cross-correlation

Theoretical mechanisms of production of CMB anisotropies include primordial energy density (scalar) perturbations and GW (tensor) perturbations generated during inflation. It is important to identify distinctive signals associated with specific physical effects to determine which mechanisms produced each. For instance, one of the main predictions of inflationary models is the existence of a background of primordial GWs [196] from inflation

which produces a distinct signature in the polarization of the CMB, referred to as B-mode polarization. The amplitude of primordial GWs can be constrained by means of observations of the B-mode polarization in the CMB. Measuring this amplitude is crucial since it is proportional to the energy scale of inflation and linked to the range of the inflaton field [197, 198].

In the following, we will focus on the existence of a non-trivial primordial scalar-scalar-tensor bispectrum, correlating the μ-distortion with the temperature anisotropies of the CMB, but in the case of a modulation of the small-scale scalar curvature power spectrum due to a long wavelength tensor mode, which also gives rise to anisotropies in temperature.

Recall that the spherical harmonic coefficients of the μ-distortions from scalar perturbations are given by

$$a^{\mu}_{\ell m} = 4\pi(-i)^{\ell}\int \frac{d^3k_1 d^3k_2}{(2\pi)^6}\zeta(\mathbf{k}_1)\zeta(\mathbf{k}_2)f(k_1,k_2,k_3)j_{\ell}(k_3 r_{\rm LS})Y^{*}_{\ell m}(\hat{\mathbf{k}}_3). \tag{5.29}$$

Now, one has to compute the scalar-scalar-tensor bispectrum (for a systematic study of scalar-tensor-tensor bispectra in CMB anisotropies see, e.g. [199–201]). For the CMB anisotropies, in general one can write [168]

$$a^{(t)X}_{\ell m} = 4\pi(-i)^{\ell}\int \frac{d^3K}{(2\pi)^3}\mathcal{T}^{(t)X}_{\ell}(K)\sum_{s=\pm 2}\left(\frac{s}{2}\right)^{x} h^{s}(\mathbf{K})\,{}_{-s}Y^{*}_{\ell m}(\hat{\mathbf{K}})\,. \tag{5.30}$$

In the case of temperature anisotropies, $X = T$ and for tensors it holds $h^{(\pm 2)}$. Here, $\mathcal{T}^{(t)X}_{\ell}(K)$ represents the tensor transfer function and $x = 0$ for $X = T$.[2] The subscript (t) stands for tensor. Here, ${}_{\lambda}Y_{\ell m}(\hat{\mathbf{K}})$ denote the spin-weighted spherical harmonics, a generalizations of the standard spherical harmonics. The most explicit form is (see e.g. [177, 202] and Refs. therein)

$$\begin{aligned}{}_{s}Y_{\ell m}(\theta,\phi) = &\sqrt{\frac{(\ell+m)!(\ell-m)!(2\ell+1)}{4\pi(\ell+s)!(\ell-s)!}}\sin^{2\ell}\left(\frac{\theta}{2}\right)\\ &\times\sum_{r=0}^{\ell-s}\binom{\ell-s}{r}\binom{\ell+s}{r+s-m}(-1)^{\ell-r-s+m}e^{im\phi}\cot^{2r+s-m}\left(\frac{\theta}{2}\right).\end{aligned} \tag{5.31}$$

The spin-weighted spherical harmonic satisfy the orthogonality and completeness conditions

$$\int_0^{2\pi}d\phi\int_{-1}^{1}d\cos\theta\,{}_{s}Y^{*}_{\ell' m'}(\theta,\phi)\,{}_{s}Y_{\ell m}(\theta,\phi) = \delta_{\ell\ell'}\delta_{mm'} \tag{5.32a}$$

$$\sum_{\ell m}{}_{s}Y^{*}_{\ell m}(\theta,\phi)\,{}_{s}Y_{\ell m}(\theta',\phi') = \delta(\phi-\phi')\delta(\cos\theta-\cos\theta')\,, \tag{5.32b}$$

[2] In general, $x = 0$ for $X = T, E$ and $x = 1$ for $X = B$.

as well as the following properties about the transformation under conjugate and parity

$$ {}_sY^*_{\ell m}(\theta,\phi) = (-1)^{s+m}\,{}_{-s}Y_{\ell(-m)}(\theta,\phi) \tag{5.33a} $$

$$ {}_sY_{\ell m}(\pi-\theta,\pi+\phi) = (-1)^{\ell}\,{}_{-s}Y_{\ell m}(\theta,\phi)\,. \tag{5.33b} $$

Notice that $Y_{\ell m}(\theta,\phi)$ are the spin-0 spherical harmonics, that is $Y_{\ell m}(\theta,\phi) = {}_0Y_{\ell m}(\theta,\phi)$. Therefore, the resulting μT angular correlation can be written as

$$ \begin{aligned} \langle a^{\mu}_{\ell m} a^{(t)T*}_{\ell' m'}\rangle \simeq\ & 16\pi^2(-i)^{\ell} i^{\ell'} \int \frac{d^3k_1 d^3k_2}{(2\pi)^6} f(k_1,k_2,k_3) j_{\ell}(k_3 r_{\rm LS}) Y^*_{\ell m}(\hat{\mathbf{k}}_3) \\ & \times \int \frac{d^3K}{(2\pi)^3} \mathcal{T}^{(t)T}_{\ell'}(K) \sum_{p=\pm 2} {}_{-p}Y^*_{\ell' m'}(\hat{\mathbf{K}}) \langle \zeta(\mathbf{k}_1)\zeta(\mathbf{k}_2) h^p(\mathbf{K})\rangle, \end{aligned} \tag{5.34} $$

indicating with p the polarization. Now consider the effect of a long wavelength GW on $\langle\zeta(\mathbf{k}_1)\zeta(\mathbf{k}_2)\rangle$. It modulates the tensor power spectrum according to [156]

$$ P^{\rm mod}_{\zeta}(\mathbf{k}) = P_{\zeta}(k)\left[1 + \sum_p F^{\zeta h}_{\rm NL} h^p_{ij}(\mathbf{K}) \hat{k}^i \hat{k}^j\right], \tag{5.35} $$

where $F^{\zeta h}_{\rm NL}$ is defined as

$$ F^{\zeta h}_{\rm NL} \simeq \frac{B_{h\zeta\zeta}(k,k,K)}{P_{\zeta}(k) P_h(K)}\,. \tag{5.36} $$

As for Eq. (5.27), the scalar-scalar-tensor correlation leads to

$$ \begin{aligned} \langle h^p(\mathbf{K})\zeta(\mathbf{k}_1)\zeta(\mathbf{k}_2)\rangle &\simeq \langle h^p(\mathbf{K}) \langle \zeta(\mathbf{k}_1)\zeta(\mathbf{k}_2)\rangle_{h^p(\mathbf{K})}\rangle \\ &\simeq (2\pi)^3 \delta^{(3)}(\mathbf{k}_1+\mathbf{k}_2+\mathbf{K}) F^{\zeta h}_{\rm NL} P_{\zeta}(k_1) P_h(K) \epsilon^p_{ij} \hat{k}^i_1 \hat{k}^j_2. \end{aligned} \tag{5.37} $$

Thus, in the squeezed limit, the anisotropic contribution leads to

$$ \begin{aligned} \langle a^{\mu}_{\ell m} a^{(t)T}_{\ell' m'}\rangle \simeq\ & -16\pi^2(-i)^{\ell}(-i)^{\ell'} \int \frac{d^3k_1 d^3k_2}{(2\pi)^6} f(k_1,k_2,k_3) j_{\ell}(k_3 r_{\rm LS}) Y^*_{\ell m}(\hat{\mathbf{k}}_3) \\ & \times \int \frac{d^3K}{(2\pi)^3} \mathcal{T}^{(t)T}_{\ell'}(K)\, {}_{-p}Y^*_{\ell' m'}(\hat{\mathbf{K}}) (2\pi)^3 \delta^{(3)}(\mathbf{k}_1+\mathbf{k}_2+\mathbf{K}) \\ & \times F^{\zeta h}_{\rm NL} P_{\zeta}(k_1) P_h(K) \epsilon^p_{ij} \hat{k}^i_1 \hat{k}^j_2 \\ =\ & 16\pi^2(-i)^{\ell+\ell'} \int \frac{d^3k_1}{(2\pi)^3} \frac{d^3K}{(2\pi)^3} f(k_1, |\mathbf{k}_1+\mathbf{K}|, K) j_{\ell}(k_3 r_{\rm LS}) Y^*_{\ell m}(\hat{\mathbf{K}}) \\ & \times \mathcal{T}^{(t)T}_{\ell'}(K) \sum_{p=\pm 2} {}_{-p}Y^*_{\ell' m'}(\hat{\mathbf{K}}) F^{\zeta h}_{\rm NL} P_{\zeta}(k_1) P_h(K) \epsilon^p_{ij} \hat{k}_{1i} \widehat{(k_1+K)}_j\,. \end{aligned} \tag{5.38} $$

We stress again that it is necessary a numerical study for more precise predictions. In this thesis, we focused on the analytical derivation of the results. The next step would be to evaluate the signal-to-noise ratio, similarly to what it has already been calculated for

the μT correlation in the case of distortions originated by dissipation of scalar modes (for instance, see [91]).

5.4 Comparison with recent results

In this Thesis we have focused on the derivation of analytic results, based on the review and extension of results already known in the literature. In order to obtain predictions about these results, it is necessary to make Fisher forecasts on the detectability of anisotropies in μT cross-correlation, but this is beyond the purposes of this work. However, very recently it has been studied how to constrain tensor non-Gaussianities with these cross-correlations [186]. The authors of [186] found that only primordial tensor bispectra with anisotropies leave distinct signatures, while isotropic tensor bispectra leave either vanishing or highly suppressed signatures. Comparing our results with [186], we can provide some comments on our results and forecasts. By adopting the BipoSH formalism (see Section 4.4) to parameterize anisotropies on the bispectra, authors of [186] made a Fisher forecast to assess the detection prospects from cross-correlation between μ spectral distortions and CMB temperature and polarization anisotropies. They found that the $\langle \mu_{\ell_1} X_{\ell_2} \rangle$, with X being the CMB T, E, B modes, may get off-diagonal values due to the anisotropies induced by the long-wavelength modes in the anisotropic squeezed primordial bispectra. Among all these possibilities, anisotropies in the squeezed limit of the $\langle \zeta\zeta h \rangle$ would be the relevant sources of these cross-correlations. Moreover, we can take advantage of their results in order to verify the mathematical consistency of ours.

Scalar-tensor-tensor bispectrum

Let us start from the calculation of the scalar-tensor-tensor bispectrum. To recover our final result, that is Eq. (5.28), we have to reproduce their calculations in the rotationally invariant case. The contribution from the $\langle \zeta hh \rangle$ primordial bispectrum to the μT cross-correlation obtained in [186] is given by

$$
\begin{aligned}
C^{\mu T,\mathrm{OMP21}}_{\ell_1\ell_2 m_1 m_2} = i^{\ell_2-\ell_1} 128\pi^3 \int \frac{dk_+ dk_-}{(2\pi)^6} k_+^2 k_-^2 \mathcal{T}^T_{\ell_2}(k_+) j_{\ell_1}(k_+ r_{\mathrm{LS}}) W_h(k_-) P_h(k_-) P_\zeta(k_+) \\
\times \sum_{L_1, M_1} f^{\mathrm{stt}}_{L_1 M_1} (-1)^{m_1+L_1} \sqrt{(2\ell_1+1)(2\ell_2+1)(2L_1+1)} \\
\times \begin{pmatrix} \ell_1 & \ell_2 & L_1 \\ 0 & 0 & 0 \end{pmatrix} \begin{pmatrix} \ell_1 & \ell_2 & L_1 \\ -m_1 & m_2 & M_1 \end{pmatrix} \left(\sum_{\lambda,\lambda'} \xi_{\lambda\lambda'} \right) .
\end{aligned} \tag{5.39}
$$

Note that from now on we will use the notation with the superscript OMP21 to indicate that we are referring to the cross-correlation reported by [186]. According to their notation, $f^{xxx}_{L_i,M_i}$ are the non-Gaussian amplitudes (which in principle can depend on the

wavelengths), $\mathcal{T}_\ell^T$ is the scalar transfer function and $\xi_{\lambda\lambda'}$ are the polarization coefficients sensitive to the polarization states of tensor perturbations appearing in the correlator. Notice that the correlation was expressed in terms of the Wigner 3-j symbols. In the rotational invariant case, Eq. (5.39) simplifies, since $L_1 = L_2 = M_1 = M_2 = 0$. The selection rules for the Wigner 3-j symbols are

$$\begin{aligned} &|m_1| \leq \ell_1, \quad |m_2| \leq \ell_2, \quad |m_3| \leq \ell_3, \quad m_1 + m_2 = m_3, \\ &|\ell_1 - \ell_2| \leq \ell_3 \leq \ell_1 + \ell_3, \quad \ell_1 + \ell_2 + \ell_3 \in \mathbb{Z}\,. \end{aligned} \tag{5.40a}$$

More properties of the Wigner 3-j symbols can be found, e.g., in [203, 204]. In our case, $\ell_3 = L_1$ and $m_3 = M_1$ and therefore, from Eq. (5.39), the selection rules set

$$m_1 = -m_2 \tag{5.41a}$$

$$0 \leq 2\ell_1 = 2\ell_2\,. \tag{5.41b}$$

Moreover, the Wigner 3-j symbols satisfy the orthogonality condition, that is

$$(2\ell_3 + 1) \sum_{\ell_3 m_3} \begin{pmatrix} \ell_1 & \ell_2 & \ell_3 \\ m_1 & m_2 & m_3 \end{pmatrix} \begin{pmatrix} \ell_1 & \ell_2 & \ell_3 \\ m_1' & m_2' & m_3 \end{pmatrix} = \delta_{m_1 m_1'} \delta_{m_2 m_2'}\,, \tag{5.42}$$

which in our case takes the form

$$\begin{pmatrix} \ell_1 & \ell_2 & 0 \\ 0 & 0 & 0 \end{pmatrix} \begin{pmatrix} \ell_1 & \ell_2 & 0 \\ -m_1 & m_2 & 0 \end{pmatrix} = \delta_{0-m_1} \delta_{0m_2}\,. \tag{5.43}$$

Therefore, using Eqs. (5.41), the cross-correlation becomes

$$\begin{aligned} C_{\ell_1 \ell_1 m_1 m_2}^{\mu T,\mathrm{OMP21}} &= 128\pi^3 \int \frac{dk_+ dk_-}{(2\pi)^6} k_+^2 k_-^2 \mathcal{T}_{\ell_1}^T(k_+) j_{\ell_1}(k_+ r_{\mathrm{LS}}) W_h(k_-) P_h(k_-) P_\zeta(k_+) \\ &\quad \times f_{00}^{\mathrm{stt}} (-1)^{m_1} (2\ell_1 + 1) \delta_{\ell_1 \ell_2} \delta_{0-m_1} \delta_{0m_2} \left(\sum_{\lambda,\lambda'} \xi_{\lambda\lambda'} \right) \\ &= \frac{2}{\pi^3} f_{00}^{\mathrm{stt}} \int dk_+ k_+^2 \int dk_- k_-^2 \mathcal{T}_{\ell_1}^T(k_+) j_{\ell_1}(k_+ r_{\mathrm{LS}}) W_h(k_-) P_h(k_-) P_\zeta(k_+) \\ &\quad \times (2\ell_1 + 1) \delta_{\ell_1 \ell_2} \delta_{0-m_1} \delta_{0m_2} \left(\sum_{\lambda,\lambda'} \xi_{\lambda\lambda'} \right), \end{aligned} \tag{5.44}$$

Let us compare this expression with our result, Eq. (5.28). One should remember that we derived our results in the SW limit (see Section 2.3). If we evaluate Eq. (5.44) in the SW limit, we obtain

$$C_{\ell_1\ell_1 m_1 m_2}^{\mu T,\mathrm{OMP21}} = \frac{2}{5\pi^3} f_{00}^{\mathrm{stt}} \int dk_+ k_+^2 \int dk_- k_-^2 j_{\ell_1}^2(k_+ r_{\mathrm{LS}}) W_h(k_-) P_h(k_-) P_\zeta(k_+) \times (2\ell_1+1)\delta_{\ell_1\ell_2}\delta_{0-m_1}\delta_{0m_2}\left(\sum_{\lambda,\lambda'}\xi_{\lambda\lambda'}\right), \tag{5.45}$$

To better compare the results, referring to Eq. (5.28), let us express the spherical harmonics in terms of the Wigner 3-j symbols. First, recall that

$$Y_{\ell m}^*(\mathbf{k}) = (-1)^m Y_{\ell -m}(\mathbf{k}), \tag{5.46}$$

and so one can write

$$\int d\hat{K} Y_{\ell m}^*(\hat{\mathbf{K}}) Y_{\ell' m'}(\hat{\mathbf{K}}) = \int d\hat{K} (-1)^m Y_{\ell -m}(\hat{\mathbf{K}}) Y_{\ell' m'}(\hat{\mathbf{K}}). \tag{5.47}$$

Let us use the properties

$$Y_{\ell_1 m_1}(\theta,\phi) Y_{\ell_2 m_2}(\theta,\phi) = \sum_{\ell_3, m_3} \sqrt{\frac{(2\ell_1+1)(2\ell_2+1)(2\ell_3+1)}{4\pi}} \times \begin{pmatrix} \ell_1 & \ell_2 & \ell_3 \\ m_1 & m_2 & m_3 \end{pmatrix} Y_{\ell_3 m_3}^*(\theta,\phi) \begin{pmatrix} \ell_1 & \ell_2 & \ell_3 \\ 0 & 0 & 0 \end{pmatrix}. \tag{5.48}$$

In the rotationally invariance hypothesis and using Eq. (5.42), the previous expression simplifies to

$$Y_{\ell_1 m_1} Y_{\ell_2 m_2} = \sqrt{\frac{(2\ell_1+1)(2\ell_2+1)}{4\pi}} Y_{00}^* \delta_{m_1 0}\delta_{m_2 0} \tag{5.49}$$

and so one gets

$$\begin{aligned} \int d\hat{K} (-1)^m Y_{\ell -m}(\hat{\mathbf{K}}) Y_{\ell' m'}(\hat{\mathbf{K}}) &= \int d\hat{K} (-1)^m \frac{(2\ell+1)\delta_{\ell\ell'}}{\sqrt{4\pi}} Y_{00}^* \delta_{-m0}\delta_{m'0} \\ &= \int d\hat{K} (-1)^m \frac{(2\ell+1)\delta_{\ell\ell'}}{\sqrt{4\pi}} \frac{1}{\sqrt{4\pi}} \delta_{-m0}\delta_{m'0} \\ &= (2\ell+1)\delta_{\ell\ell'}\delta_{-m0}\delta_{m'0}. \end{aligned} \tag{5.50}$$

Therefore, Eq. (5.28) turns out to be

$$\langle a_{\ell m}^{\mu} a_{\ell' m'}^{T*} \rangle \simeq \frac{16\pi^2}{5} i^{\ell'-\ell} F_{NL}^{\zeta\gamma} \int \frac{d^3k_1}{(2\pi)^3} W_h(k_1) j_\ell(K r_{\mathrm{LS}}) j_{\ell'}(K r_{\mathrm{LS}}) \times \int \frac{d^3K}{(2\pi)^3} Y_{\ell m}^*(\hat{\mathbf{K}}) Y_{\ell' m'}(\hat{\mathbf{K}}) P_h(k_1) P_\zeta(K) \sum_{pp'} \epsilon_{ij}^{p} \epsilon^{p',ij}$$

$$
\begin{aligned}
&= \frac{64\pi^2}{5} F_{NL}^{\zeta\gamma} \int \frac{d^3k_1}{(2\pi)^3} \frac{dKK^2}{(2\pi)^3} W_h(k_1) j_\ell^2(Kr_{\rm LS}) P_h(k_1) P_\zeta(K) \\
&\quad \times (2\ell+1)\delta_{\ell\ell'}\delta_{-m0}\delta_{m'0} \\
&= \frac{4}{5\pi^3} F_{NL}^{\zeta\gamma} \int dk_1 k_1^2 \int dK K^2 W_h(k_1) j_\ell^2(Kr_{\rm LS}) P_h(k_1) P_\zeta(K) \\
&\quad \times (2\ell+1)\delta_{\ell\ell'}\delta_{-m0}\delta_{m'0}\,, \qquad (5.51)
\end{aligned}
$$

where the sum over polarizations gives a normalization factor, since we calculated this cross correlation in the squeezed limit. Comparing Eq. (5.45) and Eq. (5.51), one can notice that the result of [186] is consistent with ours.

Tensor-scalar-scalar bispectrum

Now, let us compare the contribution from the tensor-scalar-scalar primordial bispectrum to the μT cross-correlation. First, let us recall Eq. (5.37), where the bispectrum takes the form

$$
B_{h\zeta\zeta}(k_1, k_2, K) = F_{\rm NL}^{\zeta h} P_\zeta(k_1) P_h(K) \epsilon_{ij}^{\ p} \hat{k}_1^i \hat{k}_2^j\,. \qquad (5.52)
$$

We want to see if it is possible to write our bispectrum as a subcase of the one in [186]. In the squeezed limit,

$$
\epsilon_{ij}^{\pm 2}(\mathbf{K}) \hat{k}_{1i} \hat{k}_{1j} = \frac{(8\pi)^{3/2}}{6} \sum_{M m_i m_j} {}_{\mp 2}Y_{2M}^*(\hat{\mathbf{K}}) Y_{1m_i}^*(\hat{\mathbf{k}}_1) Y_{1m_j}^*(\hat{\mathbf{k}}_1) \begin{pmatrix} 2 & 1 & 1 \\ M & m_i & m_j \end{pmatrix}. \qquad (5.53)
$$

Moreover, the Clebsch-Gordan coefficients are the expansion coefficients of a product of two spherical harmonics in terms of a single spherical harmonic. Therefore, in general, we can write

$$
Y_{\ell_1 m_1}(\Omega) Y_{\ell_2 m_2}(\Omega) = \sum_{LM} \sqrt{\frac{(2\ell_1+1)(2\ell_2+1)}{4\pi(2L+1)}} \langle \ell_1 0 \ell_2 0 | L0 \rangle \langle \ell_1 m_1 \ell_2 m_2 | LM \rangle Y_{LM}(\Omega)\,, \qquad (5.54)
$$

where the Clebsch-Gordan coefficients can only be non-zero when

$$
|\ell_1 - \ell_2| \le L \le \ell_1 + \ell_2, \qquad M = m_1 + m_2\,. \qquad (5.55)
$$

This implies that

$$
\begin{aligned}
Y_{1m_i}^*(\hat{\mathbf{k}}_1) Y_{1m_j}^*(\hat{\mathbf{k}}_1) &= (-1)^{m_i+m_j} Y_{1-m_i}(\hat{\mathbf{k}}_1) Y_{1-m_j}(\hat{\mathbf{k}}_1) \\
&= (-1)^{m_i+m_j} \sum_{LM} \sqrt{\frac{9}{4\pi(2L+1)}} \langle 1010 | L0 \rangle \langle 1 - m_i 1 - m_j | LM \rangle Y_{LM}(\hat{\mathbf{k}}_1)\,. \qquad (5.56)
\end{aligned}
$$

Thus, our bispectrum turns out to be

$$B_{h\zeta\zeta} = F_{\rm NL}^{\zeta h} P_\zeta(k_1) P_h(K) \frac{(8\pi)^{3/2}}{6} \sum_{M m_i m_j} {}_{\mp 2}Y^*_{2M}(\hat{\mathbf{K}})(-1)^{m_i+m_j}\sqrt{\frac{3}{4\pi}} \times \langle 1010|L0\rangle\langle 1-m_i 1-m_j|2M\rangle Y_{2M}(\hat{\mathbf{k}}_1) \begin{pmatrix} 2 & 1 & 1 \\ M & m_i & m_j \end{pmatrix}, \tag{5.57}$$

since, in our case, $L = 2$. If one considers the form of the squeezed limit bispectrum reported in [186], that is

$$B_{h\zeta\zeta}^{\rm OMP21} \propto \sum_{L_1 M_1} \sum_{L_2 M_2} {}_{\pm 2}Y_{L_1 M_1}(\hat{\mathbf{k}}_{\rm L}) Y_{L_2 M_2}(\hat{\mathbf{k}}_{\rm s}) f^{\rm sst}_{L_1,M_1,L_2,M_2} P_h(k_{\rm L}) P_\zeta(k_{\rm s}) \,, \tag{5.58}$$

one can notice that our bispectrum can actually be considered a subclass of theirs, since, from Eq. (5.57), we obtain

$$B_{h\zeta\zeta} \propto \sum_M {}_{\mp 2}Y^*_{2M}(\hat{\mathbf{K}}) Y_{2M}(\hat{\mathbf{k}}_1) F^{\zeta h}_{{\rm NL},M} P_\zeta(k_1) P_h(K) \,. \tag{5.59}$$

Here, the sum over m_i, m_j of the Wigner 3-j symbols gives a multiplicative factor (for each fixed value of m_i and m_j) and so it only changes the amplitude of $F^{\zeta h}_{{\rm NL},M}$ (which depends on the specific fixed values of m_i and m_j). Notice that from Eq. (5.53) and Eq. (5.57) the value of M seems to be fixed to zero.

Now, let us recall our result, given by Eq. (5.38), that is

$$\langle a^\mu_{\ell m} a^{(t)T}_{\ell' m'} \rangle \simeq 16\pi^2 (-i)^{\ell+\ell'} \int \frac{d^3k_1}{(2\pi)^3} \frac{d^3K}{(2\pi)^3} f(k_1, |\mathbf{k}_1+\mathbf{K}|, K) j_\ell(k_3 r_{\rm LS}) Y^*_{\ell m}(\hat{\mathbf{K}}) \times \mathcal{T}^{(t)T}_{\ell'}(K) \sum_{p=\pm 2} {}_{-p}Y^*_{\ell' m'}(\hat{\mathbf{K}}) F^{\zeta h}_{\rm NL} P_\zeta(k_1) P_h(K) \epsilon^p_{ij} \hat{k}_{1i} \widehat{(k_1+K)}_j \,. \tag{5.60}$$

Let us express all parts containing the angular dependence, i.e.,

$$\int d\hat{k}_1 d\hat{K}\, Y^*_{\ell m}(\hat{\mathbf{K}}) \sum_{p=\pm 2} {}_{-p}Y^*_{\ell' m'}(\hat{\mathbf{K}}) \epsilon^p_{ij} \hat{k}_{1i} \widehat{(k_1+K)}_j \,, \tag{5.61}$$

with the spin spherical harmonics. We already saw that in the squeezed limit,

$$\epsilon^{\pm 2}_{ij}(\mathbf{K}) \hat{k}_{1i} \hat{k}_{1j} = \frac{(8\pi)^{3/2}}{6} \sum_{M m_i m_j} {}_{\mp 2}Y^*_{2M}(\hat{\mathbf{K}}) Y^*_{1m_i}(\hat{\mathbf{k}}_1) Y^*_{1m_j}(\hat{\mathbf{k}}_1) \begin{pmatrix} 2 & 1 & 1 \\ M & m_i & m_j \end{pmatrix}, \tag{5.62}$$

and therefore,

$$\frac{(8\pi)^{3/2}}{6}\int d\hat{k}_1 d\hat{K}\sum_{p=\pm2} Y^*_{\ell m}(\hat{\mathbf{K}})\,{}_{-p}Y^*_{\ell' m'}(\hat{\mathbf{K}})\sum_{M m_i m_j} {}_{-p}Y^*_{2M}(\hat{\mathbf{K}})Y^*_{1m_i}(\hat{\mathbf{k}}_1)Y^*_{1m_j}(\hat{\mathbf{k}}_1) \times \begin{pmatrix} 2 & 1 & 1 \\ M & m_i & m_j \end{pmatrix}. \tag{5.63}$$

Let us fix the selection rules, that are

$$\begin{aligned} &|m_i|\leq \ell_1, \quad |m_j|\leq \ell_2, \quad |M|\leq L, \quad m_i+m_j=M, \quad |\ell_1-\ell_2|\leq L\leq \ell_1+\ell_2, \\ &|m|\leq \ell, \qquad \left|m'\right|\leq \ell', \quad |M_1|\leq L_1 \quad m+m'=M_1, \quad \left|\ell-\ell'\right|\leq L_1\leq \ell+\ell'\,. \end{aligned} \tag{5.64}$$

First, we can evaluate

$$\begin{aligned} \int d\hat{k}_1\, Y^*_{1m_i}(\hat{\mathbf{k}}_1)Y^*_{1m_j}(\hat{\mathbf{k}}_1) &= \int d\hat{k}_1 (-1)^{m_i} Y_{1-m_i}(\hat{\mathbf{k}}_1)Y^*_{1m_j}(\hat{\mathbf{k}}_1) \\ &= (-1)^{-m_i}\delta_{-m_i m_j}\,, \end{aligned} \tag{5.65}$$

which implies that $M=m_i+m_j=0$ (confirming what we have already noted previously). Thus, Eq. (5.63) becomes

$$\frac{(8\pi)^{3/2}}{6}\int d\hat{K}\sum_{p=\pm2} Y^*_{\ell m}(\hat{\mathbf{K}})\,{}_{-p}Y^*_{\ell' m'}(\hat{\mathbf{K}})\,{}_{-p}Y^*_{2M}(\hat{\mathbf{K}}) \times \sum_{M m_i}(-1)^{-m_i}(\hat{\mathbf{k}}_1)\begin{pmatrix} 2 & 1 & 1 \\ M & m_i & -m_i \end{pmatrix}. \tag{5.66}$$

Secondly, we replace the integrals of spin-weighted spherical harmonics with the Wigner 3-j symbols

$$\int d\hat{K}\,{}_{\mp2}Y^*_{\ell' m'}(\hat{\mathbf{K}})Y^*_{\ell m}(\hat{\mathbf{K}})\,{}_{\mp2}Y^*_{2M}(\hat{\mathbf{K}}) = I^{\pm2,0,\pm2}_{\ell'\ell 2}\begin{pmatrix} \ell' & \ell & 2 \\ m' & m & M \end{pmatrix}, \tag{5.67}$$

with the compact notation

$$I^{s_1 s_2 s_2}_{\ell_1\ell_2\ell_3} = \sqrt{\frac{(2\ell_1+1)(2\ell_2+1)(2\ell_3+1)}{4\pi}}\begin{pmatrix} \ell_1 & \ell_2 & \ell_3 \\ s_1 & s_2 & s_3 \end{pmatrix}. \tag{5.68}$$

Putting Eq. (5.67) in Eq. (5.66), one has

$$\frac{(8\pi)^{3/2}}{6}\sum_{m_i} I^{\pm2,0,\pm2}_{\ell'\ell 2}(-1)^{-m_i}\begin{pmatrix} \ell' & \ell & 2 \\ m' & m & 0 \end{pmatrix}\begin{pmatrix} 2 & 1 & 1 \\ 0 & m_i & -m_i \end{pmatrix}. \tag{5.69}$$

Here, the sum over m_i is a number,

$$\sum_{m_i=-1}^{1}(-1)^{-m_i}\begin{pmatrix}2 & 1 & 1\\ 0 & m_i & -m_i\end{pmatrix}=\sqrt{\frac{2}{15}}\,. \tag{5.70}$$

The remaining Wigner 3-j symbols in Eq. (5.69) set $|\ell-2|\leq\ell'\leq|\ell+2|$ and $L_1=2$. The summation over $p=\pm2$ turns out to be

$$\sum_{p=\pm2}\left(\frac{p}{2}\right)^x I^{p0-p}_{2\ell\ell'}=\begin{cases}2I^{20-2}_{2\ell\ell'} & \text{for } x+\ell+\ell'=\text{ even}\\ 0 & \text{for } x+\ell+\ell'=\text{ odd}\,.\end{cases} \tag{5.71}$$

Here, $I^{20-2}_{2\ell\ell'}$ is a numerical value (being a function of ℓ's) and therefore, it is a multiplicative constant. In our case, $x=0$ and $\ell+\ell'=$ even so that the result is not vanishing. Therefore, the final result is

$$\begin{aligned}\langle a^{\mu}_{\ell m}a^{(t)T}_{\ell'm'}\rangle=(-i)^{\ell+\ell'}16\pi^2\sqrt{\frac{2}{15}}2I^{20-2}_{2\ell\ell'}\int\frac{dk_1k_1^2}{(2\pi)^3}\frac{dKK^2}{(2\pi)^3}f(k_1,|\mathbf{k}_1+\mathbf{K}|,K)j_\ell(k_3r_{\rm LS})\\ \times\mathcal{T}^{(t)T}_{\ell'}(K)F^{\zeta h}_{\rm NL}P_\zeta(k_1)P_h(K)\begin{pmatrix}\ell' & \ell & 2\\ m' & m & 0\end{pmatrix}.\end{aligned} \tag{5.72}$$

Now, let us evaluate the result of [186]

$$\begin{aligned}C^{\mu T,\rm OMP21}_{\ell_1\ell_2m_1m_2}=i^{\ell_2-\ell_1}64\pi^3\int\frac{dk_+dk_-}{(2\pi)^6}k_+^2k_-^2\mathcal{T}^T_{\ell_2}(k_+)j_{\ell_1}(k_+r_{\rm LS})W_h(k_-)P_\zeta(k_-)P_h(k_+)\\ \times\sum_{L_1,M_1}f^{\rm sst}_{L_1M_1}(-1)^{m_1+L_1}\sqrt{(2\ell_1+1)(2\ell_2+1)(2L_1+1)}\\ \times\begin{pmatrix}\ell_1 & \ell_2 & L_1\\ 0 & 2 & -2\end{pmatrix}\begin{pmatrix}\ell_1 & \ell_2 & L_1\\ -m_1 & m_2 & M_1\end{pmatrix}\Big[\xi_{\rm L}+(-1)^{\ell_1+\ell_2+L_1}\xi_{\rm R}\Big]\,.\end{aligned} \tag{5.73}$$

Notice that, from Eq. (5.68), we can also use the compact notation

$$\sqrt{4\pi}I^{02-2}_{\ell_1\ell_2L_1}=\sqrt{(2\ell_1+1)(2\ell_2+1)(2L_1+1)}\begin{pmatrix}\ell_1 & \ell_2 & L_1\\ 0 & 2 & -2\end{pmatrix}. \tag{5.74}$$

Authors of [186] used a different parameterization from ours. For this reason, in order to recover our results, we have to compute Eq. (5.73) in the case $L_1=2$ and $M_1=0$, so that

$$\begin{aligned}C^{\mu T,\rm OMP21}_{\ell_1\ell_2m_1m_2}=i^{\ell_2-\ell_1}32\pi^{5/2}I^{02-2}_{\ell_1\ell_2L_1}\int\frac{dk_+dk_-}{(2\pi)^6}k_+^2k_-^2\mathcal{T}^T_{\ell_2}(k_+)j_{\ell_1}(k_+r_{\rm LS})W_h(k_-)P_\zeta(k_-)P_h(k_+)\\ \times f^{\rm sst}_{20}(-1)^{m_1+2}\begin{pmatrix}\ell_1 & \ell_2 & 2\\ -m_1 & m_2 & 0\end{pmatrix}\Big[\xi_{\rm L}+(-1)^{\ell_1+\ell_2+2}\xi_{\rm R}\Big]\,.\end{aligned} \tag{5.75}$$

Comparing this expression with Eq. (5.72), one can notice that the result of [186] is consistent with ours, except for the constant normalization factors (which affect the amplitude) and for the sum over the polarization coefficients which is a number and it can be reabsorbed in the amplitude.

Thanks to these comparison of the μT cross-correlations, we have been able to prove the mathematical consistency of our results. Furthermore, the fact that this paper has addressed our own studies pleases us, as it means that we have addressed an interesting, current and powerful topic. We underline that the information content of the cross-correlations between μ-distortion and CMB anisotropies is very large and worth pointing out. For this reason, advanced futuristic surveys with very high sensitivity are necessary in order to study these signals.

Conclusions

The purpose of this Thesis was to deepen one of the topics of growing interest in modern cosmology, namely the CMB spectral distortions, pointing out relevant aspects related to the cross-correlation between μ-type distortion and the CMB temperature anisotropy. The importance of these distortions is related to the fact that they provide new tools to investigate the primordial Universe at small scales so far not accessible and to provide new constraints on the inflationary scenario, testing a vast range of scales, correspoding to $1\ \mathrm{Mpc}^{-1} \lesssim k \lesssim 10^4\ \mathrm{Mpc}^{-1}$.

We started by recalling the main features of the inflationary paradigm, introducing it as a solution of some issues characterizing the Hot Big Bang model of cosmology. Then, we addressed the production and evolution of the primordial perturbations during inflation in the context of single-field slow-roll models of inflation. We performed in details the computation of the inflationary power spectrum of curvature perturbations, and we recalled the main features of the typical inflationary bispectra (i.e. the Fourier transform of the three-point correlation function). In particular, the bispectrum is important for estimates of primordial non-Gaussianity of the cosmological perturbations. Afterwards, we went through the CMB, reporting the main features and dwelling on the production of anisotropies. Moreover, we derived the angular power spectrum for the CMB, result that was useful later on to calculate the correlation with CMB spectral distortions.

We then presented the derivation of the main results present in the literature as far as the CMB spectral distortions in the CMB frequency spectrum, offering a rigorous derivation for these results. CMB spectral distortions from dissipation of acoustic waves in the primordial plasma can be used to test the statistical properties of primordial cosmological perturbations [91]. In particular, we focused on the possibility of constraining the primordial local non-Gaussianity through the cross-correlation between the μ-distortion and the CMB temperature anisotropy at first order (in the Sachs-Wolfe regime), cross-correlation that is particularly sensitive to the so-called squeezed limit of primordial bispectra. This triangle configuration is very interesting since, in this case, a perturbation mode has a wave number which is much smaller than the other two, meaning that it crosses the horizon much earlier than the other two modes. This produces a coupling between small and large scales, with the long-wavelength mode modulating the small scale power of the

two small-wavelength modes, and this has interesting physical consequences. Moreover, high-precision measurements of the μT cross-correlation can constitute a powerful tool to evaluate the bispectrum amplitude parameter $f_{\rm NL}^{\rm loc}$ in models predicting non-Gaussian signals with a significant contribution from squeezed triangles [12, 13, 92, 205]. The main interest of this approach is the possibility to test primordial non-Gaussianity at wavenumbers 50 $\mathrm{Mpc}^{-1} \lesssim k \lesssim 10^4$ Mpc^{-1}, far smaller than those accessible to other methods, for instance, the CMB temperature fluctuations. We presented a complete derivation for the $C_\ell^{\mu T}$, recovering well known results in the literature (see e.g. [13]).

Then, given the power and importance of the CMB spectral distortions, we investigated the possibility of generating anisotropic features in these distortions, focusing on μ-type. Among the various possibilities of sources of such anisotropies, there are the so-called tensor fossils, new primordial degrees of freedom which could couple with the inflaton. These fossils no longer interact, or interact very weakly, during late-time cosmic evolution and then the only observational effect due to their coupling with the inflation field would be to give rise to local departures from statistical isotropy, or from Gaussianity, in the primordial curvature perturbation field (see e.g. [9, 10]). These fossils could be scalar, vector or tensor fields. We focus on tensor modes, i.e., gravitational waves (GWs), since they are of fundamental importance in shedding light on the physics of the the early Universe. We studied the imprints of large-scale relic GWs on large-scale structure of the Universe [11]. In this case the main effect is the production of a quadrupole in the galaxy power spectrum. In standard single-field inflation scenario, the fossil signature would be too small to be detected with current and near future technology. However, non-standard variants of inflation can produce a much larger galaxy power quadrupole (this happens when the so-called consistency relations for the tensor-scalar-scalar bispectrum such as the one in [51] are violated).

In the final part of this Thesis we performed an original computation studying how the fossil tensor degree of freedom can distort the primoridal power spectrum of the scalar perturbations, on which the average value of μ-distortion depends. To that end, we calculated the tensor-scalar-scalar bispectrum in the squeezed limit configuration with the long-wavelength mode of tensor fossil modulating the small-scale power spectrum of curvature perturbations. Interestingly, we found that this primordial squeezed bispectrum induces statistical anisotropies in the average value of the $a_{\ell m}^{\mu}$ coefficients, which, however, needs to be evaluated numerically to understand the possible detectability of that signal associated with the different multipole configurations.

Moreover, extending what has been done so far in the literature, we calculated analytically the μT cross-correlation, induced by the scalar-tensor-tensor bispectrum. We considered the case of μ-distortions generated by dissipation of GWs (which depends on the tensor-tensor power spectrum) and then, we derived the primordial correlation with

CMB temperature anisotropies, generated by the long-wavelength scalar mode, in the squeezed limit.

As a final step, we calculated the μT cross-correlation in the case in which the temperature anisotropies are generated by a long-wavelength tensor mode, which modulates the scalar power spectrum of the μ-distortion. Comparing with [186], we found that indeed a quadrupole anisotropy is induced in the scalar power spectrum. These results on the μT cross-correlations involving tensor modes are new and original (including also the computation about the impact of tensor fossils on the average of μ). Notice that, while writing this Thesis, Ref. [186] appeared, dealing with the same issues about the μT cross-correlations (but not dealing with the results about the anisotropies in the average of μ induced by tensor fossils), and as we said, whenever comparable the results of Ref [186], agree with the ones in this Thesis. However, in order to provide an observable prediction, we need to numerically further develop the results we obtained in this Thesis.

Concluding, CMB spectral distortions and cross-correlations between μ-spectral distortion and CMB anisotropies are a powerfull tool to test the physics of the early stages of the Universe and primordial non-Gaussianity, providing a new way to test the physics of the primordial Universe.

Acknowledgements

I would sincerely express my gratitude to my supervisors for giving me the opportunity to work with them and for patiently guiding and following me through a completely new field, for the invaluable advice and for the great support in writing this thesis.

I would thank Prof. Nicola Bartolo for his suggestions, for the work done and for the commitment he has dedicated to me for the realization of this project.

I would thank Prof. Jens Chluba for the time he devoted to me for meaningful discussions, for the support and for the detailed explanations, always willing to help and advice me throughout my work.

I am grateful to Dr. Andrea Ravenni for his full availability, the support, the help and advice he has provided me, resolving many of my doubts.

Thank you all for accompanying me along this path.

Vorrei ringraziare i miei genitori. L'amore e la premura, gli insegnamenti e i sacrifici, tutto quello che mi avete donato sono stati fondamentali per me. Vi ringrazio infinitamente per avermi sempre sostenuto, appoggiandomi in ogni mia decisione e progetto. Dedico a voi questo lavoro.

Vorrei ringraziare mio fratello Gianrocco e mia sorella Arianna. Grazie per il vostro supporto e per la fiducia, per tutti i momenti belli e per quelli difficili che ci hanno aiutato a crescere sempre insieme. Grazie per essermi stati accanto e per aver gioito insieme a me per ogni traguardo raggiunto.

Ringrazio anche Emanuele per la disponibilità e i suoi consigli, per l'appoggio e per avermi dimostrato stima e affetto in tutti questi anni.

Grazie anche alla piccola Valentina per aver inconsapevolmente alleviato, con tutta la tua tenerezza, quest'ultimo periodo.

Ringrazio tutti i miei amici per essere rimasti tali nonostante la distanza e il tempo. Grazie per i momenti belli, spensierati e divertenti che abbiamo condiviso insieme, per l'incoraggiamento e per la comprensione che avete dimostrato nei miei confronti (soprattutto nel non vedermi per settimane a causa dello studio).

In particolare, ringrazio Arianna che ormai da una vita mi sostiene e mi è vicina. Grazie per la pazienza, per essere sempre pronta ad ascoltarmi, per la disponibilità e il supporto, per le risate e i bei momenti insieme, con la speranza di condividerne molti altri. Grazie per esserci sempre.

Un ringraziamento speciale va a Gabriele per l'incessante supporto datomi in tutti questi anni. Se sono arrivata fin qui e questo lavoro è stato portato a termine è anche merito tuo. Grazie per tutto il tempo che mi hai dedicato, per non aver mai smesso di credere in me e nelle mie capacità, per avermi aiutato ad essere audace, a credere in me stessa e a non arrendermi, anche e soprattutto nei momenti più difficili.

Grazie per essermi stati accanto, ognuno a suo modo, in questo complesso e difficile percorso.

Bibliography

[1] J. C. e. a. Mather, *Measurement of the Cosmic Microwave Background Spectrum by the COBE FIRAS Instrument*, ApJ **420**, 439 (1994).

[2] D. J. Fixsen, E. S. Cheng, J. M. Gales, J. C. Mather, R. A. Shafer, and E. L. Wright, *The Cosmic Microwave Background Spectrum from the Full COBE/FIRAS Data Set*, ApJ **473**, 576 (1996).

[3] R. A. Sunyaev and Y. B. Zeldovich, *Distortions of the Background Radiation Spectrum*, Nature **223**, 721–722 (1969).

[4] J. C. Mather and et al., *A Preliminary Measurement of the Cosmic Microwave Background Spectrum by the Cosmic Background Explorer (COBE) Satellite*, ApJL **354**, L37 (1990).

[5] J. Chluba, *Future Steps in Cosmology using Spectral Distortions of the Cosmic Microwave Background*, 2018, arXiv:1806.02915 [astro-ph.CO].

[6] M. Lucca, N. Schöneberg, D. C. Hooper, J. Lesgourgues, and J. Chluba, *The synergy between CMB spectral distortions and anisotropies*, JCAP **2020**, 026–026 (2020).

[7] J. Chluba and et al., *New Horizons in Cosmology with Spectral Distortions of the Cosmic Microwave Background*, 2019, arXiv:1909.01593 [astro-ph.CO].

[8] T. Kite, A. Ravenni, S. P. Patil, and J. Chluba, *Bridging the gap: spectral distortions meet gravitational waves*, MNRAS **505**, 4396–4405 (2021).

[9] D. Jeong and M. Kamionkowski, *Clustering Fossils from the Early Universe*, Phys. Rev. Lett. **108** (2012).

[10] L. Dai, D. Jeong, and M. Kamionkowski, *Seeking inflation fossils in the cosmic microwave background*, Phys. Rev. D **87** (2013).

[11] L. Dai, D. Jeong, and M. Kamionkowski, *Anisotropic imprint of long-wavelength tensor perturbations on cosmic structure*, Phys. Rev. D **88** (2013).

[12] M. Shiraishi, M. Liguori, N. Bartolo, and S. Matarrese, *Measuring primordial anisotropic correlators with CMB spectral distortions*, Phys. Rev. D **92** (2015).

[13] R. Emami, E. Dimastrogiovanni, J. Chluba, and M. Kamionkowski, *Probing the scale dependence of non-Gaussianity with spectral distortions of the cosmic microwave background*, Phys. Rev. D **91** (2015).

[14] E. Hubble, *A relation between distance and radial velocity among extra-galactic nebulae*, Proc. Nat. Acad. Sci. **15**, 168–173 (1929).

[15] A. A. Penzias and R. W. Wilson, *A Measurement of Excess Antenna Temperature at 4080 Mc/s.* ApJ **142**, 419–421 (1965).

[16] J. R. Primack, *The Nature of dark matter*, Frascati Phys. Ser. **24**, 449–474 (2002), arXiv:astro-ph/0112255.

[17] N. Aghanim and et al. (Planck Collaboration), *Planck 2018 results. VI. Cosmological parameters*, Astronomy & Astrophysics **641**, A6 (2020).

[18] E. W. Kolb, *Cosmology and the Unexpected*, 2007.

[19] S. Dodelson, *Modern Cosmology* (Accademic Press, Amsterdam, 2003).

[20] S. Weinberg, *Cosmology* (UK: Oxford Univ. Pr., Oxford, 2008).

[21] A. Riotto, *Inflation and the theory of cosmological perturbations*, ICTP Lect. Notes Ser. **14**, edited by G. Dvali, A. Perez-Lorenzana, G. Senjanovic, G. Thompson, and F. Vissani, 317–413 (2003), arXiv:hep-ph/0210162.

[22] P. A. R. Ade and et al. (Planck Collaboration), *Planck 2015 results. XIII. Cosmological parameters*, Astronomy & Astrophysics **594**, A13 (2016).

[23] A. D. Sakharov, *Violation of CP invariance, C asymmetry, and baryon asymmetry of the universe*, Pisma Zh. Eksp. Teor. Fiz. **5**, 32–35 (1967).

[24] J. M. Cline, "Baryogenesis", in Les Houches Summer School - Session 86: Particle Physics and Cosmology: The Fabric of Spacetime (2006), arXiv:hep-ph/0609145.

[25] J. M. Cline, *TASI Lectures on Early Universe Cosmology: Inflation, Baryogenesis and Dark Matter*, 2021, arXiv:1807.08749 [hep-ph].

[26] C. Balazs, *Baryogenesis: A small review of the big picture*, 2014, arXiv:1411.3398 [hep-ph].

[27] M. S. Turner, *The early universe* (Westview Press, 1990).

[28] R. A. Alpher, H. Bethe, and G. Gamow, *The Origin of Chemical Elements*, Phys. Rev. **73**, 803–804 (1948).

[29] N. Aghanim and et al. (Planck Collaboration), *Planck 2018 results. I. Overview and the cosmological legacy of Planck*, Astronomy & Astrophysics **641**, A1 (2020).

[30] D. Baumann, *TASI Lectures on Inflation*, 2012, arXiv:0907.5424 [hep-th].

[31] G. F. Smoot and et al., *Structure in the COBE Differential Microwave Radiometer First-Year Maps*, ApJL **396**, L1 (1992).

[32] P. A. R. Ade and et al. (Planck Collaboration), *Planck 2015 results. XVI. Isotropy and statistics of the CMB*, Astronomy & Astrophysics **594**, A16 (2016).

[33] S. Watson, *An Exposition on inflationary cosmology*, (2000), arXiv:astro-ph/0005003.

[34] G. 't Hooft, *Magnetic Monopoles in Unified Gauge Theories*, Nucl. Phys. B **79**, 276–284 (1974).

[35] E. Komatsu and et al., *Five-Year Wilkinson Microwave Anisotropy Probe (WMAP) Observations: Cosmological Interpretation*, ApJS **180**, 330–376 (2009).

[36] Y. Akrami and et al. (Planck Collaboration), *Planck 2018 results. X. Constraints on inflation*, Astronomy & Astrophysics **641**, A10 (2020).

[37] A. A. Starobinsky, *A New Type of Isotropic Cosmological Models Without Singularity*, Phys. Lett. B **91**, 99–102 (1980).

[38] D. Kazanas, *Dynamics of the universe and spontaneous symmetry breaking*, ApJL **241**, L59–L63 (1980).

[39] K. Sato, *First Order Phase Transition of a Vacuum and Expansion of the Universe*, MNRAS **195**, 467–479 (1981).

[40] A. D. Linde, *A New Inflationary Universe Scenario: A Possible Solution of the Horizon, Flatness, Homogeneity, Isotropy and Primordial Monopole Problems*, Phys. Lett. B **108**, 389–393 (1982).

[41] A. H. Guth, *Inflationary universe: a possible solution to the horizon and flatness problems*, Phys. Rev. D **23**, 347–356 (1981).

[42] A. H. Guth and E. J. Weinberg, *Cosmological consequences of a first-order phase transition in the SU_5 grand unified model*, Phys. Rev. D **23**, 876–885 (1981).

[43] D. Langlois, *Lectures on inflation and cosmological perturbations*, Lecture Notes in Physics, 1–57 (2010).

[44] D. H. Lyth and A. Riotto, *Particle physics models of inflation and the cosmological density perturbation*, Physics Reports **314**, 1–146 (1999).

[45] K. D. Lozanov, *Lectures on Reheating after Inflation*, 2019, arXiv:1907.04402 [astro-ph.CO].

[46] B. A. Bassetti, S. Tsujikawa, and D. Wands, *Inflation dynamics and reheating*, Reviews of Modern Physics **78**, 537–589 (2006).

[47] N. Bartolo, E. Komatsu, S. Matarrese, and A. Riotto, *Non-Gaussianity from inflation: theory and observations*, Physics Reports **402**, 103–266 (2004).

[48] H. V. Peiris and et al., *First Year Wilkinson Microwave Anisotropy Probe (WMAP) Observations: Implications For Inflation*, ApJS **148**, 213–231 (2003).

[49] C. L. Bennett and et al., *First Year Wilkinson Microwave Anisotropy Probe (WMAP) Observations: Preliminary Maps and Basic Results*, ApJS **148**, 1–27 (2003).

[50] P. Creminelli, *On non-Gaussianities in single-field inflation*, JCAP **2003**, 003–003 (2003).

[51] J. Maldacena, *Non-gaussian features of primordial fluctuations in single field inflationary models*, JHEP **2003**, 013–013 (2003).

[52] V. Acquaviva, N. Bartolo, S. Matarrese, and A. Riotto, *Gauge-invariant second-order perturbations and non-Gaussianity from inflation*, Nuclear Physics B **667**, 119–148 (2003).

[53] D. Babich, P. Creminelli, and M. Zaldarriaga, *The shape of non-Gaussianities*, JCAP **2004**, 009–009 (2004).

[54] E. Komatsu and et al., *Non-Gaussianity as a Probe of the Physics of the Primordial Universe and the Astrophysics of the Low Redshift Universe*, 2009, arXiv:0902.4759 [astro-ph.CO].

[55] X. Chen, *Primordial Non-Gaussianities from Inflation Models*, Advances in Astronomy **2010**, 1–43 (2010).

[56] M. Liguori, E. Sefusatti, J. R. Fergusson, and E. P. S. Shellard, *Primordial Non-Gaussianity and Bispectrum Measurements in the Cosmic Microwave Background and Large-Scale Structure*, Advances in Astronomy **2010**, 1–64 (2010).

[57] A. P. S. Yadav and B. D. Wandelt, *Primordial Non-Gaussianity in the Cosmic Microwave Background*, Advances in Astronomy **2010**, 1–27 (2010).

[58] D. H. Lyth and A. R. Liddle, *The Primordial Density Perturbation: Cosmology, Inflation and the Origin of Structure* (Cambridge University Press, 2009).

[59] C. Cheung, A. L. Fitzpatrick, J. Kaplan, and L. Senatore, *On the consistency relation of the three-point function in single-field inflation*, JCAP **2008**, 021 (2008).

[60] P. Creminelli, L. Senatore, and M. Zaldarriaga, *Estimators for local non-Gaussianities*, JCAP **2007**, 019–019 (2007).

[61] J. R. Fergusson and E. P. S. Shellard, *Shape of primordial non-Gaussianity and the CMB bispectrum*, Phys. Rev. D **80** (2009).

[62] N. Bartolo, S. Matarrese, and A. Riotto, *Non-Gaussianity in the cosmic microwave background anisotropies at recombination in the squeezed limit*, JCAP **2012**, 017–017 (2012).

[63] N. Arkani-Hamed, D. Baumann, H. Lee, and G. L. Pimentel, *The Cosmological Bootstrap: Inflationary Correlators from Symmetries and Singularities*, 2019, arXiv:1811.00024 [hep-th].

[64] L. Senatore, K. M. Smith, and M. Zaldarriaga, *Non-Gaussianities in single field inflation and their optimal limits from the WMAP 5-year data*, JCAP **2010**, 028–028 (2010).

[65] C. T. Byrnes, *Lecture notes on non-Gaussianity*, Astrophys. Space Sci. Proc. **45**, edited by J. C. Fabris, O. F. Piattella, D. C. Rodrigues, H. E. S. Velten, and W. Zimdahl, 135–165 (2016), arXiv:1411.7002 [astro-ph.CO].

[66] N. Bartolo, M. Liguori, and M. Shiraishi, *Primordial trispectra and CMB spectral distortions*, JCAP **03**, 029 (2016), arXiv:1511.01474 [astro-ph.CO].

[67] E. Komatsu and D. N. Spergel, *Acoustic signatures in the primary microwave background bispectrum*, Phys. Rev. D **63** (2001).

[68] P. Creminelli and M. Zaldarriaga, *A single-field consistency relation for the three-point function*, JCAP **2004**, 006–006 (2004).

[69] Akrami and et al. (Planck Collaboration), *Planck 2018 results. IX. Constraints on primordial non-Gaussianity*, 2019, arXiv:1905.05697 [astro-ph.CO].

[70] R. A. Alpher and R. C. Herman, *On the Relative Abundance of the Elements*, Phys. Rev. **74**, 1737–1742 (1948).

[71] E. R. Harrison, *Fluctuations at the Threshold of Classical Cosmology*, Phys. Rev. D **1**, 2726–2730 (1970).

[72] P. J. E. Peebles and J. T. Yu, *Primeval Adiabatic Perturbation in an Expanding Universe*, ApJ **162**, 815 (1970).

[73] Y. B. Zeldovich, *A hypothesis, unifying the structure and the entropy of the Universe*, MNRAS **160**, 1P (1972).

[74] C. L. Bennett, A. J. Banday, K. M. Górski, G. Hinshaw, P. Jackson, P. Keegstra, A. Kogut, G. F. Smoot, D. T. Wilkinson, and E. L. Wright, *Four-Year COBE DMR Cosmic Microwave Background Observations: Maps and Basic Results*, ApJ **464**, L1–L4 (1996).

[75] D. J. Fixsen, *The Temperature of the Cosmic Microwave Background*, ApJ **707**, 916–920 (2009).

[76] W. Hu, "*Wandering in the Background: A CMB Explorer*", PhD thesis (1995), arXiv:astro-ph/9508126 [astro-ph].

[77] R. K. Sachs and A. M. Wolfe, *Perturbations of a Cosmological Model and Angular Variations of the Microwave Background*, ApJ **147**, 73 (1967).

[78] J. Silk, *Cosmic Black-Body Radiation and Galaxy Formation*, ApJ **151**, 459 (1968).

[79] R. A. Sunyaev and Y. B. Zeldovich, *Small-Scale Fluctuations of Relic Radiation*, APSS **7**, 3–19 (1970).

[80] R. A. Sunyaev and Y. B. Zeldovich, *Small scale entropy and adiabatic density perturbations — Antimatter in the Universe*, APSS **9**, 368–382 (1970).

[81] Y. B. Zeldovich and R. A. Sunyaev, *The Interaction of Matter and Radiation in a Hot-Model Universe*, APSS **4**, 301–316 (1969).

[82] R. A. Sunyaev and Y. B. Zeldovich, *The Observations of Relic Radiation as a Test of the Nature of X-Ray Radiation from the Clusters of Galaxies*, Comments on Astrophysics and Space Physics **4**, 173 (1972).

[83] R. A. Sunyaev and Y. B. Zeldovich, *Microwave background radiation as a probe of the contemporary structure and history of the universe*, ARAA **18**, 537–560 (1980).

[84] D. N. Spergel and et al., *First-Year Wilkinson Microwave Anisotropy Probe (WMAP) Observations: Determination of Cosmological Parameters*, ApJS **148**, 175–194 (2003).

[85] P. A. R. Ade and et al. (Planck Collaboration), *Planck 2013 results. I. Overview of products and scientific results*, Astronomy & Astrophysics **571**, A1 (2014).

[86] P. A. R. Ade and et al. (Planck Collaboration), *Planck 2013 results. XVI. Cosmological parameters*, Astronomy & Astrophysics **571**, A16 (2014).

[87] W. Hu and N. Sugiyama, *Small scale integrated sachs-wolfe effect*, Phys. Rev. D **50**, 627–631 (1994).

[88] J. P. Ostriker and E. T. Vishniac, *Generation of Microwave Background Fluctuations from Nonlinear Perturbations at the ERA of Galaxy Formation*, ApJL **306**, L51 (1986).

[89] E. T. Vishniac, *Reionization and Small-Scale Fluctuations in the Microwave Background*, ApJ **322**, 597 (1987).

[90] M. J. Rees and D. W. Sciama, *Large-scale Density Inhomogeneities in the Universe*, Nature **217**, 511–516 (1968).

[91] E. Pajer and M. Zaldarriaga, *A New Window on Primordial Non-Gaussianity*, Phys. Rev. Lett. **109** (2012).

[92] J. Ganc and E. Komatsu, *Scale-dependent bias of galaxies and μ-type distortion of the cosmic microwave background spectrum from single-field inflation with a modified initial state*, Phys. Rev. D **86** (2012).

[93] J. Chluba and R. A. Sunyaev, *The evolution of CMB spectral distortions in the early Universe*, MNRAS **419**, 1294–1314 (2011).

[94] W. Hu and J. Silk, *Thermalization constraints and spectral distortions for massive unstable relic particles*, Phys. Rev. Lett. **70**, 2661–2664 (1993).

[95] P. McDonald, R. J. Scherrer, and T. P. Walker, *Cosmic microwave background constraint on residual annihilations of relic particles*, Phys. Rev. D **63**, 023001 (2000).

[96] J. Chluba, *Could the cosmological recombination spectrum help us understand annihilating dark matter?*, MNRAS **402**, 1195–1207 (2010).

[97] J. Chluba, *Distinguishing different scenarios of early energy release with spectral distortions of the cosmic microwave background*, MNRAS **436**, 2232–2243 (2013).

[98] K. Miyamoto, T. Sekiguchi, H. Tashiro, and S. Yokoyama, *CMB distortion anisotropies due to the decay of primordial magnetic fields*, Phys. Rev. D **89** (2014).

[99] K. E. Kunze and E. Komatsu, *Constraining primordial magnetic fields with distortions of the black-body spectrum of the cosmic microwave background: pre- and post-decoupling contributions*, JCAP **2014**, 009–009 (2014).

[100] J. Ganc and M. S. Sloth, *Probing correlations of early magnetic fields using μ-distortion*, JCAP **2014**, 018–018 (2014).

[101] B. J. Carr, K. Kohri, Y. Sendouda, and J. Yokoyama, *New cosmological constraints on primordial black holes*, Phys. Rev. D **81** (2010).

[102] R. Khatri and R. A. Sunyaev, *Beyond y and μ: the shape of the CMB spectral distortions in the intermediate epoch,* $1.5\times10^4 \lesssim z \lesssim 2\times10^5$, JCAP **2012**, 016–016 (2012).

[103] R. Khatri and R. A. Sunyaev, *Creation of the CMB spectrum: precise analytic solutions for the blackbody photosphere*, JCAP **2012**, 038–038 (2012).

[104] J. Chluba and et al., *Spectral Distortions of the CMB as a Probe of Inflation, Recombination, Structure Formation and Particle Physics*, 2019, arXiv:1903.04218 [astro-ph.CO].

[105] C. Burigana, L. Danese, and G. de Zotti, *Formation and evolution of early distortions of the microwave background spectrum - A numerical study*, Astronomy & Astrophysics **246**, 49–58 (1991).

[106] J. Chluba, *Green's function of the cosmological thermalization problem*, MNRAS **434**, 352–357 (2013).

[107] W. Hu, D. Scott, and J. Silk, *Power spectrum constraints from spectral distortions in the cosmic microwave background*, ApJ **430**, L5 (1994).

[108] A. Kogut and et al., *The Primordial Inflation Explorer (PIXIE): a nulling polarimeter for cosmic microwave background observations*, JCAP **2011**, 025–025 (2011).

[109] P. Andre and et al. (PRISM Collaboration), *PRISM (Polarized Radiation Imaging and Spectroscopy Mission): A White Paper on the Ultimate Polarimetric Spectro-Imaging of the Microwave and Far-Infrared Sky*, 2013, arXiv:1306.2259 [astro-ph.CO].

[110] P. André et al. (PRISM Collaboration), *PRISM (Polarized Radiation Imaging and Spectroscopy Mission): An Extended White Paper*, JCAP **02**, 006 (2014), arXiv:1310.1554 [astro-ph.CO].

[111] A. Kogut, M. H. Abitbol, J. Chluba, J. Delabrouille, D. Fixsen, J. C. Hill, S. P. Patil, and A. Rotti, *CMB Spectral Distortions: Status and Prospects*, 2019, arXiv:1907.13195 [astro-ph.CO].

[112] J. Chluba, A. Ravenni, and S. K. Acharya, *Thermalization of large energy release in the early Universe*, MNRAS **498**, 959–980 (2020).

[113] J. Chluba and D. Jeong, *Teasing bits of information out of the CMB energy spectrum*, MNRAS **438**, 2065–2082 (2014).

[114] A. S. Kompaneets, *The Establishment of Thermal Equilibrium between Quanta and Electrons*, Soviet Journal of Experimental and Theoretical Physics **4**, 730–737 (1957).

[115] Y. B. Zeldovich and R. A. Sunyaev, *The Interaction of Matter and Radiation in a Hot-Model Universe*, APSS **4**, 301–316 (1969).

[116] J. Chluba, "Spectral Distortions of the Cosmic Microwave Background", PhD thesis (2005).

[117] Y. Ali-Haïmoud, J. Chluba, and M. Kamionkowski, *Constraints on Dark Matter Interactions with Standard Model Particles from Cosmic Microwave Background Spectral Distortions*, Phys. Rev. Lett. **115** (2015).

[118] J. Chluba, *Green's function of the cosmological thermalization problem – II. Effect of photon injection and constraints*, MNRAS **454**, 4182–4196 (2015).

[119] J. Chluba, *Refined approximations for the distortion visibility function and μ-type spectral distortions*, MNRAS **440**, 2544–2563 (2014).

[120] W. Hu and J. Silk, *Thermalization and spectral distortions of the cosmic background radiation*, Phys. Rev. D **48**, 485–502 (1993).

[121] R. A. Daly, *Spectral Distortions of the Microwave Background Radiation Resulting from the Damping of Pressure Waves*, APJ **371**, 14 (1991).

[122] J. Chluba, A. L. Erickcek, and I. Ben-Dayan, *Probing the inflaton: Small-scale power spectrum constraints from measurements of the CMB energy spectrum*, ApJ **758**, 76 (2012).

[123] R. Khatri, R. A. Sunyaev, and J. Chluba, *Mixing of blackbodies: entropy production and dissipation of sound waves in the early Universe*, Astronomy & Astrophysics **543**, A136 (2012).

[124] J. Chluba, R. Khatri, and R. A. Sunyaev, *CMB at 2×2 order: the dissipation of primordial acoustic waves and the observable part of the associated energy release*, MNRAS **425**, 1129–1169 (2012).

[125] J. Chluba, J. Hamann, and S. P. Patil, *Features and new physical scales in primordial observables: Theory and observation*, International Journal of Modern Physics D **24**, 1530023 (2015).

[126] N. Kaiser, *Small-angle anisotropy of the microwave background radiation in the adiabatic theory*, MNRAS **202**, 1169–1180 (1983).

[127] R. Khatri, R. A. Sunyaev, and J. Chluba, *Does Bose-Einstein condensation of CMB photons cancel μ distortions created by dissipation of sound waves in the early Universe?*, Astronomy & Astrophysics **540**, A124 (2012).

[128] S. Weinberg, *Gravitation and Cosmology: Principles and Applications of the General Theory of Relativity* (Oxford University Press, Oxford, UK, 2008).

[129] P. A. R. Ade and et al. (Planck Collaboration), *Planck 2015 results. XVII. Constraints on primordial non-Gaussianity*, Astronomy & Astrophysics **594**, A17 (2016).

[130] L. Verde, L. Wang, A. F. Heavens, and M. Kamionkowski, *Large-scale structure, the cosmic microwave background and primordial non-Gaussianity*, MNRAS **313**, 141–147 (2000).

[131] L. Verde and et al., *The 2dF Galaxy Redshift Survey: the bias of galaxies and the density of the Universe*, MNRAS **335**, 432–440 (2002).

[132] A. Loeb and M. Zaldarriaga, *Measuring the Small-Scale Power Spectrum of Cosmic Density Fluctuations through 21 cm Tomography Prior to the Epoch of Structure Formation*, Phys. Rev. Lett. **92** (2004).

[133] G. Cabass, E. Pajer, and D. v. d. Woude, *Spectral distortion anisotropies from single-field inflation*, JCAP **2018**, 050–050 (2018).

[134] R. Khatri and R. Sunyaev, *Constraints on μ-distortion fluctuations and primordial non-Gaussianity from Planck data*, JCAP **2015**, 026–026 (2015).

[135] P. A. R. Ade and et al. (Planck Collaboration), *Planck 2015 results. XX. Constraints on inflation*, Astronomy & Astrophysics **594**, A20 (2016).

[136] P. A. R. Ade and et al. (BICEP2 Collaboration), *Detection of B-Mode Polarization at Degree Angular Scales by BICEP2*, Phys. Rev. Lett. **112** (2014).

[137] P. A. R. Ade and et al. (BICEP2 and Planck Collaborations), *Joint Analysis of BICEP2/Keck Array and PlanckData*, Phys. Rev. Lett. **114** (2015).

[138] R. Keisler and et al., *Measurements of Sub-degree B-mode Polarization in the Cosmic Microwave Background from 100 Square Degrees of SPTpol Data*, ApJ **807**, 151 (2015).

[139] A. Gangui, F. Lucchin, S. Matarrese, and S. Mollerach, *The Three point correlation function of the cosmic microwave background in inflationary models*, ApJ. **430**, 447–457 (1994).

[140] D. S. Salopek and J. R. Bond, *Nonlinear evolution of long wavelength metric fluctuations in inflationary models*, Phys. Rev. D **42**, 3936–3962 (1990).

[141] J. Martin, C. Ringeval, and V. Vennin, *Encyclopaedia Inflationaris*, 2013, arXiv:1303.3787 [astro-ph.CO].

[142] D. Wands, N. Bartolo, S. Matarrese, and A. Riotto, *An Observational test of two-field inflation*, Phys. Rev. D **66**, 043520 (2002).

[143] N. Bartolo, S. Matarrese, and A. Riotto, *Adiabatic and isocurvature perturbations from inflation: Power spectra and consistency relations*, Phys. Rev. D **64**, 123504 (2001).

[144] A. Linde, *Hybrid inflation*, Phys. Rev. D **49**, 748–754 (1994).

[145] E. J. Copeland, A. R. Liddle, D. H. Lyth, E. D. Stewart, and D. Wands, *False vacuum inflation with Einstein gravity*, Phys. Rev. D **49**, 6410–6433 (1994).

[146] D. Baumann and D. Green, *Signature of supersymmetry from the early universe*, Phys. Rev. D **85** (2012).

[147] D. H. Lyth and D. Wands, *Generating the curvature perturbation without an inflaton*, Physics Letters B **524**, 5–14 (2002).

[148] J. Beltrán Jiménez and A. L. Maroto, *Cosmological evolution in vector-tensor theories of gravity*, Phys. Rev. D **80** (2009).

[149] N. Bartolo, E. Dimastrogiovanni, S. Matarrese, and A. Riotto, *Anisotropic Bispectrum of Curvature Perturbations from Primordial Non-Abelian Vector Fields*, JCAP **2009**, 015–015 (2009).

[150] X. Chen and Y. Wang, *Quasi-single field inflation and non-Gaussianities*, JCAP **2010**, 027–027 (2010).

[151] A. Golovnev and V. Vanchurin, *Cosmological perturbations from vector inflation*, Phys. Rev. D **79** (2009).

[152] D. Seery, M. S. Sloth, and F. Vernizzi, *Inflationary trispectrum from graviton exchange*, JCAP **2009**, 018–018 (2009).

[153] E. Pajer, F. Schmidt, and M. Zaldarriaga, *The Observed squeezed limit of cosmological three-point functions*, Physical Review D **88** (2013).

[154] F. Schmidt, E. Pajer, and M. Zaldarriaga, *Large-scale structure and gravitational waves. III. Tidal effects*, Phys. Rev. D **89** (2014).

[155] E. Dimastrogiovanni, M. Fasiello, and M. Kamionkowski, *Imprints of massive primordial fields on large-scale structure*, JCAP **2016**, 017–017 (2016).

[156] E. Dimastrogiovanni, M. Fasiello, D. Jeong, and M. Kamionkowski, *Inflationary tensor fossils in large-scale structure*, JCAP **2014**, 050–050 (2014).

[157] M. Akhshik, *Clustering fossils in solid inflation*, JCAP **2015**, 043–043 (2015).

[158] R. Emami and H. Firouzjahi, *Clustering fossil from primordial gravitational waves in anisotropic inflation*, JCAP **2015**, 043–043 (2015).

[159] S. Matarrese, L. Pilo, and R. Rollo, *Resilience of long modes in cosmological observables*, JCAP **01**, 062 (2021), eprint: 2007.08877.

[160] P. Creminelli, G. D'Amico, M. Musso, and J. Noreña, *The (not so) squeezed limit of the primordial* 3*-point function*, JCAP **2011**, 038–038 (2011).

[161] X. Chen, H. Firouzjahi, M. Hossein Namjoo, and M. Sasaki, *A single field inflation model with large local non-Gaussianity*, EPL **102**, 59001 (2013).

[162] M. C. Guzzetti, N. Bartolo, M. Liguori, and S. Matarrese, *Gravitational waves from inflation*, Riv. Nuovo Cim. **39**, 399–495 (2016).

[163] M. Bruni, S. Matarrese, S. Mollerach, and S. Sonego, *Perturbations of spacetime: gauge transformations and gauge invariance at second order and beyond*, Classical and Quantum Gravity **14**, 2585–2606 (1997).

[164] J. M. Bardeen, *Gauge Invariant Cosmological Perturbations*, Phys. Rev. D **22**, 1882–1905 (1980).

[165] K. Saikawa and S. Shirai, *Primordial gravitational waves, precisely: the role of thermodynamics in the Standard Model*, JCAP **2018**, 035–035 (2018).

[166] A. Buonanno, *Gravitational waves*, 2007, arXiv:0709.4682 [gr-qc].

[167] Y. Watanabe and E. Komatsu, *Improved calculation of the primordial gravitational wave spectrum in the standard model*, Phys. Rev. D **73** (2006).

[168] N. Bartolo, G. Orlando, and M. Shiraishi, *Measuring chiral gravitational waves in Chern-Simons gravity with CMB bispectra*, JCAP **2019**, 050–050 (2019).

[169] P. Adshead, N. Afshordi, E. Dimastrogiovanni, M. Fasiello, E. A. Lim, and G. Tasinato, *Multimessenger cosmology: Correlating cosmic microwave background and stochastic gravitational wave background measurements*, Phys. Rev. D **103** (2021).

[170] V. Alba and J. Maldacena, *Primordial gravity wave background anisotropies*, JHEP **2016** (2016).

[171] N. Bartolo, D. Bertacca, S. Matarrese, M. Peloso, A. Ricciardone, A. Riotto, and G. Tasinato, *Anisotropies and non-Gaussianity of the cosmological gravitational wave background*, Phys. Rev. D **100** (2019).

[172] N. Bartolo, D. Bertacca, S. Matarrese, M. Peloso, A. Ricciardone, A. Riotto, and G. Tasinato, *Characterizing the cosmological gravitational wave background: Anisotropies and non-Gaussianity*, Phys. Rev. D **102** (2020).

[173] A. R. Liddle and D. H. Lyth, *Cosmological Inflation and Large-Scale Structure* (Cambridge University Press, 2000).

[174] K. W. Masui and U.-L. Pen, *Primordial Gravity Wave Fossils and Their Use in Testing Inflation*, Phys. Rev. Lett. **105** (2010).

[175] L. Dai, "Primordial Perturbations in the Universe: Theory, Detection, and Implication For Inflation" (2015).

[176] L. Dai, M. Kamionkowski, and D. Jeong, *Total angular momentum waves for scalar, vector, and tensor fields*, Phys. Rev. D **86** (2012).

[177] W. Hu and M. White, *CMB anisotropies: Total angular momentum method*, Phys. Rev. D **56**, 596–615 (1997).

[178] L. Dai, D. Jeong, and M. Kamionkowski, *Wigner-Eckart theorem in cosmology: Bispectra for total-angular-momentum waves*, Phys. Rev. D **87** (2013).

[179] A. Hajian, T. Souradeep, and N. Cornish, *Statistical Isotropy of the Wilkinson Microwave Anisotropy Probe Data: A Bipolar Power Spectrum Analysis*, ApJ **618**, L63–L66 (2004).

[180] L. G. Book, M. Kamionkowski, and T. Souradeep, *Odd-parity bipolar spherical harmonics*, Phys. Rev. D **85** (2012).

[181] M. Kamionkowski and T. Souradeep, *Odd-parity cosmic microwave background bispectrum*, Phys. Rev. D **83** (2011).

[182] E. Dimastrogiovanni, M. Fasiello, and G. Tasinato, *Searching for Fossil Fields in the Gravity Sector*, Phys. Rev. Lett. **124** (2020).

[183] A. Ravenni, M. Liguori, N. Bartolo, and M. Shiraishi, *Primordial non-Gaussianity with μ-type and y-type spectral distortions: exploiting Cosmic Microwave Background polarization and dealing with secondary sources*, JCAP **2017**, 042–042 (2017).

[184] A. Malhotra, E. Dimastrogiovanni, M. Fasiello, and M. Shiraishi, *Cross-correlations as a diagnostic tool for primordial gravitational waves*, JCAP **2021**, 088 (2021).

[185] S. Matarrese and L. Verde, *The Effect of Primordial Non-Gaussianity on Halo Bias*, ApJ **677**, L77–L80 (2008).

[186] G. Orlando, P. D. Meerburg, and S. P. Patil, *Primordial tensor bispectra in μ-CMB cross-correlations*, (2021), arXiv:2109.01095 [astro-ph.CO].

[187] A. Ota, *Statistical anisotropy in CMB spectral distortions*, Phys. Lett. B **790**, 243–247 (2019).

[188] J. Chluba, L. Dai, D. Grin, M. A. Amin, and M. Kamionkowski, *Spectral distortions from the dissipation of tensor perturbations*, MNRAS **446**, 2871–2886 (2014).

[189] A. Ota, T. Takahashi, H. Tashiro, and M. Yamaguchi, *CMB μ distortion from primordial gravitational waves*, JCAP **2014**, 029–029 (2014).

[190] C. Wagner, F. Schmidt, C.-T. Chiang, and E. Komatsu, *The angle-averaged squeezed limit of nonlinear matter N-point functions*, JCAP **2015**, 042–042 (2015).

[191] C.-T. Chiang, *Position-dependent power spectrum: a new observable in the large-scale structure*, 2015, arXiv:1508.03256 [astro-ph.CO].

[192] C. T. Byrnes, D. Regan, D. Seery, and E. R. Tarrant, *The hemispherical asymmetry from a scale-dependent inflationary bispectrum*, JCAP **2016**, 025–025 (2016).

[193] C.-T. Chiang, C. Wagner, F. Schmidt, and E. Komatsu, *Position-dependent power spectrum of the large-scale structure: a novel method to measure the squeezed-limit bispectrum*, JCAP **2014**, 048–048 (2014).

[194] M. H. Namjoo, S. Baghram, and H. Firouzjahi, *Hemispherical asymmetry and local non-Gaussianity: A consistency condition*, Phys. Rev. D **88** (2013).

[195] A. A. Abolhasani, S. Baghram, H. Firouzjahi, and M. H. Namjoo, *Asymmetric sky from the long mode modulations*, Phys. Rev. D **89** (2014).

[196] A. A. Starobinsky, *Spectrum of relict gravitational radiation and the early state of the universe*, JETP Lett. **30**, 682–685 (1979).

[197] K. Abazajian, K. Arnold, J. Austermann, B. Benson, C. Bischoff, J. Bock, J. Bond, J. Borrill, I. Buder, D. Burke, and et al., *Inflation physics from the cosmic microwave background and large scale structure*, Astroparticle Physics **63**, 55–65 (2015).

[198] D. H. Lyth, *What Would We Learn by Detecting a Gravitational Wave Signal in the Cosmic Microwave Background Anisotropy?*, Phys. Rev. Lett. **78**, 1861–1863 (1997).

[199] M. Shiraishi, S. Yokoyama, D. Nitta, K. Ichiki, and K. Takahashi, *Analytic formulae of the CMB bispectra generated from non-Gaussianity in the tensor and vector perturbations*, Phys. Rev. D **82** (2010).

[200] M. Shiraishi, D. Nitta, S. Yokoyama, K. Ichiki, and K. Takahashi, *CMB Bispectrum from Primordial Scalar, Vector and Tensor Non-Gaussianities*, Progress of Theoretical Physics **125**, 795–813 (2011).

[201] M. Shiraishi, N. Bartolo, and M. Liguori, *Angular dependence of primordial trispectra and CMB spectral distortions*, JCAP **2016**, 015–015 (2016).

[202] M. Zaldarriaga and U. Seljak, *An all-sky analysis of polarization in the microwave background*, Phys. Rev. D **55**, 1830–1840 (1997).

[203] N. Bartolo, E. Dimastrogiovanni, M. Liguori, S. Matarrese, and A. Riotto, *An estimator for statistical anisotropy from the CMB bispectrum*, JCAP **2012**, 029–029 (2012).

[204] M. Shiraishi, *Probing the Early Universe with the CMB Scalar, Vector and Tensor Bispectrum*, Springer Theses (2013).

[205] F. Finelli et al. (CORE), *Exploring cosmic origins with CORE: Inflation*, JCAP **04**, 016 (2018).